Stability, Control, and State Estimation of Free-Piston Engine Generators

UNIVERSITY OF SUSSEX

Tom Nsabwa Kigezi

Department of Engineering and Product Design

University of Sussex

A thesis submitted in partial fulfillment of the requirements for the degree of

Doctor of Philosophy

January 2019

Dedicated to my parents, Dr. and Mrs Yiga.

Acknowledgements

My most sincere thanks go to Professor Julian Dunne, my supervisor, for his generous stream of advice, support, and insights that carried me throughout the journey leading to this thesis. My deepest gratitude also to the team that worked exceedingly hard with me in realizing an experimentation rig developed from scratch—Dr. Chris Long, Dr. Spyros Skarvelis-Kazakos and Ian Wallace, whose expertise and mastery I greatly relied upon.

Special thanks go to the Doctoral School, for awarding me the Chancellor's International Research Scholarship. Further special thanks to the Defence Science and Technology Laboratory (Dstl) for funding the hardware used for this work.

My deep gratitude goes to the people I now consider colleagues in the Engineering Department—Dr. Kun Liang, Prof. Peter Fussey, Dr. Tai Yang, Dr. Bao K. Nguyen, Dr. Yanan Li, and of course, Dr. Luis Cuspinera, who took such an interest in my work and supported me in various ways. My heartfelt gratitude also to my fellow researchers and friends made in the Sussex community, with whom I have shared very many enjoyable moments. Jisjoe T. J., Alejandro Jesus G. A., and others, the list is long.

Finally, I thank my dear parents, family and friends back home in Uganda, for their constant belief and encouragement, all which contributed invaluably to the realization of this thesis.

Abstract

This thesis investigates stability, control, and state estimation of free-piston engines (FPEs). Emphasis is placed on FPE electric power generators, currently targeted at potential application areas including electric vehicle range extension, efficient power sources in the field, and in combined heat and power systems. A general group of FPE configurations is considered; ranging from a single piston configuration through to an opposed piston configuration, which in each case may make use of either a bounce chamber, a mechanical spring, or second combustion chamber as the rebound device. To assist in verifying the theoretical results, one configuration type is physically modelled to create numerical simulation capability. The modelling includes representative descriptions of the combustion processes, the electrical machine, and the system dynamics.

On stability, the thesis starts from first principles to newly develop a framework that relates key FPE physical parameters. Formal definitions of stability and instability are provided, and general technical statements on the stability of piston oscillations are proposed and verified. On control, the thesis newly applies model-based control theory to three control problems; namely, the control of compression ratio, engine start, and mitigation against abnormal combustion events such as misfire. Optimality and robustness are of key interest in addressing the control problems although other control approaches are investigated. On state estimation, the thesis newly develops a robust finite-time converging observer for FPE dynamics. The developed observer's effectiveness is mathematically proven and verified for the estimation of in-cylinder pressure and piston speed.

To partly verify the findings in experiment, the thesis describes the design and creation of a two-stroke gasoline FPE in hardware. The hardware rig is used to provide measurement data for model validation, observer-based state estimation, and also to discuss FPE stability. In model validation, a parameter identification scheme is proposed in form of a general optimisation problem. In state estimation, the mean observer error is found to be very small; 0.05 bar and 0.1 m/s for the estimation of in-cylinder pressure and piston speed respectively.

Contents

Nomenclature

Acronyms

APU Auxilliary Power Unit

BDC Bottom Dead Centre

BIBS Bounded Input Bounded State

BVP Boundary Value Problem

CAD Computer Aided Design

CI Compression Ignition

DAQ Data Acquisition

ECU Engine Control Unit

EGR Exhaust Gas Recirculation

emf electromotive force

FPE Free-Piston Engine

FPEG Free-Piston Engine Generator

FPLA Free-Piston Linear Alternator

FPLG Free-Piston Linear Generator

HCCI Homogeneous Charge Compression Ignition

ICE Internal Combustion Engine

LQR Linear Quadratic Regulator

LTI Linear Time Invariant

NLP Nonlinear Programme

PI Proportional Integral

PID Proportional Integral Derivative

SI Spark Ignition

SISO Single Input Single Output

TDC Top Dead Centre

Greek Symbols

η Efficiency

γ Specific heat ratio, c_p/c_v

ω Frequency

Φ Magnetic flux

ψ Volume difference

Roman Symbols

$\bar{u}$ Mean piston speed

A Area

E Energy converted/extracted

F Force

h Heat transfer coefficient

k Stiffness of generic rebound device

m Mass

N Number of electric machine coil windings

P Pressure

Q Heat energy

r Resistance

S Stroke

V Volume

W Work done

Miscelleneous Symbols

c_p Specific heat at constant pressure

c_v Specific heat at constant volume

k_s Spring stiffness

m_f Fuel mass

r_c Compression ratio

R_o Specific gas constant

x_0 Piston position

x_β Mass fraction burned

$x_T,\ x_B$ Nominal Top, nominal Bottom Dead Centre postion

$x_t,\ x_b$ Top, Bottom Dead Centre postion

Subscripts

c Cylinder

ch Chemical

cmp Compression stroke

exp Expansion stroke

f Friction

g Generator

ht Heat transfer

LHV Lower Heating Value

m Motor

p Piston

rd Rebound device

s Spring

w Wall

List of Figures

List of Tables

Chapter 1

Introduction

1.1 Motivation

The transport sector is facing ever stricter emissions reduction targets. The sector-wide apotheosis is one of total decarbonization in the form of complete electrification of the powertrain. At present, however, the economic production and subsequent mass uptake of fully electric off-grid modes of transport—such as electric vehicles, ships, and aircraft—remains elusive, owing to current limitations in battery technology [25].

Whereas batteries have served well as small, portable power sources, high capacity batteries are still bulky, slow-charging, and very expensive. Rather unsurprisingly, the limited battery capacity in passenger electric vehicles is now well-known to produce "range anxiety"[1] phenomenon among motorists, subsequently impacting the vehicles' adoption rate [31]. Furthermore, batteries contribute to an increasingly objectionable waste disposal problem that is yet to be addressed by the industry [35].

Continuous improvement of the Internal Combustion Engine (ICE) accordingly remains an important pursuit in light of the limitations of battery technology. Even

[1]Fear that an electric vehicle has insufficient charge in its batteries to reach a destination and would thus strand the vehicle's occupants.

more so when the energy per unit kilogram of liquid fuels is compared to batteries. For example, the lower heating value of gasoline is approximately 46 MJ/kg, whereas the specific energy of lithium batteries only comes close to 1 MJ/kg [1]. Thus, even modest efficiency improvements in the internal combustion engine signify large performance gains. Key improvements to the internal combustion engine lie with further increase in efficiency and reduction in weight, size, and overall complexity [83].

Free-Piston Engines (FPEs) are a promising ICE-improvement currently being pursued by various automotive manufacturers and research institutions [45]. The salient feature of FPEs is the absence of slider-crank mechanism found in conventional reciprocating engines, i.e. no crankshaft–connecting-rod assembly (see schematic comparison in Fig. 1.1). Accordingly, the piston is not mechanically constrained by slider-crank *kinematics* (and is therefore "free" in this sense) but its motion is solely governed by the *dynamics* associated with the acting forces on a moving mass (of which the piston is integral). The output work of an FPE is realized by converting piston thrust energy directly into another useful form, typically electrical (as FPE generators), hy-

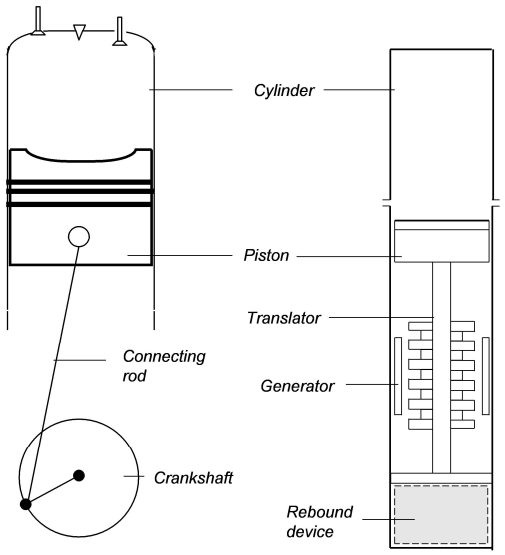

Figure 1.1: Schematic comparison of a conventional ICE (left) with a free piston engine (right).

draulic (as hydraulic FPEs), or pneumatic (as FPE air compressors) [77]. The piston return, or rebound mechanism, can be a mechanical spring [9, 41, 28, 7], an air bounce chamber (also known as a gas spring), or another combustion chamber [102, 2].

The unconstrained piston in FPEs gives the engine two distinctly exploitable features not typically found in conventional ICEs, namely:

- **A variable compression ratio, owing to a non-fixed stroke.** The implication here is that the compression ratio can be dynamically varied; for example with changes in load, allowing for optimized engine operation. An additional implication is that the engine can be adapted to run on various types of fuel as appropriate to compression ratio, making the engine very versatile.
- **Fewer moving parts.** The implication here is reduced friction loss and therefore correspondingly increased efficiency. Fewer moving parts also imply greater packaging compactness and overall mechanical simplicity.

Other advantages of FPEs have been documented. For example, Mikalsen and Roskilly [76, 78] perform extensive FPE simulations and find reduced in-cylinder heat transfer loss as a result of a faster expansion stroke than would be allowed with slider-crank kinematics. The authors go on to link this phenomenon to lower NO_x emissions [82, 79], as well as to discuss the engine's particular suitability for the lean combustion Homogeneous Charge Compression Ignition (HCCI) [116]. Yang and Aichlmay [111, 4] have investigated miniaturized engines based on free-piston designs, owing to the general mechanical simplicity that allows compactness and modularity. In the same vain, the American company Aerodyne Inc. [8, 9, 7] has produced a working version of a 300W compact FPE and tested an even more compact 5W version (see Fig. 1.2). HCCI has been the combustion scheme of choice in the miniaturized and micro engine designs, principally owing to technical limitations of installing a spark plug.

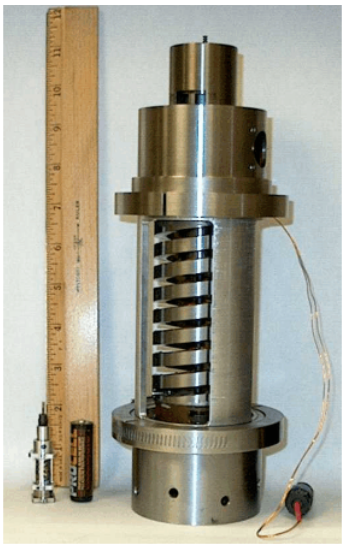

Figure 1.2: Highly compact 300W and 5W free-piston engines by Aerodyne Inc [8]. The 12" (30.48cm) ruler and AA battery provide dimensional reference. The combustion chamber is at the top, with a linear generator at the base. The piston return mechanism is a mechanical spring axially mounted in the centre with visible coils.

At present, electric power generation is the most common application of free-piston engines, targeted at various applications such as range extension of electric vehicles [45], portable power sources in the field [8], and as combined heat and power systems [28]. The potential of FPE generators as Auxiliary Power Units (APUs) in vehicles other than passenger vehicles is also of growing interest [30].

With the contextual relevance and target applications of free-piston engine technology discussed, in what follows, the background for the topic of study in this thesis is provided. In this background, the literature is surveyed to bring unanswered questions to the fore. These questions focus on modelling approaches, stability, control, and free-piston engine state estimation. Thesis objectives are subsequently stated, followed by a thesis overview and the main contributions.

1.2 Background

Free-piston engines—as power generators or otherwise—are yet to receive wide uptake despite strongly desirable features and several development prototypes in the recent and distant past [45, 77, 102]. This has largely been attributed to the difficulty in reliably stabilizing and controlling their *unconstrained* piston motion. The unconstrained piston in an FPE must be actively controlled in order to prevent instability in the form of:

i) engine stall, or

ii) piston collision with surfaces at stroke extremes,

while maintaining effective gas exchange processes at scavenging.

The precise difficulty is that since piston motion is only determined by dynamic force interaction, there is strong interdependence between energy release from combustion and energy extraction to the load. This strong interdependence implies that too "weak" a combustion and the engine stalls whereas too "strong" a combustion and the piston may exceed its allowed bounds in the device's enclosure. From both an analytical and practical standpoint therefore, the FPE presents a stability and control problem; which currently very few studies have attempted with analytical depth.

In the following subsections, background literature on free-piston engine modelling approaches, stability, control and state estimation are discussed.

1.2.1 Free Piston Engine Modelling

Free-piston engines are modelled with the main rigid body dynamics from Newton's second law, along with supporting sub-models for the forces involved. In the simplest case of a single piston configuration, Fig. 1.3 shows the free body diagram of the moving mass constituting the piston-translator assembly (motion is along a horizontal

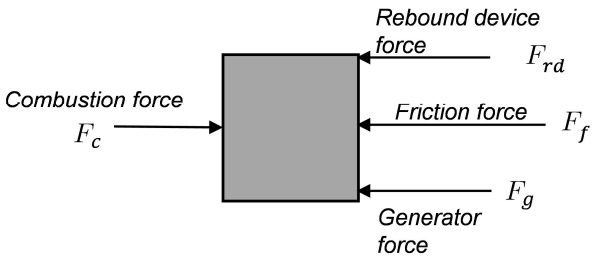

Figure 1.3: Free body diagram of free-piston engine moving mass.

axis).

For a moving mass m, Newton's second law requires:

$$m\ddot{x}_0 = \sum_i F_i \tag{1.1}$$

where x_0 is piston displacement from a reference position, and index i is used to denote a generic force F_i as depicted in Fig. 1.3; that is, the combustion force, rebound device force, generator force, and friction force. Scavenging effects on piston motion have been neglected in (1.1); justifiable under a scavenging arrangement with an external scavenging pump.

The dynamics (1.1) are highly nonlinear on the right-hand side owing to:

i) nonlinear gas compression and expansion processes in the cylinder,

ii) intermittent combustion and scavenging,

iii) nonlinear rebound device processes,

iv) nonlinear loading imposed by the generator, and

v) nonlinear frictional effects.

Model simplification by way of nonlinearity reduction is common. For example, the generator sub-model has been stated as a simple single-parameter linear equation by Mikalsen and Roskilly [78, 76], Jia et al. [55], and others [63, 42, 84]. Also, frictional effects are typically either regarded as negligible or modelled with a small number of

constant parameters [74, 78].

The gap of interest in the literature is the apparent lack of generality in modelling and analysis to include rebound devices of any type. Studies have typically focused on one rebound device; either being a mechanical spring [28], a bounce chamber [78, 76, 62], or a second combustion chamber [52, 71, 11, 117]. No study attempts to unify all three.

1.2.2 Stability of Piston Motion

Some attempts have been made towards studying the stability of FPE piston motion. In general, the quest has been to find general conditions among engine parameters that imply steady (or constant) amplitude of piston oscillations. However, this has been an enormously difficult task owing to highly nonlinear engine dynamics. No complete success towards this endeavour has yet been reported.

Li and Sun [69], for example, analyze engine stability by studying interaction of forces in an HCCI combustion hydraulic free-piston engine. They find that the intrinsic interdependency of the engine processes makes stable engine operation difficult to predict. In particular, the authors find that HCCI combustion timing is strongly affected by the gas exchange process. A cycle-to-cycle mathematical model describing the interaction of the major forces in the engine is developed.

Wu, Hu, and Huan [109] attempt to find parameter relationships that lead to constant amplitude oscillations (i.e. an energy equilibrium) by way of solving the engine's governing differential equation. They approximate the nonlinear governing differential equation with a linear model, allowing some parameter relationships influencing the piston motion to be extracted. They then validate their approximate linear model experimentally.

Zhang et al. [115] also attempt to establish the relationship between engine param-

eters and the piston oscillation characteristic in a bid to achieve constant amplitude oscillations. The idea is that if the system parameters are considered as control variables, stability can be achieved by appropriately adjusting the parameters during engine operation. However, the strongly nonlinear dynamics of the piston motion significantly frustrates their efforts to achieve their specific objectives.

1.2.3 Control of Piston Motion

Perhaps the most important control problem for the FPE is control of compression ratio. This involves controlling the piston's turnaround points, i.e. the top and bottom dead centre positions (TDC and BDC respectively). Compression ratio control has typically been achieved with an energy-based approach involving dynamic variation of supplied fuel, rebound device energy[2], or load.

Proportional Integral Derivative (PID)-type controllers have been the usual controller of choice for compression ratio control, as used by Mikalsen and Roskilly [78, 76, 80, 81], Jia et al. [52], Johansen et al. [56, 57], and others [28]. The PID-type controllers have however been commonly applied "blindly", treating the FPE system as a "black box"—the shortcoming being no real justification for the strategic basis adopted and no corresponding stability assessment.

Setting the control of compression ratio aside, there are other important FPE control problems which the literature does not address to any satisfactory analytical depth. Two of these are explained below:

- **Efficient starting**. For instance, with optimal and mechanical resonance-inducing strategies. Although resonance-inducing strategies (i.e. small starting force yielding large piston amplitude) for starting FPE generators have been proposed in a number of patent filings [9, 111] and publications [74, 53, 54],

[2]Not physically possible where the rebound device is a mechanical spring.

very little in the way of fundamental analysis or benefit assessment has been provided. Also notably, no discussion on optimal control strategies has been found in the literature. Optimal and resonance-inducing strategies are particularly suitable for FPE generators because their implementation involves operating the FPE's generator as a motor, thereby taking advantage of advances in motor control technology. For FPEs without an integrated generator, the starting process is a purely mechanical one involving either igniting an air-fuel mixture in the combustion chamber [33, 89], releasing a wound spring [33], or pre-charging the rebound device [33, 73].

- **Advanced piston motion control.** For example, in mitigation against abnormal combustion [63, 42], emissions formation [82, 79, 114], and in compression ratio control [84]. A key consequence of having an unconstrained piston as found in FPEs is that the piston trajectory *can* be controlled by manipulation of the forces acting on it. In FPE generators, operating the generator as a motor provides an extra control variable for manipulating the piston trajectory. This extra degree of freedom can be exploited in advanced piston motion control applications such as those mentioned. A model-based treatment of these important applications is absent in current FPE generator literature.

1.2.4 State Estimation of Free-Piston Engines

Current FPE literature does not cover state estimation; for instance, observer-based estimation of in-cylinder pressure and piston speed. State estimation can be a cost-effective method of acquiring engine information without installing sensors. Whereas reconstruction of engine in-cylinder pressure with observers in conventional reciprocating engines has been extensively studied, for example in [5, 24], the subject remains unaddressed for FPEs. The challenges associated with FPE observer design stem from high system nonlinearity and fast dynamics that necessitate fast observer

convergence times.

1.2.5 Summary of the Background Information

With this background, it is evident that the area of stability, control, and state estimation of FPEs (as generators or otherwise) is not well developed. Even where there has been work, the area has largely not been satisfactorily addressed with model-based approaches. Recalling that the key barrier to the wide uptake of FPE technology is reliable stabilization and control of the piston motion, there is an important need to develop analytically guided model-based approaches in this regard. A key benefit of model-based approaches is transferability of method to general FPE types and configurations, thereby facilitating repeatability. It now suffices to state the objectives of the thesis.

1.3 Thesis Objectives

The overall objective of this thesis is to develop model-based approaches in the analysis of FPEs, covering stability, control, and state estimation. The specific objectives are categorized as follows:

Stability. To develop a first-principles framework within which FPE stability can be understood.

Control. To apply control theory in developing methods for FPE control that are targeted towards achieving stability.

State Estimation. To apply observer theory in developing a robust state estimator for FPE dynamics that could be useful for feedback engine control.

In effect, this thesis lays out theoretical groundwork in the area of FPE stability,

control, and state estimation. Emphasis is placed on FPEs as power generators, also referred to as FPE generators.

The electric machine component of the FPE generator is assumed to be synchronous and of permanent magnet excitation. For simplicity, only the most fundamental principles of electric power generation observed from relative motion between a magnetic field and a conductor are used. It is now added that all analysis to be presented is based on experimentally validated free-piston engine models available in the literature.

1.4 Thesis Overview and Contributions

Generic FPE modelling has first been provided in Chapter 2, where the modelling has been unified for any rebound device type.

On the subject of *stability*, formal definitions of FPE stability and instability have been provided in Chapter 3. General statements in the form of technical facts and propositions have also been stated and verified. Accordingly, a general framework within which FPE stability can be understood has been established.

On the subject of *control*, new model-based approaches have been developed in Chapters 4, 5, and 6 respectively for:

i) the control of compression ratio,

ii) optimal and resonant engine start, and

iii) the mitigation of abnormal combustion in the form of misfire.

In compression ratio control, control-oriented models have been developed for which both simple and advanced controller design techniques can be applied. Specifically, Proportional Integral control and the Linear Quadratic Regulator have been demon-

strated. In engine start, analytical and numerical approaches have been developed for both resonance-inducing and optimal control strategies for starting free-piston engine generators. In mitigation against misfire, analytical and numerical strategies involving both constant and dynamic motoring forces have been proposed and tested. These strategies have also been adapted as an alternative to energy-based methods in achieving compression ratio control.

On the subject of *state estimation*, in Chapter 7, a newly-developed sliding mode observer has been proposed for in-cylinder pressure and piston speed estimation. The observer error converges to zero in finite time, making it useful for real-time applications. Effectiveness of the observer has been proved with Lyapunov theory.

All experimental work has been described in Chapter 8. An FPE rig developed at The University of Sussex has provided measurement data that has been exploited in three key areas; namely model validation, state estimation (using the sliding mode observer proposed in Chapter 7), and stability assessment (using the framework developed in Chapter 3). In model validation, a parameter identification scheme is proposed in form of a general optimisation problem and successfully applied. In state estimation, observer error in the estimation of in-cylinder pressure and piston speed is found to be very small; 0.05 bar and 0.1 m/s respectively.

Finally, conclusions and future work of this thesis have been discussed in Chapter 9.

Chapter 2

Classification and Modelling

2.1 Introduction

Free-piston engines are mechanically simple devices. This is indeed one of their principal merits in comparison with conventional reciprocating engines. However, several possible component combinations and configurations exist, as well as several possible combustion schemes—all with potential advantages and disadvantages in practice. An understanding of these classifications is of illustrative value before embarking on *generic* mathematical modelling for analysis.

Accordingly, this chapter briefly discusses FPE classifications and thereafter selects one generic FPE design for mathematical modelling. The selected FPE is a generator, in line the thesis scope; however the modelling is unified to cover any rebound device type in order to permit general analysis. It is noted that all modelling in this chapter has been verified experimentally, for example in work by Jia et al. [54], Zaseck et al. [113], and Li [71]. On this basis, the FPE model developed in this chapter will act as a reference model for all development work to follow in subsequent chapters. The novel features of this thesis will be tested against the FPE model developed here.

2.2 Classification of Free-Piston Engines

2.2.1 By Application

One of the most general categorizations of FPEs is by their intended purpose. This usually pertains to the type of output energy produced by the engine. The FPE has historically had three major application areas explained below:

- **Electric power generator**

  Energy extraction device: linear generator.

  Typically called a Free-Piston Engine Generator (FPEG); other names in the literature are Free-Piston Linear Alternator (FPLA) and Free-Piston Linear Generator (FPLG). The piston is rigidly attached to a translator rod along which are mounted permanent magnets, constituting the secondary units of a linear generator. The primary unit, or stator, consists of coil windings integrated in the engine housing. As the piston oscillates, electrical energy is produced by the linear generator. FPE generator development today is mainly for range extension of electric vehicles [45], portable power sources in the field [8], and as combined heat and power systems [28].

- **Hydraulic pump**

  Energy extraction device: hydraulic pump.

  Free-piston engines can be used to drive positive displacement hydraulic devices such as piston or membrane pumps to generate pressure for hydraulic actuators or motors. Many of these units are intended for off-highway vehicles such as forklift trucks and earth-moving machinery. Several designs and configurations have been developed in the past decades [3, 104, 46, 71].

- **Air compressor**

  Energy extraction device: air chamber.

The piston stroke works to compress air contained in an air chamber. The compressed air may then be supplied to various applications. Notably, FPE air compressors were used in World War II to supply compressed air for launching torpedoes [73]. In the so-called FPE gas generators (whose purpose is to supply hot exhaust gas to a power turbine), the compressed air is instead fed back to the engine as a supercharged air intake.

A brief historical note is in order. FPEs were in fact formally invented in 1928 [92] and enjoyed noteworthy success as air compressors for a brief period before becoming obsolete for various reasons, including competition from electric motor driven compressors [77, 4]. Control of FPE air compressors is reported to have involved a "self-regulating" capability from the interaction between the compressor cylinders and bounce chamber [33]. Owing to advances in sensing and computer technology, the advent of rare earth permanent magnets, and an appreciation of the limitations of conventional ICE technology, interest in FPEs has now re-emerged within the power generation and hydraulic pump applications.

2.2.2 By Piston Configuration

The number and arrangement of pistons, also sometimes called the engine architecture, is a typical way of classifying free-piston engines. Several configurations are possible but the three most common are described in Table 2.1; namely, single piston, dual piston, and opposed piston configurations.

2.2.3 By Linear or Rotary Layout

All the free-piston designs discussed thus far are of linear type i.e. the oscillatory motion of the piston is along a straight line. This design has persisted from history and still dominates free-piston engine research today. However, to attain even greater

Table 2.1: Free-Piston Engine Architectures

Type	Illustration	Remarks
Single piston	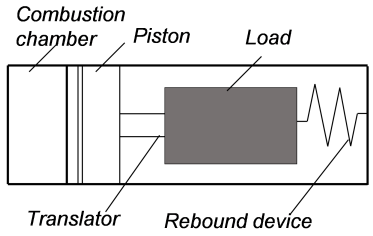	• One piston, one combustion chamber, and one rebound device. • Simple design. • Unbalanced, therefore produces heavy vibration.
Dual piston	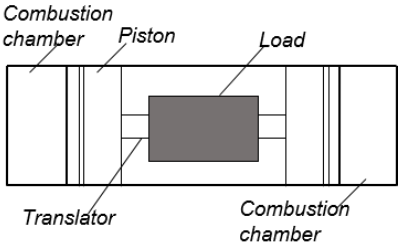	• No rebound device. Combustion occurs alternately in opposing combustion chambers. • Two power strokes in one cycle implying high power-weight ratio. • High sensitivity to combustion variation.
Opposed piston	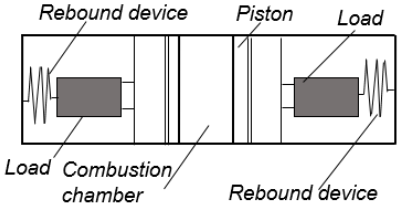	• Two single piston units sharing common combustion chamber. • Perfectly balanced. Reduced heat transfer loss owing to elimination of cylinder head. • Reduced compactness due to parts mirroring.

compactness, rotary designs have been recently proposed [29, 49].

2.2.4 Other Classifications

Just like conventional engines, free-piston engines may be classified according to number of piston strokes in an operating cycle i.e. two-stroke or four-stroke; combustion type e.g. spark ignition (SI) or compression ignition (CI); and other attributes such as engine size in terms of nominal piston displacement volume.

2.3 Modelling of Free-Piston Engines

This section presents a mathematical model of a two-stroke single piston FPE generator, on which all subsequent stability and control techniques in later chapters are tested. The model constitutes rigid body dynamics and a description of relevant forces from the various parts of the device, i.e. combustion chamber, rebound device, and generator.

Note that as shown in Table 2.1, there are other possible FPE piston configurations other than the single piston configuration; namely the dual and opposed piston configurations. The choice of the single piston configuration as a reference here stems from the fact that other FPE piston configurations are equivalent to the single piston configuration under the following considerations: In the dual piston configuration, one combustion chamber is treated as a bounce chamber, whereas in the opposed piston configuration, mirror-like symmetry is assumed about the combustion chamber vertical centre line, yielding two opposing single piston FPEs.

Verification of the presented FPE model under experimental conditions has been reported in [55, 113, 71]. The scope of the model is now summarized by the following main assumptions:

- Zero-dimensional thermodynamic modelling is used to describe thermodynamic processes. This modelling approach is sufficient for control design, but of limited scope in describing performance aspects such as fuel efficiency or emissions formation.
- All fuel available within a given engine cycle is combusted, with negligible effects included from air-fuel ratio variability. Indeed, air-fuel ratio is considered to be a static parameter.
- Ideal scavenging occurs, where all exhaust gas is instantaneously replaced with fresh charge. Therefore, the effect of residual gases or exhaust gas recirculation

(EGR) to combustion chamber thermodynamics is not considered.

- As the focus in subsequent chapters is to study piston motion, investigation into electrical energy conversion efficiencies is deemed out of scope.

The first three assumptions pertaining to engine thermodynamics are not unusual in ICE engine analysis for control design [32].

2.3.1 Equation of Motion

An idealized two-stroke single piston FPE generator schematic is shown in Fig. 2.1. The engine comprises three major parts: a piston-translator assembly, known as the moving or active mass; a rebound device to return the piston to TDC from BDC; and an integrated generator for power generation.

Considering the direction of the compression stroke as positive for piston displacement x_0, application of Newton's second law to the piston-translator mass m gives the equation of motion as

$$-m\ddot{x}_0 = F_c + F_{rd} + F_g + F_f \tag{2.1}$$

where F_c is the force due to in-cylinder gas pressure in the combustion chamber, F_{rd} is the rebound device force, F_g is the generator force, and F_f is the friction force. These forces will now be described.

2.3.2 In-Cylinder Gas Pressure Force

The in-cylinder gas pressure force F_c is related to the in-cylinder gas pressure P_c according to the equation

$$F_c = A_p P_c \tag{2.2}$$

where A_p is the piston crown area.

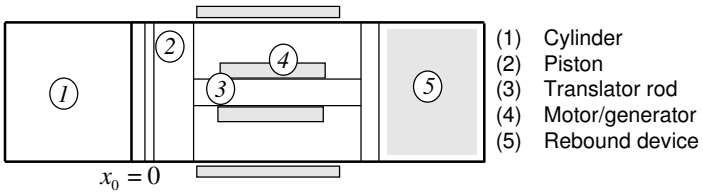

Figure 2.1: Generic FPE generator schematic. The piston, translator, and generator permanent magnet constitute the moving mass. The rebound device may be a mechanical spring, an air bounce chamber or another cylinder. 1—Cylinder, 2—piston, 3—translator rod, 4—piston load (generator), and 5—rebound device.

2.3.2.1 In-Cylinder Pressure

The in-cylinder or combustion chamber pressure is determined according to thermodynamic processes taking place in the cylinder. Consider the following assumptions:

- When both inlet and exhaust ports are covered (as is the case during compression and expansion strokes), the cylinder volume is *closed*.
- The mixture of burned and unburned gases within the cylinder is *uniform.* As such, a single control volume can be used to characterize the thermodynamic behavior of the contained gas.
- The gas inside the cylinder is *ideal*, i.e. it obeys the ideal gas law.
- There are no crevices on any surface forming the closed cylinder volume. In line with the closed volume assumption, there is no "blow by", i.e. gas leakages from the cylinder through any space between the piston and cylinder walls.
- Potential energy influences and velocity effects (i.e. inertial effects) of the gas are not considered.

Heywood [47] uses the above assumptions when applying the first law of thermodynamics to the combustion chamber volume in order to derive the in-cylinder pressure dynamics as

$$\frac{dP_c}{dt} + \frac{\gamma_c}{V_c}\frac{dV_c}{dt}P_c = \frac{\gamma_c - 1}{V_c}\left(\frac{dQ_{ch}}{dt} - \frac{dQ_{ht}}{dt}\right) \tag{2.3}$$

where V_c is the cylinder volume, Q_{ch} is the chemical energy (or gross heat) released from burned fuel—also known as combustion heat release, Q_{ht} is the energy lost through heat transfer out of the cylinder and γ_c is the ratio of specific heat of constant pressure to that of constant volume for the cylinder contents. Equation (2.3) is also called a *single-zone* thermodynamic model [34] because the entire combustion chamber is treated as one system, or "zone".

2.3.2.2 Combustion Heat Release

A model of the gross heat release rate from combustion is commonly given as

$$\frac{dQ_{ch}}{dt} = \eta_c Q_{LHV} m_f \frac{dx_\beta}{dt} \tag{2.4}$$

where η_c is the combustion efficiency i.e. the proportion of fuel actually ignited (usually measured between 95–98 %), Q_{LHV} is the fuel's lower heating value, m_f is the fuel mass and x_β is the mass fraction of fuel burned, commonly approximated over the combustion duration by a sigmoid curve known as the Weibe function [47]. The Wiebe function is modified here to be time-dependent (as opposed to crank angle dependent) in

$$x_\beta = 1 - \exp\left[-a\left(\frac{t - t_0}{t_c}\right)^{c+1}\right] \tag{2.5}$$

where $t_0 \leq t \leq t_0 + t_c$ is time, t_0 is start of combustion time, t_c is the total combustion duration (associated with $x_\beta = 0$ to $x_\beta = 1$), and parameters a and c are experimentally fitted. Heywood [47] has reported that actual mass fraction burned curves have been fitted with $a = 5$ and $c = 2$.

Combining (2.5) and (2.4) produces the explicit equation for the gross heat release rate as

$$\frac{dQ_{ch}}{dt} = \eta_c Q_{LHV} m_f \frac{a(c+1)}{t_c}\left(\frac{t - t_0}{t_c}\right)^c \exp\left[-a\left(\frac{t - t_0}{t_c}\right)^{c+1}\right] \tag{2.6}$$

2.3.2.3 Heat Transfer

Most heat loss equations used for combustion engine modelling are of the standard convection heat transfer form given by

$$\frac{dQ_{ht}}{dt} = hA_s(T_c - T_w) \tag{2.7}$$

where A_s is the surface area enclosing the combustion volume, T_c is the mean gas temperature within the cylinder, T_w is the mean wall temperature and h is the heat transfer coefficient.

The most significant challenge with applying the relation (2.7) is in choosing a heat transfer coefficient. Borman and Nishiwaki [20] have written an extensive review of different models for conventional engines. A commonly used one is Woschni's correlation [108]. The heat transfer coefficient used here is the one proposed by Hohenberg [48], and also used by Mikalsen and Roskilly [78, 76, 55], i.e.

$$h = 130V_c^{-0.06}\left(\frac{P_c}{10^5}\right)^{0.8} T_c^{-0.4}\left(\bar{u} + 1.4\right)^{0.8} \tag{2.8}$$

where $\bar{u}$ is the mean piston speed.

2.3.2.4 Scavenging

Much of the research on free-piston engines has been with two-stroke cycles, for which the scavenging process applies (notable recent work with four-stroke cycles is by Lin et al. [72]). Scavenging is the operation of clearing the cylinder of burned gases and filling it with fresh charge before the start of a new compression stroke. This process is extensively characterized both analytically and empirically by Heywood [47] and by Blair [17]. Indeed, sophisticated scavenging models have been used in free-piston engine simulations [74, 112].

However, the vast majority of the literature on free-piston engine modelling for *control design* assumes that scavenging is a perfect process; meaning that during scavenging, while both intake (from scavenge case) and exhaust ports are open, the cylinder pressure instantaneously drops to the intake pressure and remains at this value until both intake and exhaust ports are closed. Thus, the in-cylinder pressure during scavenging can be expressed as

$$P_c = P_0 \tag{2.9}$$

where P_0 is the intake pressure of fresh charge, e.g. from a scavenge case. Therefore, in the computation of in-cylinder pressure, Equation (2.9) is implemented at one time instant in a cycle—the instant of scavenging—while Equation (2.3) is solved for the rest of the cycle. This ideal scavenging description is akin to the "perfect displacement model" of scavenging, among others surveyed by Merker and Gerstle [75].

Where a scavenge case is present, one must note that work is done by the piston in compressing the scavenge case during the FPE's expansion stroke. Accordingly, presence of a scavenge case must necessitate introduction of a "scavenge case force" F_{sc} to the dynamics (2.1), given by

$$F_{sc} = -A_{sc}P_{sc} \tag{2.10}$$

where P_{sc} is the scavenge case pressure and A_{sc} is the area of the surface interfacing the piston-translator rod to the scavenge case. The pressure P_{sc} is generally not trivial to model, even with a zero dimensional approach [87]. For simplicity, Jia et al.[55] model the variation of P_{sc} as an adiabatic isentropic process. Alternatively, modelling P_{sc} (and therefore F_{sc}) could be done away with if scavenge case compression is considered as part of a friction model that is to be experimentally validated.

2.3.3 Generator Force

Relative motion between the translator and armature coil windings (stator) causes an induced electromotive force (emf) across the armature coil terminals, which in turn sets up a current flow through a connected load. The resulting armature reaction magnetic field (due to induced current flow) interacts with the permanent magnet field in the air gap to produce a thrust force in the opposite direction of piston motion. This opposing thrust force is sometimes called a generator *reaction* force. However it is more common to simply refer to it as a generator force.

Detailed calculation of the generator force is generally complicated as it requires solving Maxwell's equations while accounting for magnetic field temporal and spatial variation. Furthermore, model accuracy tends to be specific to machine topology, geometry and component physical properties. Boldea and Nasar [19] have extensively modelled linear electric machines, going further to discuss detailed practical design methodologies. Mueller [85] has a detailed mathematical modelling account of a linear generator motivated by wave energy conversion applications. For free-piston engines, a tubular machine with modular windings is modelled and analyzed extensively by Wang and Howe [106].

A commonly used simplistic approach to calculating the generator force is the following: Induced emf e_g across the armature coils is produced according to Faraday's law. Taking piston position as an independent variable, Faraday's law can then be manipulated by chain rule as follows

$$e_g = N\frac{d\Phi}{dt} \tag{2.11a}$$

$$= N\frac{d\Phi}{dx_0}\frac{dx_0}{dt} \tag{2.11b}$$

$$= k_g\dot{x}_0 \tag{2.11c}$$

where N is the number of armature coil windings (turns), Φ is the magnetic flux

linking one coil winding, and k_g is a constant determined by the physical properties of the generator (topology, geometry and component physical properties). Energy conversion from mechanical power to electrical power can be represented by the power continuity equation

$$F_g \dot{x}_0 = \frac{1}{\eta} e_g i_g \tag{2.12}$$

where i_g is the armature current and η is an energy conversion efficiency from mechanical to electrical power. Combining (2.12) with (2.11c) yields

$$F_g = \frac{1}{\eta} k_g i_g \tag{2.13}$$

which shows that the generator force is proportional to the produced armature current. It is now assumed that the generator circuit is at resonance [23]; i.e. the induced current and voltage are in phase, accordingly rendering the circuit nearly purely resistive (that is to say of power factor close to 1). The armature current is then given according to Ohm's law as

$$i_g = \frac{e_g}{r_g} \tag{2.14}$$

where r_g is the overall generator circuit resistance. Substituting (2.14) in (2.13) and using (2.11) gives the final expression of the generator force as

$$F_g = \mu_g \dot{x}_0 \tag{2.15}$$

where $\mu_g = \frac{k_g^2}{\eta r_g}$ is sometimes ambiguously called the generator parameter or generator coefficient. The essence of (2.15) is that the generator force is proportional to piston speed.

Figure 2.2 shows an equivalent circuit diagram of a synchronous generator. The impedances Z_{g1} and Z_{g2} are in general reactive, and respectively represent the synchronous and electrical load impedances of the generator. The validity of the derived

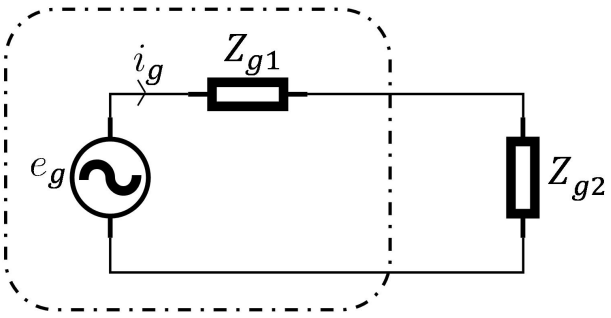

Figure 2.2: Equivalent circuit of synchronous generator.

expression for generator force (2.15) hinges on the generator circuit having a power factor close to 1. One way of achieving such a circuit is by power factor correction, a well-known concept in power systems engineering [96].

2.3.4 Rebound Device Force

A rebound device is responsible for returning the piston to TDC from BDC during the compression stroke. A rebound device could be a mechanical spring, a bounce chamber (gas spring), or a combustion chamber. The combustion chamber force has been discussed in (2.2) – (2.9). The remaining two rebound device forces are modelled as

$$F_{rd} = \begin{cases} k_s x_0 & \text{mechanical spring} \\ -A_{rd} P_{rd} & \text{bounce chamber} \end{cases} \tag{2.16}$$

where k_s is the spring constant or spring stiffness (as per Hooke's law), A_{rd} is the area of the translator surface interfacing with the bounce chamber, and P_{rd} corresponds to the bounce chamber pressure that is taken to satisfy an adiabatic isentropic process [74]

$$P_{rd} V_{rd}^{\gamma_{rd}} = \text{constant} \tag{2.17}$$

or equivalently in dynamic form when (2.17) is differentiated with respect to time,

$$\frac{dP_{rd}}{dt} = -\gamma_{rd}\frac{P_{rd}}{V_{rd}}\frac{dV_{rd}}{dt} \tag{2.18}$$

In (2.17) and (2.18), V_{rd} is the rebound device volume and the index γ_{rd} is the ratio of specific heats for air (constant pressure to constant volume), assuming air fills the bounce chamber.

2.3.5 Friction Force

Friction losses in the free-piston engine are in general expected to be lower than for the conventional engines due to the elimination of the crank mechanism. The frictional force will originate from contact between both the piston rings and piston skirt with the cylinder wall. Note that this force always acts in the opposite direction of piston motion.

Blair [17] provides a correlation for calculating the friction force for conventional engines. Assuming a constant frictional force over a stroke, Atkinson et al. [11] and Mikalsen et al. [78] have followed the correlation provided by Blair to calculate the friction force in their simulations. However, Atkinson et al. calculate the force to be so small compared to the magnitude of other forces that they completely neglect it in their simulations. Kosaka et al. [63] also neglect friction completely on the basis that it is much smaller compared to the generator force.

More detailed parametric friction modelling has been used. For example, Zaseck et al. [113] model piston ring and piston skirt frictional force with detailed models adapted from Zweiri et al. [119] and a bearing friction model based on Petroff's law

from Rezeka et al. [97] and Cameron [22]:

$$\begin{aligned} F_f =& \mu_f \sum_{i=1}^{n_r} \left[\frac{E_{Y,i} L_g}{7.07 d_r} \left(\frac{d_r}{L_{r,i}} - 1 \right)^3 + z_i \left| P_c - P_{sc} \right| \right] \pi d_r L_{r,i} \\ &+ \frac{\mu_o \dot{x}_0}{L_0} d_{CV} L_s \\ &+ \frac{2\pi \mu_o \dot{x}_0 r_b L_b}{L_c} \end{aligned} \tag{2.19}$$

The first, second, and third terms of (2.19) describe the frictional force owing to the piston rings, piston skirt, and translator rod bearings respectively. Parameter μ_f is the friction coefficient, $E_{Y,i}$ is the modulus of elasticity of the piston ring i, L_g is the piston ring gap closure, d_r is the piston ring diameter, L_r is the piston ring thickness, n_r is the number of piston rings, P_c is the cylinder pressure, P_{sc} is the scavenge case pressure while z_i incorporates the pressure drop across ring i. Parameter L_0 is the oil clearance, d_{CV} is the cylinder diameter, and L_s is the skirt length. Parameter μ_o is the oil viscousity, $\dot{x}_0$ is the piston speed, L_b is the bearing length, r_b is the bearing radius, and L_c is the radial clearance.

Here, as in Mao et al. [74], the friction force is modelled with a Coulomb friction and viscous friction component as

$$F_f = a_f \text{sgn}(\dot{x}_0) + b_f \dot{x}_0 \tag{2.20}$$

where a_f and b_f are empirical parameters obtained by measurement.

2.4 Chapter Conclusions

A generic mathematical model for a single piston free-piston engine generator has been introduced in this chapter. The model accommodates any rebound device type and includes both rigid body dynamics and thermodynamics modelling with heat

transfer. All model descriptions have been adopted from the literature, where they have been experimentally validated. The key significance of the model is that it forms the reference model for all simulation work in Chapters 4–7. The same model is validated for an FPE test rig in Chapter 8.

Chapter 3

Stability Analysis with the Energy Conservation Principle

3.1 Introduction

Piston motion in free-piston engines (FPEs) is characterised by oscillations between bottom-dead-centre (BDC) and top-dead-centre (TDC); i.e. compression and expansion strokes. This chapter investigates the stability of these oscillations. Stability will mean the tendency to maintain such oscillations in spite of variations in operating conditions. The opposite of stability, i.e. instability, will mean a decay of these oscillations to zero, i.e. stall, or a growth of these oscillations beyond the allowed bounds of the engine cylinder, i.e. collision.

Chapter 2 has described the FPE governing dynamic equation as nonlinear. In analyzing stability of solutions to nonlinear dynamic equations, one usually first finds an approximate analytic solution by an approximation scheme such as perturbation [105, 13, 59, 86, 88] or harmonic balance [107, 37, 93]. If successful, stability of the known solution can then be investigated. However, applying these well-known

solution-approximation schemes to FPE dynamics is particularly problematic owing to the intermittent, or discrete-time occurrence of events such as combustion and scavenging alongside continuous-time dynamics. Strictly speaking therefore, the FPE is a *hybrid* dynamical system; i.e. one that exhibits both continuous-time and discrete-time behaviour. An excellent but highly abstract stability treatment of such systems, with focus on a Lyapunov function approach, can be found in the recent work by Goebel, Sanfelice, and Teel [38].

Here, stability of piston oscillations is analyzed from a more physically intuitive point of view. With the energy conservation principle (also known as the first law of thermodynamics), this chapter deduces general technical statements about the stability of FPE piston oscillations. These statements, which broadly explain FPE stability, are the main contribution of this chapter.

The chapter starts by introducing the notion of an operating point. An energy conservation analysis is then undertaken to work out the relationships between the parameters forming an operating point. A nominal operating point is then chosen, and stability of piston oscillations at the nominal operating point is discussed. The implications (on FPE stability) of perturbing an operating point are then considered, and the chapter ends with a brief discussion on the stability of an FPE in closed loop.

3.2 The Notion of an Operating Point

In studying stability of FPE piston oscillations using the energy conservation principle, it is helpful to introduce the notion of an FPE *operating point*. An operating point will constitute key physical parameters influencing piston motion, such as fueling, loading, and rebound device stiffness. An operating point may or may not be physically viable, and may therefore lead to stability or instability of FPE piston oscillations.

To build an understanding of what an FPE operating point constitutes and its relevance to FPE stability, definitions of FPE instability and stability are first given.

Definition 1 (FPE instability). *An FPE is unstable if piston oscillation amplitude decays to zero (i.e. stall) or if piston oscillation amplitude grows beyond cylinder bounds (i.e. collission).*

From engine design practice [53, 46, 42, 62, 3, 18], it has been established that FPE instability can be triggered by a number of factors, broadly categorized here as the following:

- Thermodynamic factors (relating to in-cylinder pressure and temperature):
  - Insufficient compression ratio, leading to misfire and ultimately stall.
  - Insufficient scavenging (i.e. gas exchange) efficiency, leading to misfire and ultimately stall.
- Energy factors (relating to energy supply, extraction, and internal energy storage):
  - Excessively high or low fuel supply relative to loading and rebound device stiffness, respectively leading to collision and stall.
  - Excessively high or low loading relative to fuel supply and rebound device stiffness, respectively leading to stall and collision.
  - Excessively high or low rebound device stiffness relative to fuel supply and loading, respectively leading to stall and collision.

It is thus apparent that insufficiency, or excess, of engine thermodynamic or energy parameters can lead to instability as per Definition 1. Next, FPE stability is defined.

Definition 2 (FPE stability). *An FPE is stable if piston oscillation amplitude neither decays to zero nor exceeds cylinder bounds amidst small variations in operating conditions.*

The "operating conditions" in Definition 2 simply constitute the thermodynamic and energy factors listed following Definition 1. Thus, in studying FPE stability, one studies the effects of changes in thermodynamic and energy factors to piston oscillations. Definition 2 is restricted to small variations in operating conditions, as arbitrarily large variations can be expected to lead to physically invalid operating conditions and therefore instability.

In this work, only the effects of energy factors—i.e. energy supplied (fueling), energy extracted (loading), and energy stored (rebound device stiffness)—to piston oscillation amplitude (i.e. stroke) are examined. The precise effects of thermodynamic factors (i.e. compression ratio and scavenging efficiency) on FPE stability do not lie within the scope of the zero-dimensional thermodynamic models introduced in Chapter 2 and for this reason are not considered.

Having defined FPE instability and stability, it suffices to define an FPE *operating point*. An FPE operating point is a set of parameters characterizing FPE operation; for this work they are: the three energy-related parameters (constituting fuel supplied, loading, and rebound device stiffness), and the piston stroke. A developing idea here is that a stable FPE operates at a physically viable operating point, while an unstable FPE does not. Whereas establishing physical viability of an operating point is no trivial task, it is possible to relate the FPE operating point parameters with the energy conservation principle. An understanding of these relationships will guide physical reasoning towards making some general statements about FPE stability *at* an operating point.

3.3 Energy Conservation Analysis at an Operating Point

The parameters constituting an operation point (i.e. fuel supplied, loading, rebound device stiffness and stroke) will now be formally related by the energy conservation principle. This will start with the compression stroke, followed by the expansion stroke, and lastly the full cycle constituting both the compression and expansion stroke. Key facts that facilitate later discussions on stability at an operating point are highlighted. For notation, the use of subscripts b and t will denote BDC and TDC respectively throughout the chapter.

3.3.1 Compression Stroke Energy Balance

Consider a piston moving from a BDC position x_b to a TDC position x_t in a compression stroke (solid line in Fig. 3.1). In a compression stroke, all energy that drives the

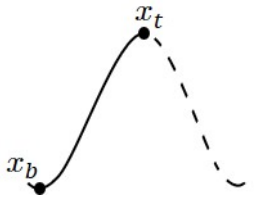

Figure 3.1: Visualization of compression stroke in time.

piston from x_b to x_t originates from the rebound device (energy supply). A portion of this energy goes into compressing the gas contained in the cylinder (internal energy storage) and the rest is extracted as useful work *and* lost in frictional effects (loading).

A compression stroke energy balance is accordingly constructed as

$$\underset{b\to t}{W_{rd}} = \underset{b\to t}{W_c} + E_{cmp} \tag{3.1}$$

where $\underset{b\to t}{W_{rd}}$ is the work done by the rebound device in driving the piston from x_b to x_t, $\underset{b\to t}{W_c}$ is the work done on the cylinder gas when the piston moves from x_b to x_t, and E_{cmp} is the energy converted by piston motion into useful output energy and into the energy lost as friction when the piston moves from x_b to x_t.

It is now shown that $\underset{b\to t}{W_{rd}}$ on the left hand-side of (3.1) is related to rebound device stiffness. When the rebound device is a mechanical spring, the evaluation of $\underset{b\to t}{W_{rd}}$ reveals its relationship to spring stiffness k_s as

$$\underset{b\to t}{W_{rd}} = \frac{1}{2}k_s\left(x_b^2 - x_t^2\right) \tag{3.2}$$

When the rebound device is a bounce chamber, the stiffness of the bounce chamber is considered as its air mass. Assuming the bounce chamber pressure follows the isentropic process

$$PV^{\gamma} = \text{constant}; \tag{3.3}$$

then the evaluation of $\underset{b\to t}{W_{rd}}$ reveals its relation to bounce chamber air mass m_{rd} as

$$\underset{b\to t}{W_{rd}} = \frac{P_{rd_b}\left(V_{rd_b}^{\gamma_{rd}}V_{rd_t}^{1-\gamma_{rd}} - V_{rd_b}\right)}{1-\gamma_{rd}} \tag{3.4}$$

where

$$P_{rd_b} = \frac{R_o T_{rd_b}}{V_{rd_b}} m_{rd_b} \tag{3.5}$$

as per the ideal gas law (R_o in (3.5) is the specific gas constant). Thus, it has been shown that $\underset{b\to t}{W_{rd}}$ is related to rebound device stiffness m_{rd}.

Now, let k denote the rebound device stiffness for either a mechanical spring or bounce chamber. Also, let $S(x_b, x_t)$ denote the compression stroke length from x_b to x_t, i.e.

$$S(x_b, x_t) = |x_b - x_t| \tag{3.6}$$

When a piston travels from x_b to x_t in a compression stroke, the energy balance (3.1) relates the piston travel $S(x_b, x_t)$ to the energy supply in terms of rebound device stiffness k and energy extraction (i.e. loading) E_{cmp}. Visually, one can imagine the parameter interconnection in Fig. 3.2, which aids the deduction of the following fact:

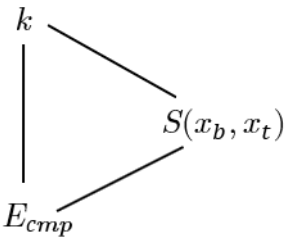

Figure 3.2: Operating point parameter interconnection for the compression stroke.

Fact 1. *For a compression stroke $S(x_b, x_t)$ and an energy extraction E_{cmp} there exists an associated rebound device stiffness k.*

Fact 1 is verified when rebound device stiffness is made the subject of (3.1) and shown to exist for all compression strokes $S(x_b, x_t) > 0$. For illustration, taking a mechanical spring as the rebound device, (3.2) is used in (3.1) to find

$$k_s = \frac{2\left(\underset{b\to t}{W_c} + E_{cmp}\right)}{x_t^2 - x_b^2} \tag{3.7}$$

Since $x_t \neq x_b$, it is concluded that stiffness k_s exists for all $S(x_b, x_t) > 0$.

3.3.2 Expansion Stroke Energy Balance

Now consider the piston moving from the TDC position x_t to a BDC position x_{b^+} in the following expansion stroke (solid line in Fig. 3.3). In an expansion stroke, the energy that drives the piston from x_t to x_{b^+} originates from the added fuel quantity (energy supply), assuming combustion at TDC. A fraction of this energy is captured

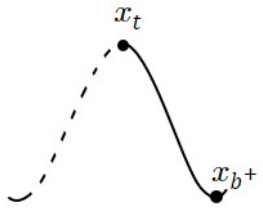

Figure 3.3: Visualization of expansion stroke in time.

by the rebound device (internal energy storage) and the rest is extracted as useful work *and* lost in frictional effects (loading).

An expansion stroke energy balance is accordingly constructed as

$$\underset{t\to b^+}{W_c} = \underset{t\to b^+}{W_{rd}} + E_{exp} \tag{3.8}$$

where $\underset{t\to b^+}{W_c}$ is the work done by the cylinder gas in driving the piston from x_t to x_{b^+}, $\underset{t\to b^+}{W_{rd}}$ is the work done on the rebound device when the piston moves from x_t to x_{b^+}, and E_{exp} is the energy converted by piston motion into useful output energy and into the energy lost as friction when the piston moves from x_t to x_{b^+}.

Next, the relation between $\underset{t\to b^+}{W_c}$ and fuel mass is shown. Assuming pressure follows an isentropic process (3.3); the evaluation of $\underset{t\to b^+}{W_c}$ reveals the relation to added fuel mass m_f as

$$\underset{t\to b^+}{W_c} = \frac{(P_{c_t} + \Delta P_{c_t})\left(V_{c_t}^{\gamma_c} V_{c_{b^+}}^{1-\gamma_c} - V_{c_t}\right)}{1-\gamma_c} \tag{3.9}$$

where it can be shown that

$$\Delta P_{c_t} = \frac{\eta_c Q_{LHV} R_o}{c_v V_{c_t}} m_f \tag{3.10}$$

is the pressure rise at TDC due to combustion of fuel mass m_f. In (3.10), η_c is the proportion of actual fuel burned (the combustion efficiency), Q_{LHV} is the fuel's lower heating value, c_v is the fuel's specific heat at constant volume, and R_o is the specific gas constant.

Let $S(x_t, x_{b^+})$ denote the expansion stroke length from x_t to x_{b^+}, i.e.

$$S(x_t, x_{b^+}) = |x_t - x_{b^+}| \tag{3.11}$$

When a piston travels from x_t to x_{b^+} in an expansion stroke, the energy balance (3.8) relates the piston travel $S(x_t, x_{b^+})$ to the energy supply in terms of added fuel mass m_f and energy extraction (i.e. loading) E_{exp}. Visually, one can imagine the parameter interconnection in Fig. 3.4, which aids the deduction of the following fact:

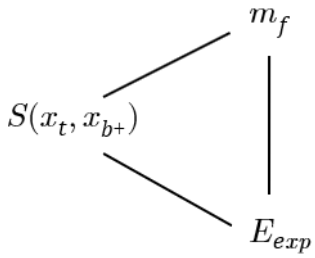

Figure 3.4: Operating point parameter interconnection for the expansion stroke.

Fact 2. *For an expansion stroke $S(x_t, x_{b^+})$ and an energy extraction E_{exp} there exists an associated fuel mass m_f.*

Fact 2 is verified when fuel mass is made the subject of (3.8) and shown to exist for all expansion strokes $S(x_t, x_{b^+}) > 0$. Indeed, using (3.9) and (3.10) in (3.8), it is easy to show that

$$m_f = \frac{c_v V_{c_t}}{\eta_c Q_{LHV} R_o} \left\{ \frac{\left(\underset{t \to b^+}{W_{rd}} + E_{exp} \right)(1 - \gamma_c) - P_{c_t} \left(V_{c_t}^{\gamma_c} V_{c_{b^+}}^{1-\gamma_c} - V_{c_t} \right)}{V_{c_t}^{\gamma_c} V_{c_{b^+}}^{1-\gamma_c} - V_{c_t}} \right\} \tag{3.12}$$

The final step is to check existence of m_f for all $S(x_t, x_{b^+}) > 0$. An expansion stroke $S(x_t, x_{b^+}) > 0$ implies $\underset{t \to b^+}{W_c} > 0$ in (3.9), which further implies in the same equation that the right-hand side term $\left(V_{c_t}^{\gamma_c} V_{c_{b^+}}^{1-\gamma_c} - V_{c_t} \right) \neq 0$. Hence, (3.12) has no singularity, and therefore m_f exists for all $S(x_t, x_{b^+}) > 0$.

3.3.3 Full-Cycle Consideration at Steady State

FPE operating point parameter relationships have been established in both compression stroke (Fact 1, Fig. 3.2) and expansion stroke (Fact 2, Fig. 3.4). The picture is now simply completed for a full cycle involving a compression and an expansion stroke at *steady state*.

At steady state, the start of the compression stroke coincides with the end of the expansion stroke, i.e. $x_b = x_{b^+}$. Hence, the compression stroke matches the expansion stroke. Accordingly, from Fig. 3.2 and Fig. 3.4, a parameter interconnection can be visualized as Fig. 3.5 depicting an operating point in the complete parameter set (k, E_{cmp}, S, m_f, E_{exp}). It is remarked that the energy quantities E_{cmp} and E_{exp} need not be equal for an equal compression and expansion stoke S.

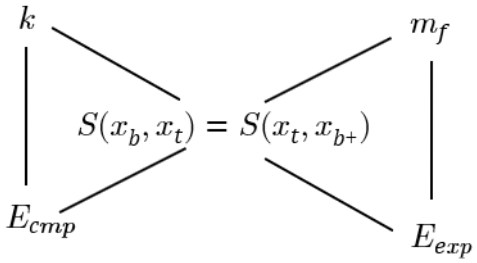

Figure 3.5: Operating point parameter interconnection for a full cycle at steady state.

Having introduced a complete operating point parameter set for a full cycle at steady state, a *nominal* operating point is considered next, and an FPE's stability at such an operating point discussed.

3.4 Stability at a Nominal Operating Point

This section examines FPE stability at a nominal operating point, where a nominal operating point is one at which an FPE is desired to operate at steady state. First, the idea of a nominal operating point is motivated by the need to operate at one

compression ratio. After this motivation, Fact 1 and Fact 2 are combined into one, following which a proposition on FPE stability at the nominal operating point is made. Simulation results are presented to verify this proposition.

3.4.1 Main Developments

In practice, an FPE is typically required to operate at one compression ratio, i.e. the nominal compression ratio—for reasons such as fuel type suitability and requirements on engine efficiency and emissions. A nominal compression ratio r_c^* is related to a nominal stroke S^* according to

$$r_c^* = \frac{\underline{V_c} + A_p S^*}{\underline{V_c}} \tag{3.13}$$

where $\underline{V_c}$ is the cylinder clearance volume and A_p is the piston crown area. Thus, with a nominal compression ratio, a nominal stroke S^* can be calculated from (3.13).

From Fact 1 and Fact 2, the nominal stroke S^* is associated with a nominal stiffness k^*, a nominal converted energy E_{cmp}^*, a nominal fuel mass m_f^* and a nominal converted energy E_{exp}^*. This nominal operating point parameter set (k^*, E_{cmp}^*, S^*, m_f^*, E_{exp}^*) may be visualized by the parameter interconnection in Fig. 3.6.

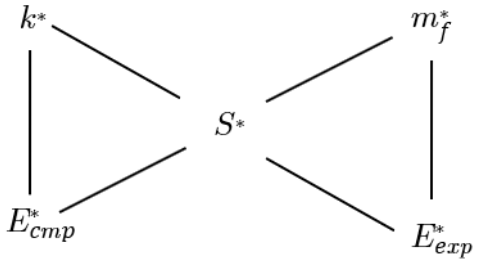

Figure 3.6: Nominal operating point parameter interconnection for a full cycle at steady state.

Recall from generator modelling in (2.15) that a generator force is defined with the generator coefficient μ_g. Accordingly, let μ_g^* denote the nominal generator coefficient

associated with production of the nominal energy quantities E^*_{cmp} and E^*_{exp}. Fact 1 and Fact 2 can now be combined into the following fact pertaining to a nominal operating point:

Fact 3. *Consider an FPE with generator coefficient μ^*_g;*

- *For a compression stroke S^* and an energy extraction E^*_{cmp} there exists an associated rebound device stiffness k^*.*
- *For an expansion stroke S^* and an energy extraction E^*_{exp} there exists an associated fuel mass m^*_f.*

Fact 3 is trivially implied when Fact 1 and Fact 2 are considered at an FPE nominal operating point.

The Fact points to the following key implication: *Regardless* of what the compression or expansion stroke is initially, provided the nominal rebound device stiffness k^*, nominal fuel mass m^*_f, and nominal generator coefficient μ^*_g are in place, then the nominal stroke S^* can always be expected, along with nominal energy extraction E^*_{cmp} and E^*_{exp}. Stated differently, having the nominal rebound device stiffness k^*, nominal fuel mass m^*_f, and nominal generator coefficient μ^*_g in place is *sufficient* to achieve the nominal stroke S^* and nominal energy extraction E^*_{cmp} and E^*_{exp}.

With this key implication in mind, let x_B and x_T respectively denote the nominal BDC and nominal TDC positions associated with nominal stroke S^*, i.e.

$$S^* = |x_B - x_T| \tag{3.14}$$

The following proposition regarding stability of an FPE at a nominal operating point can be made:

Proposition 1 (FPE stability at a nominal operating point). *An FPE beginning a compression stroke at, or other than, the nominal BDC position achieves the nominal stroke S^* and nominal energy extraction E^*_{cmp} and E^*_{exp} in subsequent*

compression and expansion strokes, provided the nominal rebound device stiffness k^*, the nominal fuel mass m_f^* and nominal generator coefficient μ_g^* are in place.

Proposition 1 is verified by studying the three possible cases of proximity to nominal BDC at the start of a compression stroke, i.e. exactly at nominal ($x_b = x_B$), below nominal ($|x_b| < |x_B|$), and above nominal ($|x_b| > |x_B|$). Physical reasoning is used on occasion.

Case I : $x_b = x_B$

This is the trivial case, depicted in Fig. 3.7. The proposition supposes a rebound device stiffness $k = k^*$, a generator coefficient $\mu_g = \mu_g^*$, and a fuel mass $m_f = m_f^*$. According to Fact 3, these conditions imply the compression and expansion stroke S^* and energy extraction E_{cmp}^* and E_{exp}^*. As the stroke S^* has by definition been associated with BDC position x_B in (3.14), it is trivial to conclude that $x_b = x_B$ implies stroke S^* with the energy extraction E_{cmp}^* and E_{exp}^*.

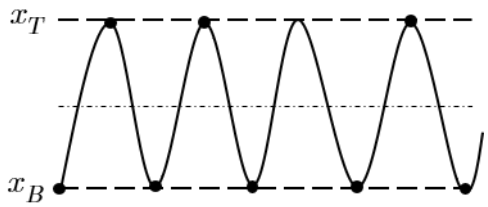

Figure 3.7: Evolution of BDC and TDC with beginning of compression stroke at nominal BDC.

Case II : $|x_b| < |x_B|$

Figure 3.8 is used for reference.

Let $x_b = x_{b_1}$ be the BDC position of the start of a compression stroke with $|x_b| < |x_B|$. The compression stroke to TDC position x_{t_1}, i.e. $S(x_{b_1}, x_{t_1})$, is shorter than the nominal stroke S^* since $|x_b| < |x_B|$.

The following expansion stroke to BDC position x_{b_2}, i.e. $S(x_{t_1}, x_{b_2})$, is longer than its preceding compression stroke $S(x_{b_1}, x_{t_1})$. This is because only with a

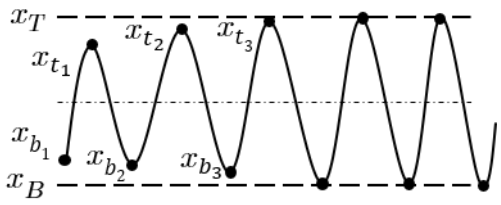

Figure 3.8: Evolution of BDC and TDC with beginning of compression stroke above nominal BDC.

longer expansion stroke (as opposed to an equal or shorter one) can the FPE attain the stroke S^* with energy extraction E^*_{exp} , given that m^*_f and μ^*_g are in place (owing to Fact 3).

Indeed, the proceeding compression stroke to TDC position x_{t_2}, i.e. $S(x_{b_2}, x_{t_2})$, is also longer than its preceding expansion stroke $S(x_{b_1}, x_{t_1})$ because only with a longer expansion stroke (as opposed to an equal or shorter one) can the FPE attain the stroke S^* with energy extraction E^*_{cmp} , given that k^* and μ^*_g are in place.

Subsequently, the stroke S^* as defined in (3.14) is attained, along with nominal energy extraction E^*_{cmp} and E^*_{exp}.

Case III : $|x_b| > |x_B|$

Figure 3.9 is used for reference.

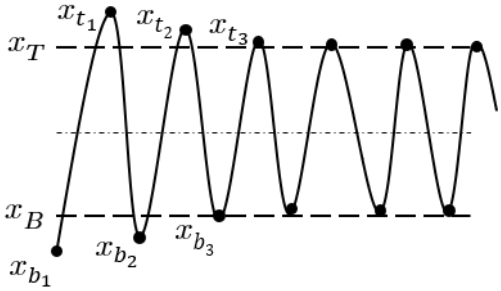

Figure 3.9: Evolution of BDC and TDC with beginning of compression stroke below nominal BDC.

Let $x_b = x_{b_1}$ be the BDC position of the start of a compression stroke with $|x_b| > |x_B|$. The compression stroke to TDC position x_{t_1}, i.e. $S(x_{b_1}, x_{t_1})$, is

longer than the nominal stroke S^* since $|x_b| > |x_B|$.

The following expansion stroke to BDC position x_{b_2}, i.e. $S(x_{t_1}, x_{b_2})$, is shorter than its preceding compression stroke $S(x_{b_1}, x_{t_1})$. This is because only with a shorter expansion stroke (as opposed to an equal or longer one) can the FPE attain the stroke S^* with energy extraction E^*_{exp} , given that m^*_f and μ^*_g are in place (owing to Fact 3).

Indeed, the proceeding compression stroke to TDC position x_{t_2}, i.e. $S(x_{b_2}, x_{t_2})$, is also shorter than its preceding expansion stroke $S(x_{b_1}, x_{t_1})$ because only with a shorter expansion stroke (as opposed to an equal or longer one) can the FPE attain the stroke S^* with energy extraction E^*_{cmp} , given that k^* and μ^*_g are in place.

Subsequently, the stroke S^* as defined in (3.14) is attained, along with nominal energy extraction E^*_{cmp} and E^*_{exp}.

3.4.2 Simulation Testing

A simulation to test Proposition 1 is conducted with an FPE whose rebound device is a mechanical spring. The FPE properties and other simulation parameters are detailed in Table 3.1. Friction is neglected for simplicity. The nominal generator coefficient is set to zero in Table 3.1 to allow direct computation of the nominal rebound device stiffness and nominal fuel mass from (3.7) and from (3.12) respectively. A zero nominal generator coefficient also means zero energy extraction but does not invalidate the simulation test for Proposition 1. Piston responses with three different BDC positions at the start of the first compression stroke are examined.

Figures 3.10a and 3.10b respectively show the time response and phase space response in the trivial case where the beginning of a compression stroke coincides with the nominal BDC position. As expected, the piston oscillations remain at the nominal stroke for all time in Fig. 3.10a. The phase space response is correspondingly a closed

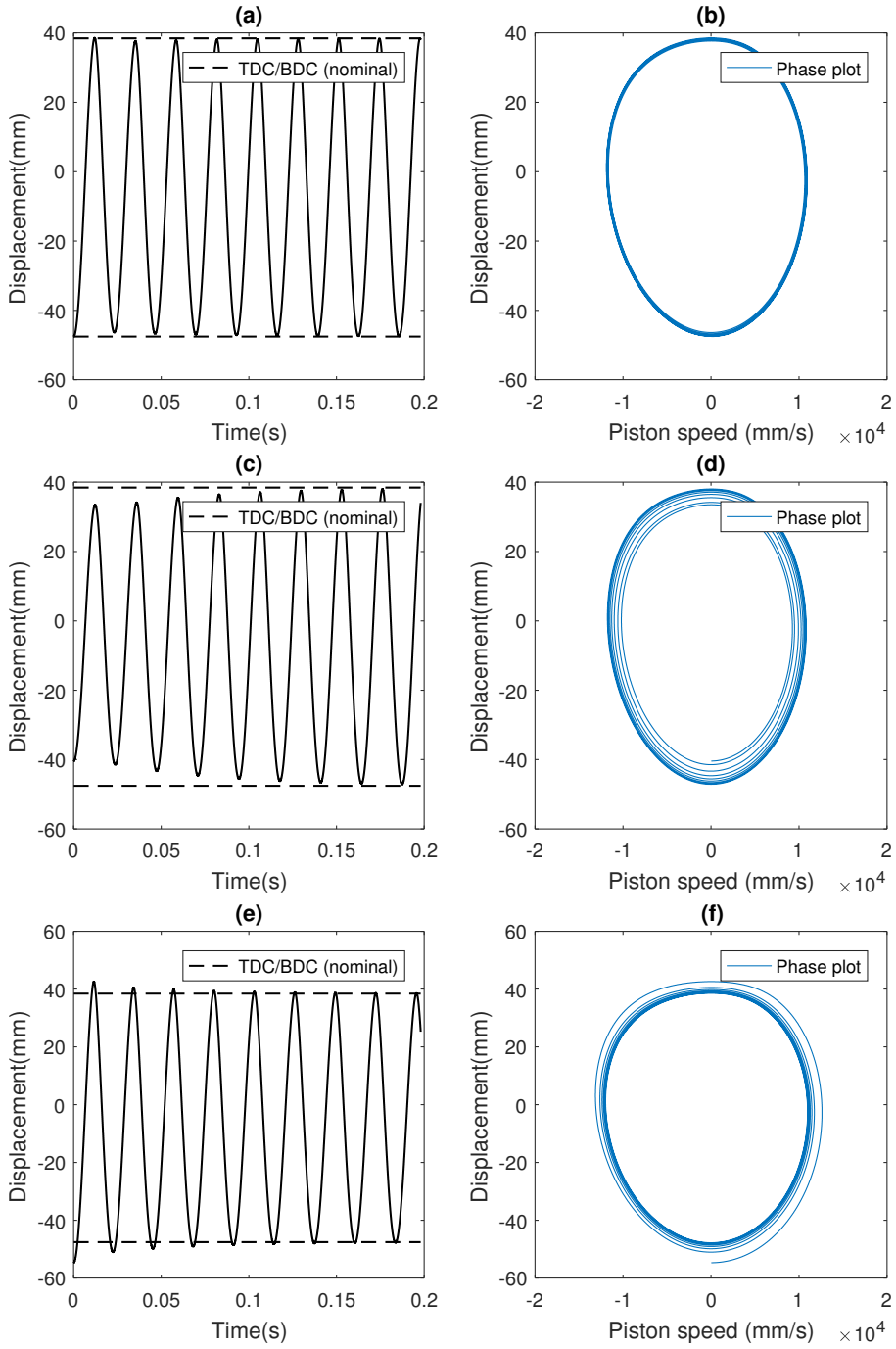

Figure 3.10: Time and phase space responses with three BDC positions at start of compression stroke. Both the compression and expansion strokes subsequently achieve the nominal stroke; and hence a closed orbit in the phase space.

Table 3.1: Simulation Parameters

Parameter	**Value**
Compression ratio (nominal)	10.44
Bore	86 mm
Stroke (nominal)	86 mm
piston-translator mass	9 kg
generator coefficient (nominal)	0 kg/s

orbit in Fig 3.10b.

Figures 3.10c and 3.10d correspond to the case where the beginning of a compression stroke is below the nominal BDC position. Here, it is seen (in Fig. 3.10c) that the piston oscillations move towards the nominal stroke as expected. In Fig. 3.10d, the phase response correspondingly starts inside a closed orbit and moves towards it.

Figures 3.10e and 3.10f correspond to the converse case where the beginning of a compression stroke is above the nominal BDC position. It is seen in Fig. 3.10e that the piston oscillations move towards the nominal stroke as expected. In Fig. 3.10f, the phase response correspondingly starts outside a closed orbit and moves inside it.

3.5 Perturbations to the Nominal Operating Point

The stability of an FPE at a nominal operating point has been stated in Proposition 1. The proposition stated what happens to piston oscillations when they start at, or away from, the nominal stroke (under conditions of nominal rebound device stiffness and nominal fuel added). Indeed, the proposition is very much a statement of what happens to piston oscillations when the nominal stroke is perturbed. By contrast, this section investigates what happens to piston oscillations when the nominal fuel added and rebound device stiffness are perturbed. Note that it is not necessary to separately examine perturbation of the energy extraction (i.e. the load) as this is

equivalent to perturbing either of the former parameters.

3.5.1 Main Developments

The following proposition is made pertaining to FPE stability under perturbation to the nominal operating point.

Proposition 2 (FPE stability under perturbation to a nominal operating point). *Consider an FPE with nominal generator coefficient μ_g^* operating at its nominal operating point (k^*, E_{cmp}^*, S^*, E_{exp}^*, m_f^*).*

- *A perturbation δm_f such that $m_f = m_f^* + \delta m_f$ causes the FPE to transition to a new operating point.*
- *A perturbation δk such that $k = k^* + \delta k$ causes the FPE to transition to a new operating point.*

Proposition 2 is verified as follows. By definition, there is only one nominal operating point parameter set $(k^*, E_{cmp}^*, S^*, m_f^*, E_{exp}^*)$. Using Fact 1 and Fact 2, a change (i.e. perturbation) to k^* and m_f^* implies new parameter associations with the perturbed k^* and m_f^* that are different from nominal; i.e. a new operating point.

It is then natural to ask if an FPE remains stable at the new operating point. The answer to this question lies with the fundamental question of whether the new operating point is physically viable for normal engine operation or not. To illustrate this point, consider an FPE running at a nominal operating point. Now consider a perturbation as a complete cut off of the fuel, i.e. $\delta m_f = -m_f$, such that $m_f = 0$. Since no energy is being added to the FPE system while energy is being extracted, the new FPE operating point becomes the zero piston position; i.e. engine stall, which is defined as instability in Definition 1. Whereas this has been an extreme case, it is not difficult to imagine that excessively large deviations from nominal can lead to new operating points where an FPE may have poor gas exchange (poor scavenging),

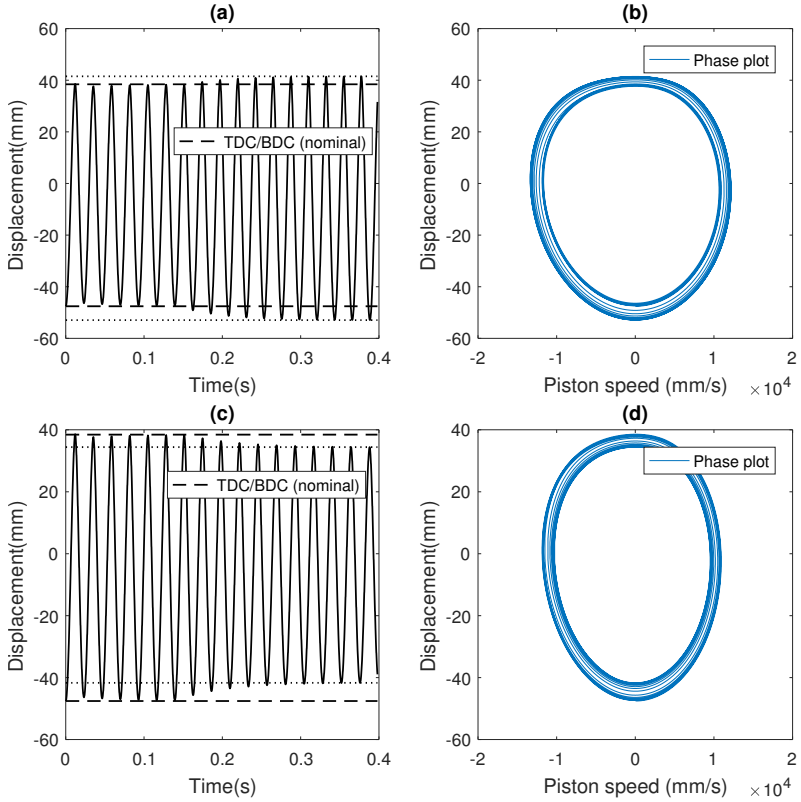

Figure 3.11: Time and phase space response under perturbation of added fuel mass from nominal by ±15%. The FPE finds a new operating point.

poor gas compression, and so on, potentially resulting in FPE instability.

3.5.2 Simulation Testing

A simulation to test Proposition 2 is now conducted with an FPE whose rebound device is a mechanical spring. Again, the simulation parameters are as in Table 3.1. Piston responses are captured following perturbations on added fuel and rebound device stiffness.

Figures 3.11a and 3.11c show the piston responses when the added fuel is perturbed from nominal by +15% and −15% respectively at approximately 0.15 seconds. As expected, the FPE finds a new operating point as evidenced by the new piston oscillation amplitude. Correspondingly Figures 3.11b and 3.11d show two closed orbits,

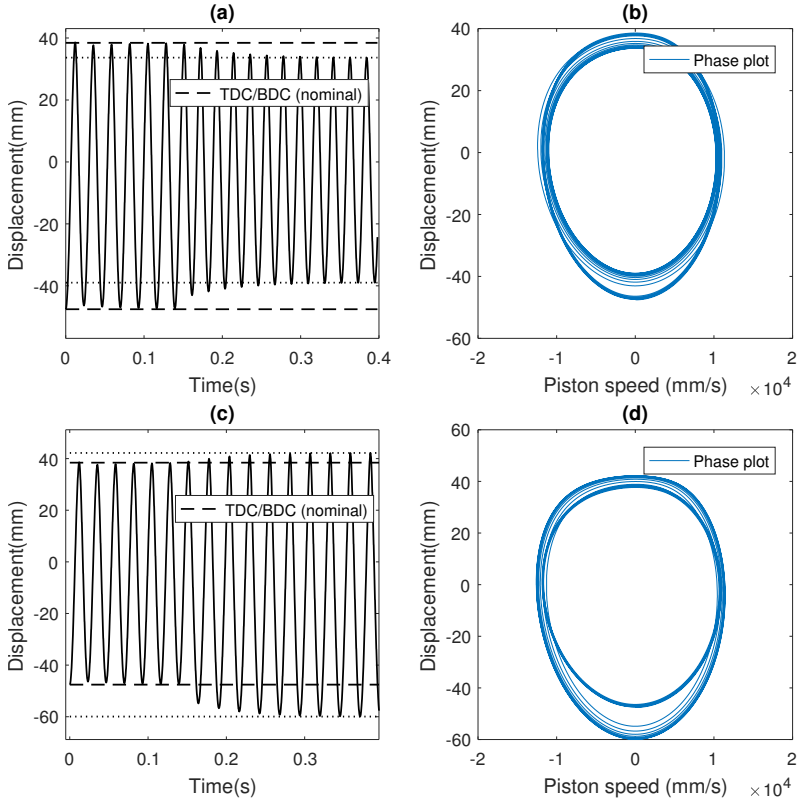

Figure 3.12: Time and phase space response under perturbation of rebound device stiffness from nominal by ±15%. The FPE finds a new operating point.

corresponding to an old and new operating point. If the newly-found operating point is physically viable, the oscillations persist (stable). If not, either collision or stall occurs (unstable).

Similarly, Figures 3.12a and 3.12c show the piston responses when the rebound device stiffness is perturbed from nominal +15% and −15% respectively at approximately 0.15 seconds. As expected, the FPE finds a new operating point as evidenced by the new piston oscillation amplitude. Correspondingly Figures 3.12b and 3.12d show two closed orbits, corresponding to an old and new operating point. If the newly-found operating point is physically viable, the oscillations persist (stable). If not, either stall or collision occurs (unstable).

3.6 Remarks on Stability in Open Loop Vs Closed Loop

Proposition 1 has put forward conditions at which a nominal stroke and associated nominal energy extraction are achieved. Proposition 2 has conversely put forward conditions at which a nominal stroke and associated nominal energy extraction are lost. In these propositions, there have been three key influencing parameters, namely: the added fuel mass, the rebound device stiffness, and generator coefficient. These three parameters therefore form what can be termed as *control variables* of an FPE. Throughout this chapter, these control variables have been calculated beforehand and fixed. Accordingly, FPE stability has been analyzed in "open loop".

However, it is possible to dynamically manipulate these control variables based on feedback information on the state of the piston. For instance, piston position and speed could be used to actively manipulate the control variables in order to achieve a desired stroke—say, the nominal stroke. Here, the FPE is said to operate in "closed loop". Various feedback *control design* approaches are available to the engineer as seen in Chapter 4, where stability is discussed in closed loop.

3.7 Chapter Conclusions

Starting with the energy conservation principle, a framework for understanding stability of FPE piston motion has been developed. The framework includes definitions of stability and technical facts and propositions that relate key physical FPE parameters. The key developments in this chapter have been the conditions under which a nominal piston stroke is achieved, in Proposition 1, and conditions under which it is lost, in Proposition 2. These two Propositions broadly explain FPE stability.

Chapter 4

Control of Compression Ratio

4.1 Introduction

Free-piston engines (FPEs) are typically designed to operate at one nominal compression ratio. Operating too far below this compression ratio may result in unacceptably low thermal efficiencies or misfire. Operating too far above the nominal compression ratio may result in engine knock or compromise the mechanical integrity of the device. Accordingly, this chapter applies control theory in developing feedback strategies for control of FPE compression ratio. The feedback control strategies are designed with newly-developed FPE control-oriented models that are derived from further exploitation of the energy conservation principle.

For clarity, it is immediately remarked that control of compression ratio is equivalent to control of piston stroke, which in turn is equivalent to control of BDC and TDC positions. This three-way equivalence is easily seen from the definition of compression ratio r_c, i.e.

$$r_c(S) = \frac{\underline{V_c} + A_p S}{\underline{V_c}} \tag{4.1}$$

where S is the stroke, A_p is the piston crown area, and $\underline{V_c}$ is the clearance cylinder

volume. The stroke S is related to BDC position x_b and TDC position x_t as

$$S(x_b, x_t) = |x_t - x_b| \tag{4.2}$$

Thus, it is seen in (4.2) that by controlling BDC position x_b and TDC position x_t, the stroke $S(x_b, x_t)$ is controlled. Subsequently, the compression ratio r_c in (4.1) is controlled.

Recalling that piston motion in an FPE is governed entirely by dynamic force interaction—i.e. there are no kinematic constraints imposed by a slider-crank to predetermine a piston motion profile—*active* piston motion control is necessary for stable and repeatable engine cycles. As the piston dead-center positions (BDC and TDC) are free to vary cycle-by-cycle, accurate control of the dead-centre positions is not only essential for ensuring a sufficient compression ratio needed for combustion, but also for ensuring a sufficient clearance to avoid piston collision at the extremities of a stroke. Thus, it can be said that the most important control problem for FPEs is the control of BDC and TDC, and therefore accordingly, the control of compression ratio.

Although a number of prototype FPEs have been developed [77, 102, 2], no studies have adopted a fully analytical model-based approach to piston BDC/TDC control in a general way so as to include various FPE configurations and types. Reported control approaches have largely considered the engine as a "black box"—the shortcoming being that there is no real justification for the strategic basis adopted and no corresponding stability assessment.

In TDC and BDC control, usually two separate control loops are involved. One control loop achieves BDC control by regulating the fuel supply, whereas the second achieves TDC control by regulating the energy stored in the rebound device, consequently regulating the rebound device stiffness. Tikkanen and Vilenius [101] are early

proponents of a similar energy-based approach, highlighting the difficulty of achieving reliable piston motion control in practice. They propose analytically guided control of TDC and BDC using total energy flows, thereby controlling compression ratio, while using a combination of fuel and piston load regulation strategies—a potentially useful approach, although is left untested. By contrast, Johansen et al. [56, 57] derive a detailed dynamic model of a diesel FPE. Their control-oriented analysis reveals that TDC control can be achieved by varying rebound stiffness, whereas BDC control can be achieved by the regulation of injected fuel per cycle. They implement PI and PID controllers. Similarly, Mikalsen and Roskilly [78, 76] implement separate TDC and BDC control strategies in their simulations of both spark ignition (SI) and compression ignition (CI) FPEs. They propose TDC control by regulating rebound stiffness per cycle and BDC control by fuel regulation. Mikalsen and Roskilly [80] also identify the main difficulty of FPE control as being able to achieve sufficient compression ratio across what they call the entire load range. This difficulty is further addressed in [81], with PID and other approaches examined in [52].

This chapter sets out to develop and achieve a general, model-based, analytical approach to BDC and TDC control of a two-stroke FPE. In direct contrast to this work are non-model-based attempts to control BDC and TDC, where engineering insight into the control problem is achieved through trial and error—a potentially problematic approach, prone to unanticipated engine responses. The proposed model-based approach has two important benefits:

- In controller parameter selection: A range of viable parameters to warrant stable BDC and TDC can be computed prior to controller testing on hardware.
- In availing a basis for advanced control design: A framework for advanced control design is established, with the possibility of enforcing more stringent objectives other than stability; for example, requirements on optimality, robustness, or constraint enforcement.

In the analysis presented here, energy conservation is exploited to derive control-oriented BDC and TDC dynamic models. These models are subsequently used to obtain a formal FPE stability condition in terms of the parameters of the widely adopted PI controller. Furthermore, how the models can be used to develop advanced control strategies such as linear quadratic regulation (LQR) for optimality is demonstrated. This chapter involves detailed extensions to the work of Gong et al. [39] and Zaseck et al. [113], where model-based control for TDC is developed for a specific FPE configuration. A further step is taken in this chapter to unify the approach into four common FPE configuration cases.

4.2 Control-Oriented Engine Models

The FPE model introduced in Section 2.3 describes continuous time dynamics of the piston throughout a cycle, including the intermittent combustion and scavenging events. Noting that the piston only arrives at BDC and TDC once every cycle, this section develops models that capture the discrete time dynamics from one dead-centre position to another, starting with the energy conservation principle. The models developed form control-oriented models to be used in designing feedback controllers for the control of BDC and TDC. As before, the subscripts b and t will respectively denote BDC and TDC. A generic FPE generator schematic with the said notation is shown in Fig. 4.1 for convenience.

4.2.1 A BDC Control-Oriented Energy Balance Model

A BDC control-oriented energy balance model is developed starting with simplifying assumptions and definitions associated with the cycle of an FPE as follows:

- A new cycle commences at the start of the compression stroke at piston position

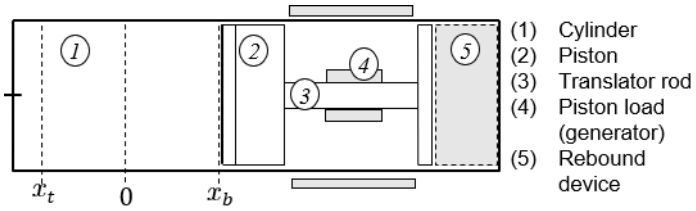

Figure 4.1: Generic FPE schematic. The piston, translator, and generator permanent magnet constitute the moving mass. The rebound device may be a mechanical spring, an air bounce chamber or another cylinder. 1—Cylinder, 2—piston, 3—translator rod, 4—piston load (generator), and 5—rebound device.

x_b.

- The end of the compression stroke occurs at piston position x_t.
- The start of the expansion stroke occurs at piston position x_t.
- The end of the expansion stroke occurs at piston position x_{b^+}.

These simplifying assumptions and definitions allow two energy balance relations to be constructed. The first is a compression stroke energy balance statement as follows:

$$\underset{b\to t}{W_{rd}} = \underset{b\to t}{W_c} + E_{cmp} \tag{4.3}$$

where $\underset{b\to t}{W_{rd}}$ is the work done by the rebound device in driving the piston from x_b to x_t, $\underset{b\to t}{W_c}$ is the work done on the cylinder gas when the piston moves from x_b to x_t, and E_{cmp} is the energy converted by piston motion into useful output energy and into the energy lost as friction when the piston moves from x_b to x_t. The second energy balance relation is an expansion stroke statement

$$\underset{t\to b^+}{W_c} = \underset{t\to b^+}{W_{rd}} + E_{exp} \tag{4.4}$$

where $\underset{t\to b^+}{W_c}$ is the work done by the cylinder gas in driving the piston from x_t to x_{b^+}, $\underset{t\to b^+}{W_{rd}}$ is the work done on the rebound device when the piston moves from x_t to x_{b^+}, and E_{exp} is the energy converted by piston motion into useful output energy and into

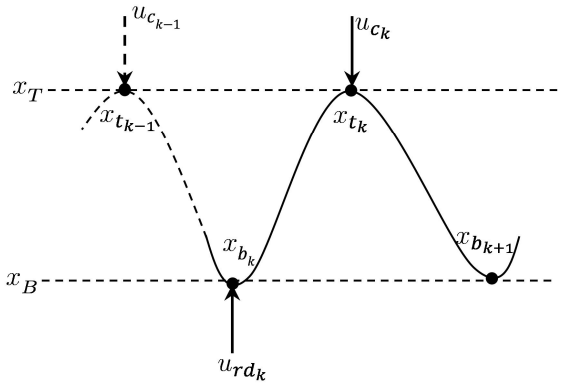

Figure 4.2: Visualization of piston motion over time. One complete cycle is from x_{b_k} to $x_{b_{k+1}}$.

the energy lost as friction when the piston moves from x_t to x_{b^+}.

Addition of the energy balance equation (4.3) and Equation (4.4) gives the full cycle energy balance

$$\left(\underset{b\to t}{W_{rd}} - \underset{t\to b^+}{W_{rd}}\right) + \left(\underset{t\to b^+}{W_c} - \underset{b\to t}{W_c}\right) - (E_{cmp} + E_{exp}) = 0 \tag{4.5}$$

Equation (4.5) can be used to predict x_{b^+} when x_t and x_b are known. A visual description of the piston motion in one cycle is given in Fig. 4.2 (it shows the motion from one trough to the next, as a solid line). Index $k = 1, 2, 3, \ldots$ is used to denote the cycle count of the piston end points, where x_T and x_B are the nominal end points, and u_c is the fuel added to the cylinder for a given cycle. The input variable u_{rd} varies once every cycle to adjust the stiffness of the rebound device. In a bounce chamber, for example, u_{rd} is the trapped air mass which when varied once in a cycle adjusts the bounce chamber's stiffness on a cycle-by-cycle basis. Control variable u_{rd} has no relevance for a mechanical spring.

In general, assuming isentropic compression and expansion processes, the first two parenthesized terms of Equation (4.5) can be expressed in terms of the piston endpoint variables ($x_{b_{k+1}}$, x_{t_k}, x_{b_k}, $x_{t_{k-1}}$) and the input variables (u_{c_k}, u_{rd_k})—this generality is

later demonstrated in the development of three numerical case studies in Section 4.4 using the same six variables. Furthermore, the last parenthesized term of (4.5) which represents the total energy converted in a cycle is assumed to be approximated by a polynomial function of the piston endpoints, where, for small load changes, the total energy converted is approximately constant. Equation (4.5) may alternatively be expressed as an implicit nonlinear function in the form

$$f_1(x_{b_{k+1}}, x_{t_k}, x_{b_k}, x_{t_{k-1}}, u_{c_k}, u_{rd_k}) = 0 \tag{4.6}$$

By defining a nominal point for the variables of interest, i.e.,

$$\underline{\theta} = (x_B, x_T, u_C, u_{RD}) \tag{4.7}$$

where u_C and u_{RD} respectively depict the cylinder and rebound device inputs required to send the piston from x_T to x_B and x_B to x_T, the associated error variables from nominal $\underline{\theta}$ are accordingly defined as

$$\delta x_b = x_b - x_B \tag{4.8a}$$

$$\delta x_t = x_t - x_T \tag{4.8b}$$

$$\delta u_c = u_c - u_C \tag{4.8c}$$

$$\delta u_{rd} = u_{rd} - u_{RD} \tag{4.8d}$$

Equation (4.6), when expanded in the form of a Taylor series about the point $\underline{\theta}$, can can be used to generate the following predictive equation:

$$\delta x_{b_{k+1}} = a_1 \delta x_{b_k} + b_1 \delta u_{c_k} + \xi_{1_k} \tag{4.9}$$

where

$$\xi_{1_k} = c_1 \delta x_{t_k} + d_1 \delta x_{t_{k-1}} + e_1 \delta u_{rd_k} + g_1 \tag{4.10}$$

and where

$$a_1 = -\frac{\partial f_1}{\partial x_{bk}} \Bigg/ \left.\frac{\partial f_1}{\partial x_{bk+1}}\right|_{\underline{\theta}} \tag{4.11a}$$

$$b_1 = -\frac{\partial f_1}{\partial u_{ck}} \Bigg/ \left.\frac{\partial f_1}{\partial x_{bk+1}}\right|_{\underline{\theta}} \tag{4.11b}$$

$$c_1 = -\frac{\partial f_1}{\partial x_{tk}} \Bigg/ \left.\frac{\partial f_1}{\partial x_{bk+1}}\right|_{\underline{\theta}} \tag{4.11c}$$

$$d_1 = -\frac{\partial f_1}{\partial x_{tk-1}} \Bigg/ \left.\frac{\partial f_1}{\partial x_{bk+1}}\right|_{\underline{\theta}} \tag{4.11d}$$

$$e_1 = -\frac{\partial f_1}{\partial u_{rdk}} \Bigg/ \left.\frac{\partial f_1}{\partial x_{bk+1}}\right|_{\underline{\theta}} \tag{4.11e}$$

$$g_1 = -f_1 \Bigg/ \left.\frac{\partial f_1}{\partial x_{bk+1}}\right|_{\underline{\theta}} \tag{4.11f}$$

Equation (4.9) is the BDC control-oriented prediction model which describes the deviation from nominal as a discrete time, first order, linear time invariant (LTI) equation with input δu_c, output δx_b, and residual term ξ_1 from the Taylor series expansion procedure, evaluated according to (4.10).

4.2.2 A TDC Control-Oriented Energy Balance Model

The development of a TDC control-oriented energy balance model is similar to the BDC control-oriented model but with different cycle endpoints, namely

- A new cycle starts at the beginning of the expansion stroke at piston position x_t.
- The end of the expansion stroke occurs at piston position x_b.
- The beginning of the compression stroke occurs at piston position x_b.
- The end of the compression stroke occurs at piston position x_{t^+}.

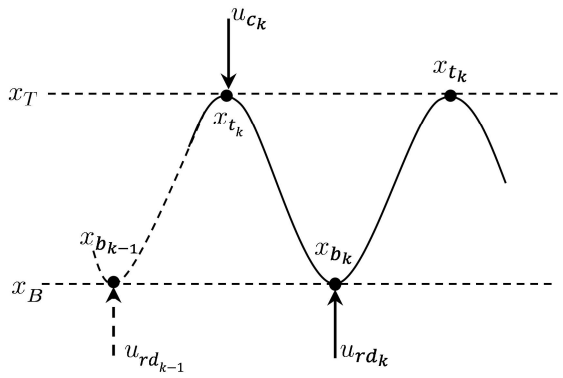

Figure 4.3: Visualization of piston motion over time. One complete cycle is from x_{t_k} to $x_{t_{k+1}}$.

The corresponding expansion and compression stroke energy balance equation, analogous to (4.5), is

$$\left(W_{\substack{rd \\ b\to t^+}} - W_{\substack{rd \\ t\to b}}\right) + \left(W_{\substack{c \\ t\to b}} - W_{\substack{c \\ b\to t^+}}\right) - (E_{exp} + E_{cmp}) = 0 \tag{4.12}$$

Equation (4.12) can be used to predict x_{t^+} when x_b and x_t are known. Visualization making use of Fig. 4.3 helps to picture a full engine cycle (peak-to-peak on the solid line) and associated piston endpoints, where k is the count index. Assuming isentropic compression and expansion, the first two parenthesized terms of (4.12) can be directly expressed in terms of the piston endpoint variables ($x_{t_{k+1}}$, x_{b_k}, x_{t_k}, $x_{b_{k-1}}$) as well as the input variables (u_{rd_k},u_{c_k},$u_{rd_{k-1}}$). The last parenthesized term in (4.12) can be expressed as a polynomial function of the piston endpoint variables, which is nearly constant for small load changes. Similarly, (4.12) may be equivalently expressed as an implicit function

$$f_2\left(x_{t_{k+1}}, x_{b_k}, x_{t_k}, x_{b_{k-1}}, u_{rd_k}, u_{c_k}, u_{rd_{k-1}}\right) = 0 \tag{4.13}$$

which, when expanded as a Taylor series about $\underline{\theta}$ and rearranged, yields the predictive equation

$$\delta x_{t_{k+1}} = a_2 \delta x_{t_k} + b_2 \delta u_{rd_k} + \xi_{2_k} \tag{4.14}$$

where

$$\xi_{2_k} = c_2 \delta x_{b_k} + d_2 \delta x_{b_{k-1}} + e_2 \delta u_{c_k} + g_2 \delta u_{rd_{k-1}} + h_2 \tag{4.15}$$

and where

$$a_2 = -\frac{\partial f_2}{\partial x_{tk}} \Bigg/ \left.\frac{\partial f_2}{\partial x_{tk+1}}\right|_{\underline{\theta}} \tag{4.16a}$$

$$b_2 = -\frac{\partial f_2}{\partial u_{rdk}} \Bigg/ \left.\frac{\partial f_2}{\partial x_{tk+1}}\right|_{\underline{\theta}} \tag{4.16b}$$

$$c_2 = -\frac{\partial f_2}{\partial x_{bk}} \Bigg/ \left.\frac{\partial f_2}{\partial x_{tk+1}}\right|_{\underline{\theta}} \tag{4.16c}$$

$$d_2 = -\frac{\partial f_2}{\partial x_{bk-1}} \Bigg/ \left.\frac{\partial f_2}{\partial x_{tk+1}}\right|_{\underline{\theta}} \tag{4.16d}$$

$$e_2 = -\frac{\partial f_2}{\partial u_{ck}} \Bigg/ \left.\frac{\partial f_2}{\partial x_{tk+1}}\right|_{\underline{\theta}} \tag{4.16e}$$

$$g_2 = -\frac{\partial f_2}{\partial u_{rdk-1}} \Bigg/ \left.\frac{\partial f_2}{\partial x_{tk+1}}\right|_{\underline{\theta}} \tag{4.16f}$$

$$h_2 = -f_2 \Bigg/ \left.\frac{\partial f_2}{\partial x_{tk+1}}\right|_{\underline{\theta}} \tag{4.16g}$$

4.3 Control Design

With BDC and TDC predictive models constructed, the design of feedback control action is possible to satisfy specific control objectives. Equations (4.9) and (4.14) (when suffixes 1,2, b and t are omitted) are of the same general form

$$\delta x_{k+1} = a \delta x_k + b \delta u_k + \xi_k \tag{4.17}$$

and can, therefore, be treated alike in subsequent analysis. The control objective is to design control action δu to stabilize the output, i.e., to drive δx to zero as $k \to \infty$. But for convenience, (4.17) can be simplified further, and by doing so, allows simplification of the subsequent analysis. Consider an equivalent input ν defined as

$$\nu_k = b\delta u_k + \xi_k \tag{4.18}$$

which allows (4.17) to be rewritten as

$$\delta x_{k+1} = a\delta x_k + \nu_k \tag{4.19}$$

The control objective now becomes the design of an equivalent input ν that drives the output δx_{k+1} to zero as $k \to \infty$. Note that when the equivalent control ν is designed for (4.19), it is ultimately implemented for (4.17) as

$$\delta u_k = \frac{1}{b}\left(\nu_k - \xi_k\right) \tag{4.20}$$

as per the relation between ν and δu in (4.18).

4.3.1 Proportional-Integral Control Design

Proportional-Integral (PI) control, which is well-suited to low-order linear systems, has been shown to provide effective control in simulation and experimental work on FPEs [77, 102, 78, 76]. Since (4.19) represents a first-order linear system, PI control is appropriate for BDC and TDC control of FPEs. Moreover, an associated stability condition can be derived. The input-output transfer function for (4.19) is found as

$$G(z) = \frac{z^{-1}}{1 - az^{-1}} \tag{4.21}$$

where z is the unit delay operator. For a reference value $r = 0$, the feedback error is defined as

$$e_k = r - \delta x_k \tag{4.22}$$

Defining the integral of the feedback error as $I_k = e_{k-1} + I_{k-1}$, a PI controller is realized as

$$\nu_k = k_p e_k + k_i I_k \tag{4.23}$$

where $k_p > 0$ and $k_i > 0$. The transfer function of (4.23), i.e. the feedback error to control input, is given as

$$C(z) = \frac{k_p + (k_i - k_p)z^{-1}}{1 - z^{-1}} \tag{4.24}$$

The plant model (4.21) and controller (4.24) are in a closed negative feedback loop, whose transfer function relates the reference input to the output, and has the well-known form

$$G_{CL}(z) = \frac{CG}{1 + CG} \tag{4.25}$$

with two poles p_1 and p_2 being evaluated as

$$p_1 = \frac{-\beta + \sqrt{\beta^2 - 4\alpha\gamma}}{2\alpha} \tag{4.26a}$$

$$p_2 = \frac{-\beta - \sqrt{\beta^2 - 4\alpha\gamma}}{2\alpha} \tag{4.26b}$$

where

$$\alpha = 1 \tag{4.27a}$$

$$\beta = k_p - a - 1 \tag{4.27b}$$

$$\gamma = k_i - k_p + a \tag{4.27c}$$

in terms of the parameters k_p and k_i. For stability of this closed-loop system, the poles p_1 and p_2 must lie within the unit circle to imply that the output δx decays to

zero as time goes to infinity. Another way to express this statement is

$$|p_1 p_2| < 1 \tag{4.28}$$

which manifests as the closed-form stability condition for PI control in terms of parameters k_p and k_i. In simple terms, for a given value of k_p, the integral gain k_i must be chosen to satisfy (4.28). Indeed, a useful map showing regions of stable and unstable parameter combinations can easily be generated, as is shown in Fig. 4.4.

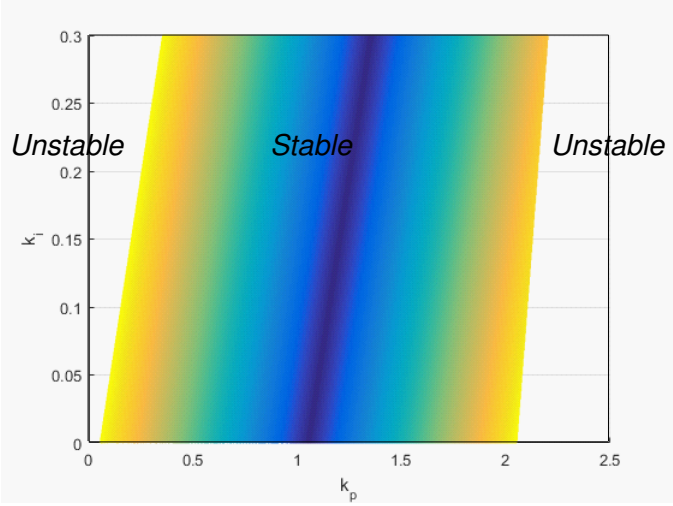

Figure 4.4: PI controller parameter combinations k_p, k_i and associated regions of stability and instability, where $a = 1.05$ in system (4.19). The specific value of a is obtained from Case I in Sec. 4.4.1, with FPE parameters in Table 4.1. The blue region corresponds to high robustness, i.e. when the left-hand side of (4.28) is furthest from 1.

4.3.2 Advanced Control Design

Other requirements on control action—other than system stability and system output decay to zero—may be imposed. Such requirements may include optimality, robustness, or even constraint enforcement by the control action, typically designed with advanced control design techniques. For example, Gong et al. [39] and Zaseck et al. [113] implement constraint enforcement on piston motion with model predictive

control. Li et al. [70] implement robust control action with a technique the authors call robust repetitive control, which is applied to achieve piston trajectory tracking and therefore also the desired compression ratio.

Here, optimality of the control action (relating to minimization of a mathematically defined performance index) is considered, i.e., achieving an optimal fuel supply or optimal regulation of the rebound device stiffness. Linear quadratic regulation (LQR) via a state space control design formalism is pursued for illustrative purposes.

State Equations. The first step is to develop the state equations to which LQR will be applied. For improved controller performance, it is not uncommon to apply integral action to the system output. Let υ be the integral of the output to system (4.19) as follows

$$\upsilon_{k+1} = \delta x_k + \upsilon_k \tag{4.29}$$

By constructing the state vector $w = [\ \delta x \quad \upsilon\ ]^T$, both (4.19) and (4.29) can then be directly expressed in state space form as

$$w_{k+1} = Aw_k + B\nu_k \tag{4.30}$$

where

$$A = \begin{bmatrix} a & 0 \\ 1 & 1 \end{bmatrix} \tag{4.31a}$$

$$B = \begin{bmatrix} 1 \\ 0 \end{bmatrix} \tag{4.31b}$$

LQR Solution. Detailed development of LQR has been treated by Anderson and Moore [6]. Here, it is the final solution to the discrete time LQR problem which is provided, since the choice of LQR over other control design methodologies has been for illustrative purposes only. The control objective is to find a control v of the

discrete time plant (4.30) which minimises the performance index

$$J = \sum_{k=0}^{\infty} \left(w_k^T Q w_k + u_k^T R u_k \right) \tag{4.32}$$

where Q and R in (4.32) are, respectively, positive semidefinite and positive definite. It is assumed that pair $[A, B]$ is controllable.

The LQR control is found as

$$\nu_k = -K w_k \tag{4.33}$$

with

$$K = \left(B^T P B + R \right)^{-1} B^T P A \tag{4.34}$$

where P is a positive definite matrix that is a solution to the so-called discrete algebraic Riccati equation

$$Q + A^T P A - P - A^T P B \left(B^T P B + R \right)^{-1} B^T P A = 0 \tag{4.35}$$

The LQR solution as stated in (4.33)–(4.35) is taken from Goodwin, Graebe, and Salgado [40] where it is developed.

4.4 FPE Case Studies

The generic modelling and control design developed in Sections 4.2 and 4.3 will now be tailored to specific FPE configuration cases—all physically dissimilar, but with conceptually identical configurations. Detailed development for each particular case will precede the test simulation results. Two cases of FPEs, differing only by rebound device type, namely the case of a mechanical spring and the case of a bounce chamber, are first studied. In these studies, Figs. 4.2 and 4.3 will be used for reference purposes.

Examination will then follow for two other common FPE cases, with one involving two opposed pistons in the same cylinder.

4.4.1 Case I: Mechanical Spring as Rebound Device

In this configuration, the FPE rebound device is simply a mechanical spring [9, 41, 28, 7]. As the spring stiffness is fixed, the only control variable available for BDC control is fuel supply. Whereas the objective of BDC control is to ensure the piston is driven to nominal BDC, it is possible to compute the spring stiffness needed to send the piston from nominal BDC to nominal TDC.

4.4.1.1 Detailed Development of the Control-Oriented Model for BDC Control

The first task is to construct the specific form of (4.5). If the spring stiffness is denoted by k_s, the first parenthesized term in (4.5) becomes

$$\underset{b\to t}{W_{rd}} - \underset{t\to b^+}{W_{rd}} = \left\{\frac{1}{2}k_s\left(x_{b_k}^2 - x_{t_k}^2\right)\right\} - \left\{-\frac{1}{2}k_s\left(x_{t_k}^2 - x_{b_{k+1}}^2\right)\right\} \tag{4.36}$$

which, as expected, is a function only of the piston endpoints. Pressure varies with volume in an isentropic process according to

$$PV^{\gamma} = \begin{cases} \text{constant 1}; & \text{compression stroke} \\ \text{constant 2}; & \text{expansion stroke} \end{cases} \tag{4.37}$$

where γ is the heat capacity ratio of the working gas. Therefore, from the isentropic work done, the second parenthesized term is

$$\underset{t\to b^+}{W_c} - \underset{b\to t}{W_c} = \left\{\frac{P_{c_{b^+}}V_{c_{b^+}} - \left(P_{c_t} + \Delta P_{c_t}\right)V_{c_t}}{1-\gamma_c}\right\} - \left\{-\frac{P_{c_t}V_{c_t} - P_{c_b}V_{c_b}}{1-\gamma_c}\right\} \tag{4.38}$$

where P_c is in general the cylinder gas pressure, ΔP_c is the pressure rise at constant volume, V_c is the cylinder volume, and P_{c_b} is the air intake pressure during scavenging (which must be known). Using (4.37) in (4.38) allows elimination of $P_{c_{b^+}}$ in (4.38) to yield

$$\underset{t\to b^+}{W_c} - \underset{b\to t}{W_c} = \left\{ \frac{(P_{c_t} + \Delta P_{c_t})\left(V_{c_t}^{\gamma_c} V_{c_{b^+}}^{1-\gamma_c} - V_{c_t}\right)}{1-\gamma_c} \right\} - \left\{ -\frac{P_{c_b}\left(V_{c_b}^{\gamma_c} V_{c_t}^{1-\gamma_c} - V_{c_b}\right)}{1-\gamma_c} \right\} \quad (4.39)$$

where the pressure P_{c_t} can be evaluated from (4.37) as

$$P_{c_t} = P_{c_b}\left(\frac{V_{c_b}}{V_{c_t}}\right)^{\gamma_c} \quad (4.40)$$

Turning to the combustion pressure rise term ΔP_{c_t}, if the total amount of fuel burned at constant volume V_{c_t} is u_c, then the corresponding pressure rise is given by

$$\Delta P_{c_t} = \frac{\eta_c Q_{LHV} R_o}{c_v}\left(\frac{1}{V_{c_t}}\right) u_{c_t} \quad (4.41)$$

where η_c is the combustion efficiency, u_{c_t} is the fuel mass input for a given cycle, Q_{LHV} is the fuel lower heating value, R_o is the specific gas constant, and c_v is the specific heat capacity at constant volume.

Thus, using (4.40), and (4.41), equation (4.39) can be expressed as a function of cylinder volume and fuel input only. Since the cylinder volume depends on piston position, equation (4.39) therefore depends only on the piston end points and the fuel mass input. The third term of (4.5) as stated earlier, can, under low load changes, be approximated as a constant, i.e.,

$$E_{cmp} + E_{exp} = \{E_1\} + \{E_2\} \quad (4.42)$$

where E_1 and E_2 are constants. The sum of (4.36), (4.39), and (4.42) forms a nonlinear

equation of the form

$$f_1\left(x_{b_{k+1}}, x_{t_k}, x_{b_k}, u_{c_k}\right) = 0 \tag{4.43}$$

as shown by (4.6). A Taylor series expansion of (4.43) will generate the particular form of the BDC control-oriented model for (4.9)—the subsequent controller follows directly from the steps described in Section 4.3.

4.4.1.2 Assignment of the Spring Stiffness

The energy required by the piston to move from nominal BDC to nominal TDC during the compression stroke is supplied entirely by the rebound device—in this case, a mechanical spring. An appropriate choice of the spring stiffness ensures that the piston moving from nominal BDC precisely reaches nominal TDC. This is achieved using the compression stroke energy balance equation (4.3) evaluated at nominal piston endpoints. The spring stiffness is

$$k_s = \frac{2P_{c_b}V_{c_b}^{\gamma_c}V_{c_t}^{1-\gamma_c}\left(1 - r_c^{1-\gamma_c}\right) + 2\left(\gamma_c - 1\right)E_1}{\left(\gamma_c - 1\right)\left(x_B^2 - x_T^2\right)} \tag{4.44}$$

where $r_c = V_{c_b}/V_{c_t}$ is the nominal compression ratio, x_B and x_T are the nominal BDC and nominal TDC piston displacement positions, respectively.

To make the spring stiffness computation with (4.44) exact, the electrical generator can be turned-off during the compression stroke, therefore, rendering E_1 equal to zero. The nominal piston endpoints x_B and x_T are known, or easily calculated from the required compression ratio.

4.4.1.3 TDC Estimation

Implementation of the control action in (4.20) for BDC control requires BDC feedback (as δx_{b_k} in ν_k) and feedback of the immediately following TDC position (as δx_{t_k} in

ξ_k). Whereas the BDC feedback can be made available by a sensor, the immediately following TDC position must be estimated when the piston is at the BDC position. This can be done as follows: in Fig. 4.1, let l be the length from the left end of the cylinder to centreline $x_0 = 0$. Considering the direction to the left of centerline $x_0 = 0$ as positive and to the right of centerline as negative, then the instantaneous in-cylinder volume for a piston crown of area A_p is given as

$$V_c = A_p \left(l - x_0\right) \tag{4.45}$$

Hence, using (4.45), a TDC estimate is given as

$$\hat{x}_t = l - \frac{\hat{V}_{c_t}}{A_p} \tag{4.46}$$

where $\hat{V}_{c_t}$ is an estimate of the cylinder volume at the estimated TDC position $\hat{x}_t$.

Using the compression stroke energy balance equation (3.1), an algebraic equation can be constructed for $\hat{V}_{c_t}$ as follows

$$\lambda_3 \hat{V}_{c_t}^2 + \lambda_2 \hat{V}_{c_t} + \lambda_1 V_{c_t}^{1-\gamma_c} + \lambda_0 = 0 \tag{4.47}$$

where the coefficients are

$$\lambda_0 = P_{c_b} V_{c_b}^{\gamma_c} + (1 - \gamma_c) \left(E_1 + E_2 + \frac{1}{2} k_s \left(l^2 - x_b^2\right)\right) \tag{4.48a}$$

$$\lambda_1 = -P_{c_b} V_{c_b}^{\gamma_c} \tag{4.48b}$$

$$\lambda_2 = -\frac{1}{A_p} k_s l (1 - \gamma_c) \tag{4.48c}$$

$$\lambda_3 = \frac{1}{2A_p^2} k_s \left(1 - \gamma_c\right) \tag{4.48d}$$

Equation (4.47) can be solved numerically, for example, with Newton's method, and used in (4.46) to compute the TDC estimate. The iterations can be expected to

converge quickly given that an initial solution guess (for example nominal TDC) is not far from the true TDC solution in a transient. In the simulation results, the number of iterations to find a solution was never greater than five.

4.4.1.4 Simulation Results and Discussion

Testing the control of BDC and TDC (and therefore control of compression ratio) for the case of a mechanical spring as a rebound device can now proceed. The FPE

Table 4.1: Simulation Parameters

Parameter	**Value**
Compression ratio (nominal)	10.44
Bore	86 mm
Stroke (nominal)	86 mm
piston-translator mass	9 kg
generator coefficient (nominal)	418.5 kg/s
spring stiffness	510.8 kN/m
bounce chamber compression ratio (nominal)	10

geometry is taken from Table 4.1, with the PI controller parameters k_p and k_i selected from the stability map in Fig. 4.4, and the LQR weighting parameters Q and R selected as positive definite. It should be emphasized that only model-based control, such as developed, allows the confident selection of the controller parameters, i.e., from a predetermined set. The alternative is non-model-based control, which relies on a trial and error approach to obtain meaningful engineering insight.

Figure 4.5 shows the piston error at BDC and TDC for both PI and LQR control, having started with an offset and going to zero after a relatively small number of cycles. Hence, the nominal compression ratio is achieved. The piston error at BDC and TDC is expressed as the percentage

$$\frac{\text{Deviation from nominal BDC/TDC}}{\text{Nominal BDC/TDC}} \times 100 \tag{4.49}$$

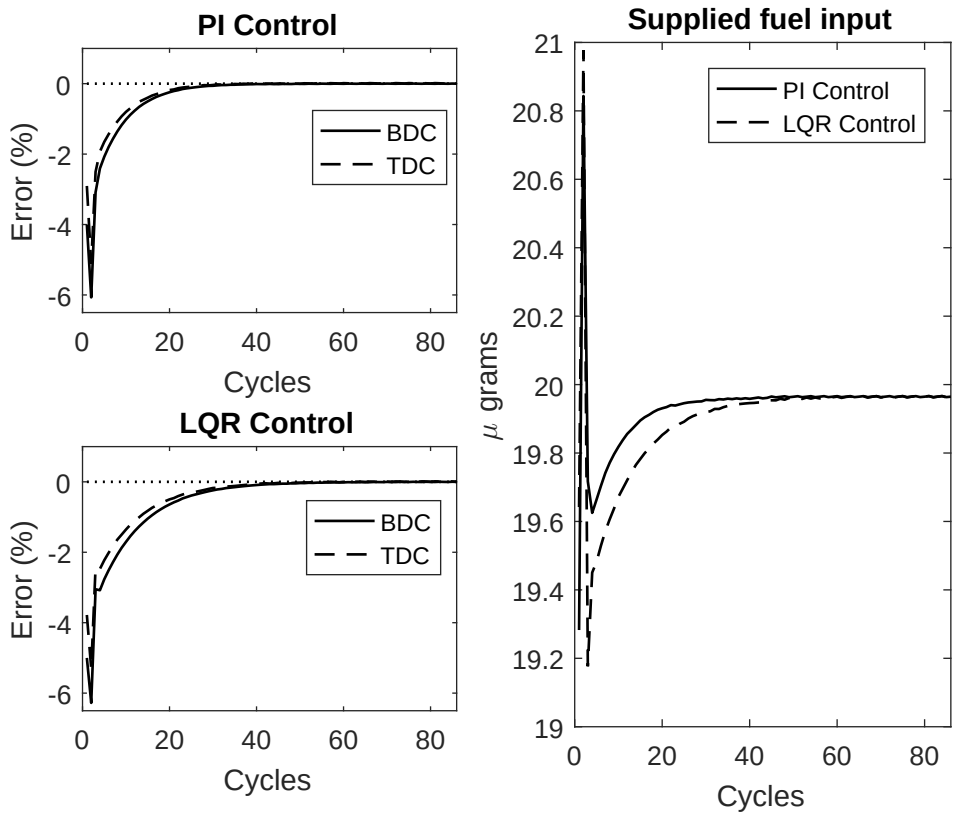

Figure 4.5: BDC/TDC error and input fuel response for PI and LQR controllers with a mechanical spring as rebound device. Controller parameters are chosen within their stability bounds. LQR response transient is slower than the PI response transient owing to a minimization of input objective.

which must stay below a critical value (which for the geometry considered is 24%, indicating where the deviation corresponds to the cylinder clearance length). In this case, the LQR control transient is slower than the PI control transient, owing to a minimization of an objective function that involves the fuel input (see (4.32)). Correspondingly, the "supplied fuel input" in Fig. 4.5 shows that the LQR transient fuel supply is lower than that with PI control. However, the FPE being an energy balance system at oscillations of constant amplitude (i.e., constant compression ratio), the fuel supplied at steady state is the same amount required to overcome a given load, regardless of the controller implemented. Therefore, the choice of one controller over another should be made based on transient response performance.

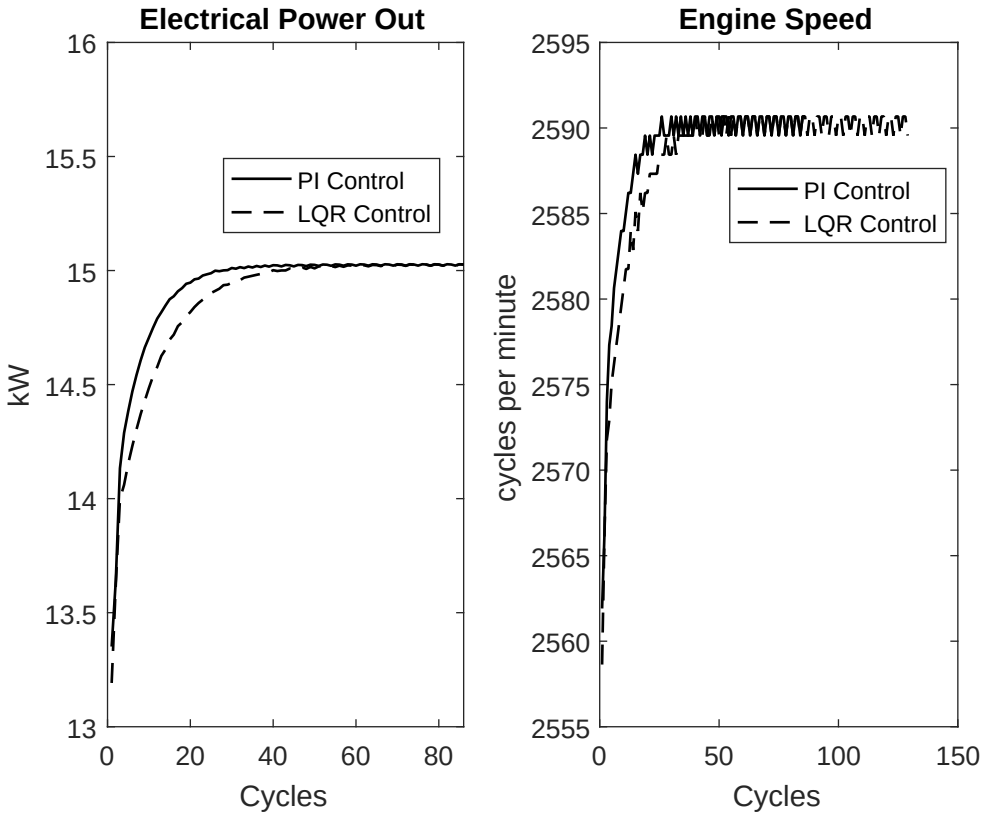

Figure 4.6: Output power and engine speed responses with a mechanical spring as rebound device. The same power and speed are achieved at steady-state regardless of controller type.

The performance responses of the electrical power produced (deduced from (2.15)) and piston oscillation frequency (or engine speed) are shown in Fig. 4.6. As expected, when steady compression ratio is achieved, both show stable convergence to the same value at steady state. In the simulation, an initial piston position is chosen such that the initial BDC/TDC error is small but significant (around 5%). In practice, a starting arrangement is required to bring the piston from its rest position to as close to nominal BDC/ TDC as possible before engine firing. This ensures that the nominal compression ratio is achieved fast. The largest possible initial BDC/TDC error that yields a compression ratio sufficient for combustion can be investigated experimentally.

4.4.2 Case II: Bounce Chamber as Rebound Device

In this configuration, the rebound device is a stiffness adjustable air bounce chamber (or gas spring). The chamber usually changes the air mass once every cycle to achieve TDC control. By varying the air mass, the bounce chamber stiffness is varied.

4.4.2.1 Detailed Development of the Control-Oriented Model for BDC Control

As in the previous example, the first task is to construct the BDC control model with (4.5). Considering isentropic expansion and compression of the rebound device, this specializes to

$$\underset{b\to t}{W_{rd}} - \underset{t\to b^+}{W_{rd}} = \left\{ -\frac{P_{rd_b}\left(V_{rd_b}^{\gamma_{rd}} V_{rd_t}^{1-\gamma_{rd}} - V_{rd_b}\right)}{1-\gamma_{rd}} \right\} - \left\{ -\frac{P_{rd_b}\left(V_{rd_b}^{\gamma_{rd}} V_{rd_{b^+}}^{1-\gamma_{rd}} - V_{rd_b}^{\gamma_{rd}} V_{rd_t}^{1-\gamma_{rd}}\right)}{1-\gamma_{rd}} \right\} \tag{4.50}$$

Assuming an ideal gas, and denoting the mass of air in the bounce chamber as u_{rd}, the pressure term P_{rd_b} in (4.50) is evaluated according to the ideal gas law as

$$P_{rd_b} = R_o T_{rd_b} \left(\frac{1}{V_{rd_b}}\right) u_{rd_b} \tag{4.51}$$

where R_o is the specific gas constant and T_{rd_b} is the bounce chamber air temperature at BDC (assumed to be a known constant). The second parenthesized term of (4.5) remains as evaluated in (4.39)–(4.41) because the cylinder side is no different from the previous example. Also, the same approximation equation (4.42) holds. Thus, (4.5) is again expressed in general nonlinear form

$$f_1\left(x_{b_{k+1}}, x_{t_k}, x_{b_k}, x_{t_{k-1}}, u_{c_k}, u_{rd_k}\right) = 0 \tag{4.52}$$

Subsequent linearization by Taylor series expansion to achieve the BDC control-oriented model equation (4.9) and subsequent control design are as described in Section (4.3).

4.4.2.2 Detailed Development of the Control-Oriented Model for TDC Control

For the TDC model, the first parenthesized term of (4.12) can be adapted to the form

$$\underset{b\to t^+}{W_{rd}} - \underset{t\to b}{W_{rd}} = \left\{ \frac{P_{rd_b}\left(V_{rd_b}^{\gamma_{rd}} V_{rd_{t^+}}^{1-\gamma_{rd}} - V_{rd_b}\right)}{1-\gamma_{rd}} \right\} - \left\{ -\frac{P_{rd_t}\left(V_{rd_t}^{\gamma_{rd}} V_{rd_b}^{1-\gamma_{rd}} - V_{rd_t}\right)}{1-\gamma_{rd}} \right\} \quad (4.53)$$

where the pressure term P_{rd_b} is computed as in (4.51). The pressure P_{rd_t} is obtained from

$$P_{rd_t} = P_{rd_{b^-}} \left(\frac{V_{rd_{b^-}}}{V_{rd_t}} \right)^{\gamma_{rd}} \quad (4.54)$$

where the subscript b^- refers to the BDC position $x_{b_{k-1}}$. According to the ideal gas law, $P_{rd_{b^-}}$ in (4.54) is obtained as

$$P_{rd_{b^-}} = R_o T_{rd_{b^-}} \left(\frac{1}{V_{rd_{b^-}}} \right) u_{rd_{b^-}} \quad (4.55)$$

The second parenthesized term of (4.12) can be computed as

$$\underset{t\to b}{W_c} - \underset{b\to t^+}{W_c} = \left\{ \frac{(P_{c_t} + \Delta P_{c_t})\left(V_{c_t}^{\gamma_c} V_{c_b}^{1-\gamma_c} - V_{c_t}\right)}{1-\gamma_c} \right\} - \left\{ -\frac{P_{c_b}\left(V_{c_b}^{\gamma_c} V_{c_{t^+}}^{1-\gamma_c} - V_{c_b}\right)}{1-\gamma_c} \right\} \quad (4.56)$$

And similar to (4.40), P_{c_t} is evaluated as

$$P_{c_t} = P_{c_b} \left(\frac{V_{c_{b^-}}}{V_{c_t}} \right)^{\gamma_c} \quad (4.57)$$

where P_{c_b} is the air intake pressure during scavenging, and the pressure rise ΔP_{c_t} is as stated in (4.41). The third parenthesized term of (4.12) is the same as that of (4.5),

and is therefore, evaluated no differently from (4.42). Equation (4.12) can thus be stated in the general nonlinear form

$$f_2\left(x_{t_{k+1}}, x_{b_k}, x_{t_k}, x_{b_{k-1}}, u_{rd_k}, u_{c_k}, u_{rd_{k-1}}\right) = 0 \tag{4.58}$$

Taylor series expansion of (4.58) yields the control-oriented model corresponding to (4.14). Subsequent controller design follows the process described in Section 4.3.

4.4.2.3 TDC Estimation

Estimation of TDC is important in the implementation of the BDC controller. As in the previous case, the compression stroke energy balance is used to obtain

$$P_{rd_b} V_{rd_b}^{\gamma_c}\left(\hat{V}_{rd_t}^{1-\gamma_c} - V_{rd_b}^{1-\gamma_c}\right) + P_{c_b} V_{c_b}^{\gamma_c}\left(\hat{V}_{c_t}^{1-\gamma_c} - V_{c_b}^{1-\gamma_c}\right) - E_1\left(1-\gamma_c\right) = 0 \tag{4.59}$$

where $\hat{V}_{rd_t}$ and $\hat{V}_{c_t}$are estimates of the rebound device volume and the cylinder volume at the immediately following TDC position, respectively. Volumes $\hat{V}_{rd_t}$ and $\hat{V}_{c_t}$ are known functions the TDC position estimate $\hat{x}_t$. Thus, when these functions are substituted into (4.59), $\hat{x}_t$ can be found as a direct solution with a root-finding scheme such as Newton's method.

4.4.2.4 Simulation Results and Discussion

The basic engine geometry for the numerical simulation is again given in Table 4.1, with the PI controller parameters k_p and k_i selected from the stability map in Fig. 4.4, and the LQR weighting parameters Q and R selected as positive definite.

Figure 4.7 shows the piston response for PI and LQR control, as well as the fuel supply input for both controllers. Both TDC and BDC errors can be seen to converge to zero (implying convergence to a steady compression ratio). Owing to minimization of

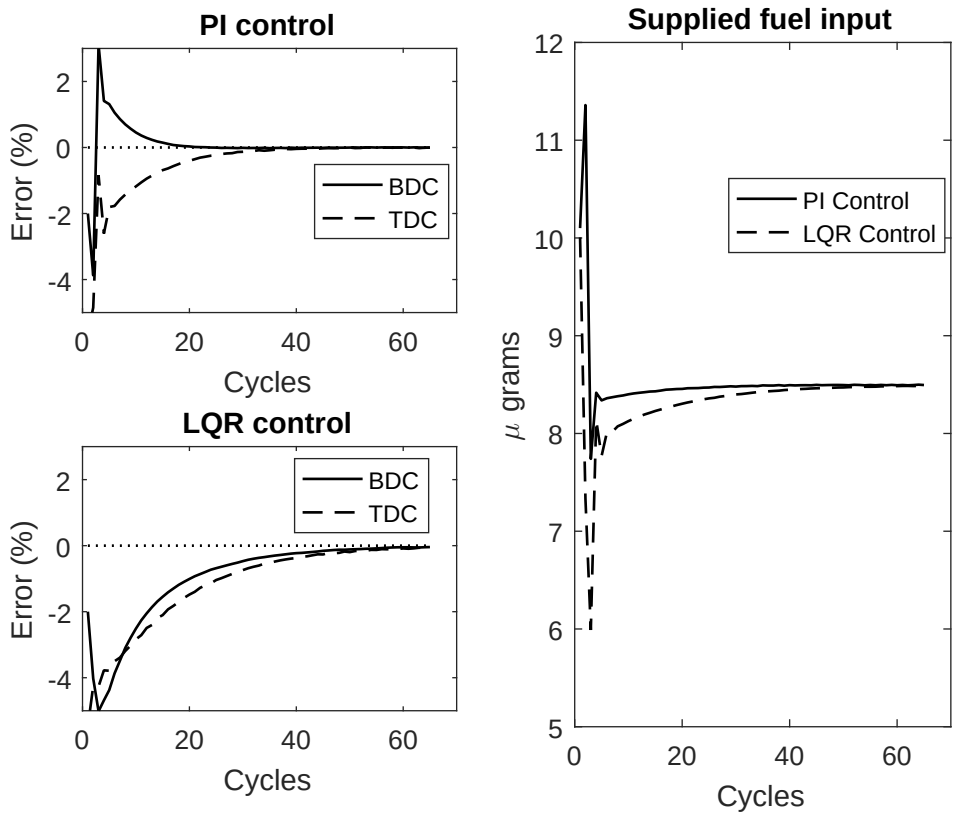

Figure 4.7: BDC/TDC error and input fuel response for PI and LQR controllers with a bounce chamber as rebound device . Controller parameters were chosen within their stability bounds.

the supplied input fuel in (4.32), the LQR response transient is evidently slower than the PI response. But the LQR response transient appears to be "smoother", and on this basis, is preferable to the PI transient for the parameters chosen. Note that at steady state, the same fuel is supplied regardless of the type of controller.

The generated electrical power and the engine speed are shown in Fig. 4.8, both converging to their respective steady-state values when a steady compression ratio is achieved. There is a brief initial deviation from a converging path for both transients. This can be attributed to the interaction of the BDC and TDC controllers, as well as possibly unmodelled dynamics in control design—for example, instantaneous fuel combustion is assumed during control design (see (4.41)), whereas the engine is simulated with finite time fuel combustion (see (2.4)).

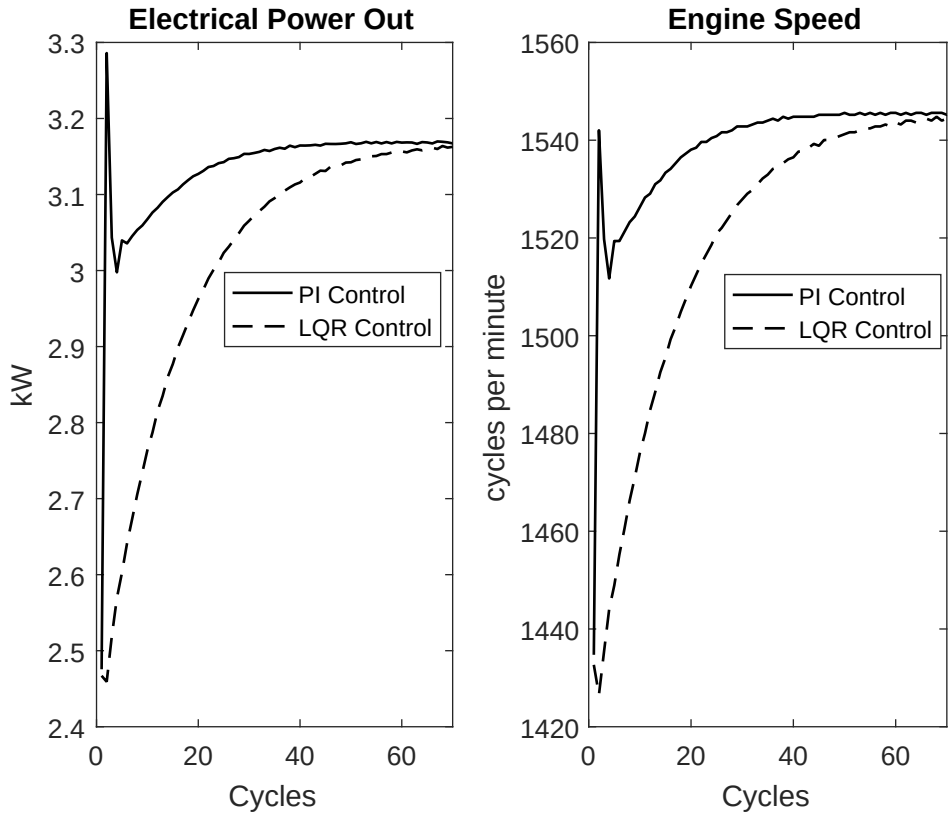

Figure 4.8: Output power and engine speed responses with a bounce chamber as rebound device . The same power and speed are achieved at steady-state regardless of controller type.

4.4.3 Case III: Combustion Chamber as Rebound Device

In this configuration (also known as a dual-piston FPE), the rebound device is a combustion chamber [53, 18] identical to the left-hand cylinder in Fig. 4.1. The engine, therefore, comprises two pistons on either end (hence the "dual-piston" reference) which produces two power strokes in a cycle—one in gas compression and the other in gas expansion. The treatment of this case reduces to analyzing two identical combustion chambers, but considering one as a rebound device. Since a combustion chamber has already been accounted for in the previous two cases, this third case does not present any particular new challenge. The first parenthesized term of (4.5)

is found as

$$W_{\underset{b\to t}{rd}} - W_{\underset{t\to b^+}{rd}} = \left\{ \frac{\left(P_{rd_b} + \Delta P_{rd_b}\right)\left(V_{rd_t}^{\gamma_{rd}} V_{rd_t}^{1-\gamma_{rd}} - V_{rd_b}\right)}{1-\gamma_{rd}} \right\} - \left\{ -\frac{P_{rd_t}\left(V_{rd_t}^{\gamma_{rd}} V_{rd_b}^{1-\gamma_{rd}} - V_{rd_t}\right)}{1-\gamma_{rd}} \right\} \tag{4.60}$$

where P_{rd_t} is the rebound device intake pressure during scavenging. Following the arguments used to obtain (4.54) and (4.41), P_{rd_b} and ΔP_{rd_b} are functions of (i) rebound device cylinder volume (which itself is expressible as a function of piston endpoints) and (ii) the rebound device fuel input u_{rd}. Since the left-hand cylinder remains unchanged following-on from the previous case, the second parenthesized term of (4.9) is evaluated the same way as in (4.39)–(4.41). Also, the same approximation (4.42) holds. This allows (4.5) to be expressed in the general nonlinear form

$$f_1\left(x_{b_{k+1}}, x_{t_k}, x_{b_k}, x_{t_{k-1}}, u_{c_k}, u_{rd_k}\right) = 0 \tag{4.61}$$

By Taylor series expansion, the control-oriented model (4.9) and subsequent controller design again follow from the procedure described in Section 4.4. Finally, by swapping the cylinder functions on either end, the TDC control-oriented model is realized through the same process as the BDC control-oriented model.

Figure 4.9 shows the BDC and TDC error responses using the same simulation settings as described in the previous cases. As expected, both errors converge to zero to yield a steady compression ratio at steady-state. The LQR response transient is slower–owing to a fuel minimization requirement in (4.32)—but also less oscillatory than the PI controller response, for the controller parameters used.

4.4.4 Case IV: Opposed Piston Free-Piston Engine

In this configuration, two opposing pistons share a combustion chamber to form an opposed piston FPE [2] as shown in Fig. 4.10. It is shown here that under symmetry

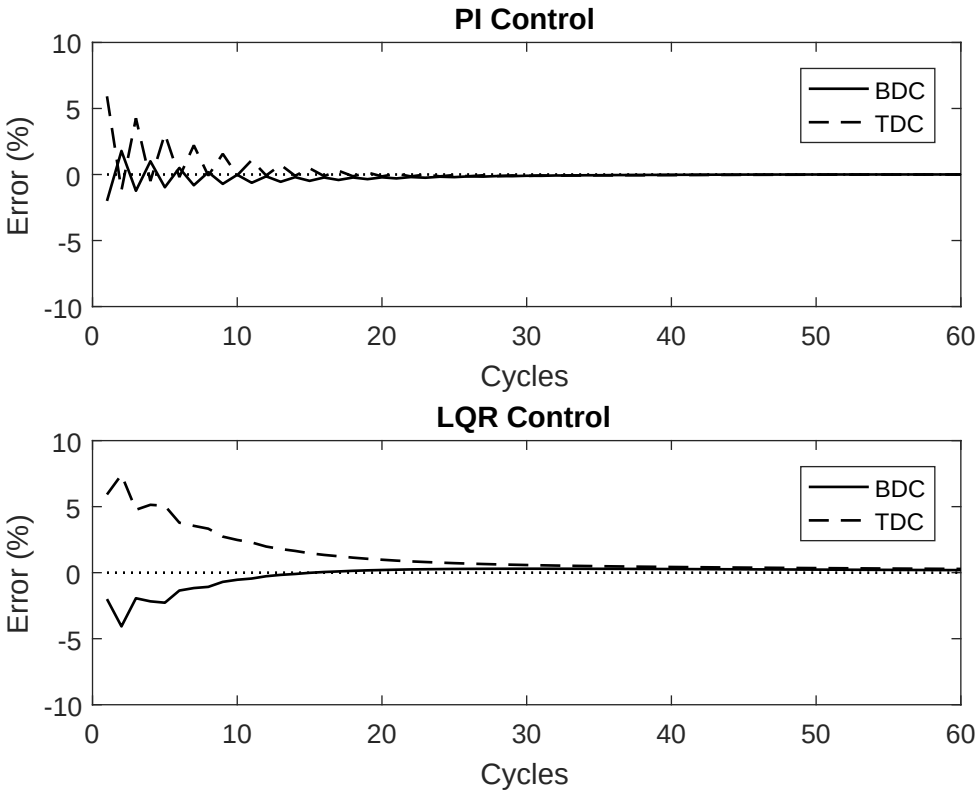

Figure 4.9: BDC/TDC error response for PI and LQR controllers with a combustion chamber as rebound device. Controller parameters were chosen within their stability bounds.

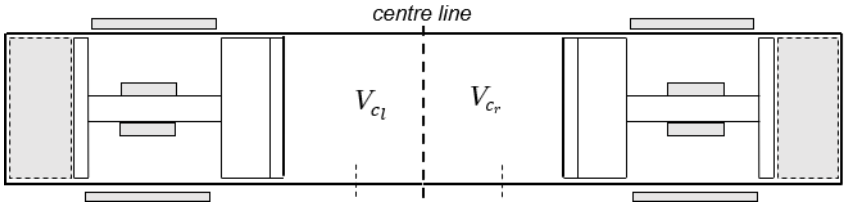

Figure 4.10: An opposed piston FPE. Two pistons sharing a combustion volume oppose each other about the centerline.

conditions, the analysis of this configuration case for BDC and TDC control is no different from that for the previously studied cases. Symmetry about the centerline simplifies analysis by reducing the device to an equivalent single piston FPE configuration. This is achieved after noting that in Fig. 4.10, the common combustion volume is given by

$$V_c = V_{c_l} + V_{c_r} \tag{4.62}$$

where V_{c_l} and V_{c_r} are instantaneous gas chamber volumes on either side of the centerline. Assuming symmetry of piston motion and identical physical properties on either side of the centerline, the two gas volumes are then equal, i.e., $V_{c_l} = V_{c_r}$, giving

$$V_c = 2V_{c_l} = 2V_{c_r} \tag{4.63}$$

From (4.63), the common volume is equivalently described either by the left or right gas chamber volume. The common volume V_c is the only form of coupling between the two pistons; therefore, symmetry acts as a decoupling condition. Consequently, it can be concluded from (4.63) that opposed piston FPE analysis under symmetry conditions is equivalent to single piston FPE analysis, but with twice the volume to the centerline. If the symmetry assumption does not hold, then this amounts to quantifying the asymmetry between the two opposing piston FPEs. Knowledge of this asymmetry can then be as a compensator in the equivalent single piston model. So, under asymmetry conditions, by defining the left-side volume V_{c_l} as

$$V_{c_l} = V_{c_r} + \psi(t) \tag{4.64}$$

where $\psi(t)$ is the instantaneous time-varying volume difference between the left and right cylinder volumes to the centerline, for which $\psi(t) = 0$ implies complete symmetry, substituting (4.64) into (4.63) yields

$$V_c = 2V_{c_r} + \psi(t) \tag{4.65}$$

or, in terms of the left cylinder,

$$V_c = 2V_{c_l} - \psi(t) \tag{4.66}$$

Equations (4.65) and (4.66) are generalized forms of (4.63), when taking into account asymmetry of the left and right cylinders as quantified by parameter $\psi(t)$. The common volume V_c is described only in terms of the left or right cylinder volume from the top of the relevant piston head to the centerline. The general finding is that the analysis of an opposed piston FPE configuration is equivalent to the analysis of just one piston, for example, in Cases I–III, assuming that the level of asymmetry between the two pistons is known, and adequately compensated for. It can be investigated whether the asymmetry parameter $\psi(t)$ can be modeled with simple and convenient functions that can be fitted to experimental data. This serves as a possible future line of investigation.

4.5 Chapter Conclusions

A model-based procedure for control of BDC and TDC in a free-piston engine has been developed, thereby achieving analytically guided compression ratio control. The limited scope of zero dimensional thermodynamic modeling does not permit a first principled investigation into performance aspects such as fuel efficiency or emissions formation. However, the basic objective of analytically deriving controller parameter combinations that produce stable BDC/TDC responses has been achieved and demonstrated with PI control. Additionally, using LQR control, advanced control yielding transient responses that satisfy stated performance objectives has been demonstrated. Of greater significance, however, is the unified context in which four FPE configurations can be treated to demonstrate the generality of the proposed approach.

Chapter 5

Optimal and Resonant Engine Start

5.1 Introduction

Like conventional engines, free-piston engines (FPEs) have a brief *starting* period in which the engine gets thermodynamically ready for the first combustion event; i.e. a prelude to *firing*. The goal of engine start in FPEs is to drive the piston from its rest state to a required piston amplitude corresponding to a compression ratio needed for firing.

Broadly speaking, there are two methods with which an FPE can be started:

i) Mechanically; for example by sending the piston to nominal bottom dead centre (BDC) with aid of a compressed air supply, and, having compressed the rebound device, releasing the piston, or

ii) Electrically (for FPE generators only); by operating the FPE generator as a motor to drive the piston—a process known as *motoring*.

This chapter focuses on the second method, which is to electrically start an FPE by

way of motoring. From this point forward, the term "motoring force" will be used interchangeably with the term "starting force".

While building up the required piston amplitude (and therefore compression ratio) during FPE starting, it would appear that the motoring force must overcome large opposing forces from the cylinder and rebound device. Yet, arbitrarily large motoring forces are not possible, as the motoring force is greatly limited by the peak current rating of the motor coils. To overcome this problem, a mechanical resonance inducing strategy has been proposed in the literature [53, 74, 8, 118], where a motoring force always acts in the direction of the piston motion such that growing oscillation amplitudes are realized. However, despite the strategy's apparent success in practice [53, 54], it has not been the subject of analytical consideration.

This chapter has two objectives. The first is to propose an analytical approach to starting FPEs by mechanical resonance, and by so-doing fill a gap in the literature. The second is to consider a previously unexplored strategy; that of optimally starting FPEs. In optimally starting an FPE, one seeks to minimize the motoring force during the starting process. In turn, the current drawn from an external battery is minimized, and consequently so are the resistive losses in the motor circuit. Indeed, an optimal starting strategy with minimal battery discharge current is especially useful in field or remote FPE deployment where access to an alternative power supply is limited.

Two FPEs of different rebound device types are considered: one with a mechanical spring and the other with an air bounce chamber. Development of explicit motoring force functions is elaborated and tested by simulation.

5.2 Modelling

This section provides the FPE modelling on which this chapter's analysis is based. For convenience, an idealized schematic of a single piston two-stroke FPE generator

is shown again here in Fig. 5.1. The engine comprises three major parts, namely: a piston-translator assembly (the moving mass), a rebound device (for returning the piston), and an integrated generator (for power generation or motoring).

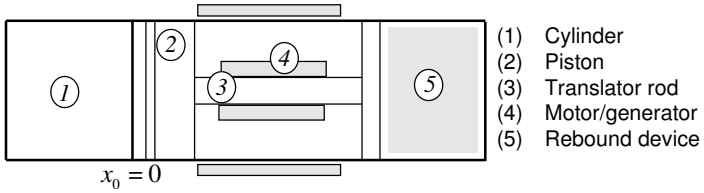

Figure 5.1: Idealized FPE generator schematic.

Considering the compression stroke as the positive direction for piston displacement, piston motion is described by Newton's second law as:

$$-m\ddot{x}_0 = F_c + F_{rd} + F_f + F_m \tag{5.1}$$

where m is the piston-translator mass (also known as the moving or active mass), F_c is the cylinder gas force in the combustion chamber, F_{rd} is the rebound device force, F_f is the friction, and F_m is the motoring force (as opposed to generator force).

For a piston of crown area A_p, forces F_c and F_{rd} are modelled as

$$F_c = A_p P_c \tag{5.2a}$$

$$F_{rd} = \begin{cases} k_s x_0 & \text{mechanical spring} \\ -A_p P_{rd} & \text{bounce chamber} \end{cases} \tag{5.2b}$$

Here, P_c is the in-cylinder pressure, P_{rd} is the bounce chamber pressure, and k_s is a spring stiffness. The pressure P_c and P_{rd} are respectively related to their associated volumes $V_c(x_0)$ and $V_{rd}(x_0)$ through the polytropic process

$$P_i(x_0) = \frac{K_i}{V_i(x_0)^{\underline{n}_i}}, \qquad i = c, rd. \tag{5.3}$$

In (5.3), K is constant and $\underline{n}$ is a polytropic index. Assuming a sufficiently fast starting process for which heat exchange with the surrounding is negligible, $\underline{n}$ can be taken as the ratio of specific heats of the contents of the volume V. Friction force F_f in (5.1) is modelled as in (2.20) with a Coulomb friction and viscous friction component, i.e.

$$F_f = a_f \text{sgn}(\dot{x}_0) + b_f \dot{x}_0 \tag{5.4}$$

where a_f and b_f are constants determined empirically.

5.3 Starting using mechanical resonance

Starting by mechanical resonance requires that a small motoring force be supplied to produce large piston oscillation amplitudes. The idea is to supply a motoring force that constantly acts in the direction of piston motion. Such a force always does positive work on the piston, yielding continued growth of piston oscillations until limited by some form of system damping. The starting process ends when the piston oscillations reach the required amplitude, i.e. a required compression ratio. In the following subsections, resonance is exploited to derive a small motoring force that yields a required piston oscillation amplitude. An analytical solution is successfully developed for an FPE whose rebound device is a mechanical spring. A boundary value problem is constructed for an FPE whose rebound device is a bounce chamber.

5.3.1 Mechanical Spring as rebound device

5.3.1.1 Main Developments

A mechanical spring is first considered as the rebound device. It is proposed that the combustion chamber remains vented, or open, during the starting process, i.e. $F_c = 0$ in (5.1). To safely limit growth of piston oscillations, rather than rely on friction, a

viscous damper of coefficient b is proposed to be active during the starting process. Accordingly, the force

$$F_d = b\dot{x}_0 \tag{5.5}$$

is introduced on the right-hand side of (5.1). With these considerations, equations (5.1)–(5.5) reveal the dynamics of a linear oscillator if the rebound device is a mechanical spring. The said dynamics being of a linear oscillator, proposed is a simple motoring force in the form of a sinusoid of amplitude $\bar{F}_m$ and frequency ω:

$$F_m(t) = -\bar{F}_m \cos \omega t \tag{5.6}$$

where the minus sign on the right-hand side of (5.6) is introduced to mean motoring (as opposed to generation). Both $\bar{F}_m$ and ω in (5.6) are to be designed. Neglecting friction and incorporating (5.6) into (5.1), and introducing damping force (5.5) on the right-hand side of (5.1) yields

$$\ddot{x}_0 + \gamma \dot{x}_0 + \omega_0^2 x_0 = \bar{F} \cos \omega t \tag{5.7}$$

where

$$\gamma = \frac{b}{m} \tag{5.8a}$$

$$\omega_0 = \sqrt{\frac{k_s}{m}} \tag{5.8b}$$

$$\bar{F} = \frac{\bar{F}_m}{m} \tag{5.8c}$$

The task is to find $\bar{F}_m$ (see (5.8c)) that produces a required oscillation amplitude—one that is arbitrarily chosen based on desired compression ratio—while exploiting mechanical resonance.

To this end, it can be shown that Equation (5.7) has the general solution [94]

$$x_0(t) = A_0 \cos(\omega t + \phi) + e^{-\frac{\gamma}{2}t}\left(A_{h1}\cos\omega_h t + A_{h2}\sin\omega_h t\right) \tag{5.9}$$

where A_{h1} and A_{h2} are arbitrary constants and

$$A_0 = \frac{\bar{F}}{\sqrt{(\omega_0^2 - \omega^2) + \gamma^2\omega^2}} \tag{5.10a}$$

$$\tan\,\phi = \frac{-\gamma\omega}{\omega_0^2 - \omega^2} \tag{5.10b}$$

$$\omega_h = \omega_0\sqrt{1 - \left(\frac{\gamma}{2\omega_0}\right)^2} \tag{5.10c}$$

As time increases, the second term in (5.9) diminishes, allowing the first term which represents a constant amplitude sinusoid to dominate. Also observe from (5.10a) that A_0 is a function of the motoring force frequency ω. The maximum of $A_0(\omega)$ occurs when the derivative of its denominator in (5.10a) is zero; i.e. at

$$\omega = \sqrt{\omega_0^2 - \frac{\gamma^2}{2}} \tag{5.11}$$

The stiffness of an FPE rebound spring tends to be very high, usually greater than 100 kN/m [8]. It can therefore be expected that $\gamma \ll \omega_0$. Consequently it can be said that the maximum of $A_0(\omega)$, and hence that of $x_0(t)$, occurs with $\omega \approx \omega_0$. Taking $\omega = \omega_0$ in (5.10a) and (5.10b) respectively gives

$$A_0(\omega_0) = \frac{\bar{F}}{\gamma\omega_0} \tag{5.12a}$$

$$= \frac{\bar{F}_m}{b\omega_0} \tag{5.12b}$$

where (5.8a) has been used, and

$$\phi(\omega_0) = -\frac{\pi}{2} \tag{5.13}$$

For a *target* oscillation amplitude s, $\bar{F}_m$ is found from (5.12b) as

$$\bar{F}_m = sb\omega_0 \tag{5.14}$$

thereby completing the design of $\bar{F}_m(t)$ in (5.6). Note that in general $s \ll 1$ (taken in metres), and so $\bar{F}_m$ and hence $F_m(t)$ are by no means large. It should also be noted that at phase $\phi(\omega_0)$ in (5.13), $F_m(t)$ always acts in the same direction—i.e. is in phase—with the piston speed $\dot{x}_0$.

Linear system resonance analysis described by Equations (5.7)–(5.13) is well-known. However, the formal application of Equation (5.14) to starting an FPEs is new.

5.3.1.2 Simulation Testing

A simulation is now conducted to test a resonance-inducing motoring force as per Equation (5.14) in starting an FPE. Table 5.1 contains the relevant simulation parameters.

Table 5.1: Simulation Parameters

Parameter	**Value**
Piston-translator mass	0.5 kg
Length from zero position to cylinder end	0.0168 m
Top dead centre position (nominal)	0.0136 m
Bottom dead centre position (nominal)	-0.0152 m

The spring is of stiffness $k_s = 170$ kN/m and the damping coefficient is set to $b = 10$. The piston is required to achieve an amplitude $s = 0.0152$ (the absolute value of the

bottom dead centre position). Figure 5.2 shows the piston response when motored with force (5.6) at $\omega = \omega_0$ and $\bar{F}_m$ designed as in (5.14). It is evident that the target amplitude s is achieved in 0.4 seconds without exceeding the cylinder end (solid horizontal line) although nominal top dead centre is exceeded (upper dotted line). The root-mean-square (RMS) of the motoring force is computed to be 62.7 N.

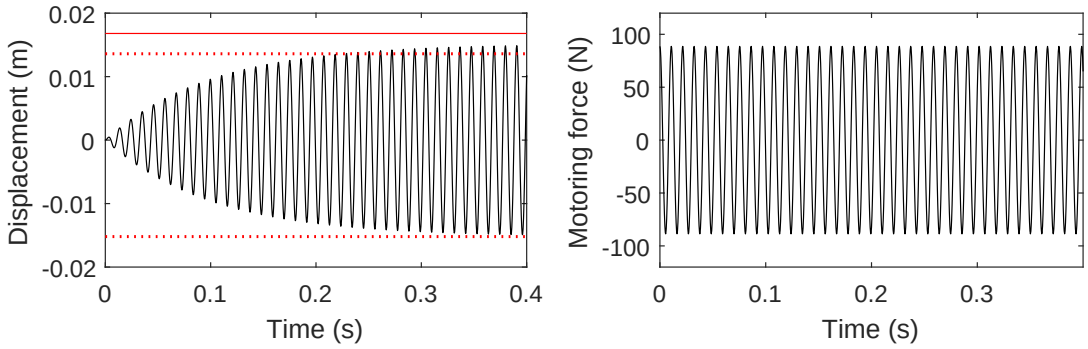

Figure 5.2: FPE start by mechanical resonance with spring as rebound device.

5.3.2 Air bounce chamber as rebound device

5.3.2.1 Main Developments

Where a bounce chamber is the rebound device, it is proposed that the combustion chamber remains closed throughout the start period. This is to allow for alternate energy storage and release between the combustion chamber and bounce chamber (a bounce chamber may itself constitute a combustion chamber, as in the dual-piston FPE configuration).

The gas compression and expansion processes as modelled by (5.3) make the FPE dynamics (5.1) highly nonlinear, yet it is non-trivial to compute characteristics of nonlinear resonances or to even predict their very appearance [58]. To overcome analytical difficulty, one may supply a *feedback* motoring force that is designed to

always act in phase with piston velocity, i.e.

$$F_m(\dot{x}_0) = -\bar{F}_m \text{sgn}(\dot{x}_0) \tag{5.15}$$

where the minus sign once again denotes motoring and $\bar{F}_m$ is for simplicity considered constant. The question for starting an FPE becomes: what value of $\bar{F}_m$ is required to achieve a target oscillation amplitude when (5.15) is applied to the dynamics (5.1)?

An attempt can be made to solve (5.1) with a solution-approximation method that could relate $\bar{F}_m$ to oscillation amplitude. However, accurately approximating the polytropic process nonlinearities (5.3) over the entire amplitude in question may require a Taylor polynomial of unamenably high degree. Moreover, presence of the discontinuous sgn term in (5.15) can further complicate the analysis. A numerical approach to estimating $\bar{F}_m$ is hence proposed; namely, to solve for $\bar{F}_m$ as a parameter for which the dynamics (5.1) have a solution that satisfies the four boundary conditions

$$x_0(0) = \delta \tag{5.16a}$$

$$\dot{x}_0(0) = 0 \tag{5.16b}$$

$$x_0(t_f) = x_B \tag{5.16c}$$

$$\dot{x}_0(t_f) = 0 \tag{5.16d}$$

where δ is a small perturbation to start the oscillations, x_B is the nominal bottom dead centre position and t_f is an unknown terminal time. Such a problem can be solved using commercially available boundary value problem solvers. To ensure finding $\bar{F}_m$ for which response $x_0(t)$ is oscillatory (as opposed to a single-stroke response), $\bar{F}_m$ cannot be arbitrarily large.

5.3.2.2 Simulation Testing

In testing (5.15), the FPE of parameters in Table 5.1 is considered for simulation. Note that the sgn term in (5.15) is a perfect switch that may be difficult to implement in practice. It is approximated to a continuous function as

$$\mathrm{sgn}(\dot{x}_0) = \frac{\dot{x}_0}{|\dot{x}_0| + \varepsilon} \tag{5.17}$$

where ε is a small positive scalar. Indeed, it holds that

$$\lim_{\varepsilon \to 0} \frac{\dot{x}_0}{|\dot{x}_0| + \varepsilon} = \mathrm{sgn}(\dot{x}_0), \qquad \varepsilon \neq 0 \tag{5.18}$$

A bounce chamber of compression ratio 12 is considered, and the motoring force amplitude $\bar{F}_m$ is set at 4 N. This parameterisation produces the response in Figure 5.3, showing a growing but limited piston response amplitude in 0.8 seconds. It is now noted that the FPE system is frictionless and has no dampers employed. If the FPE system is *not* frictionless, the motoring force $\bar{F}_m$ must be set to ensure that it always overcomes the friction in the FPE system, or the piston response amplitude growth may be severely limited. It is also noted in Fig. 5.3 that although the piston exceeds the nominal top dead centre position (upper dotted line), it crucially does not exceed the cylinder end (solid horizontal line) or the nominal bottom dead centre position (lower dotted line).

5.4 Optimal start

This section considers the design of *minimal* motoring force—as per some mathematically defined criterion—for an *imposed* start duration. The minimal motoring force shall be that which minimizes a chosen objective function, and is therefore optimal

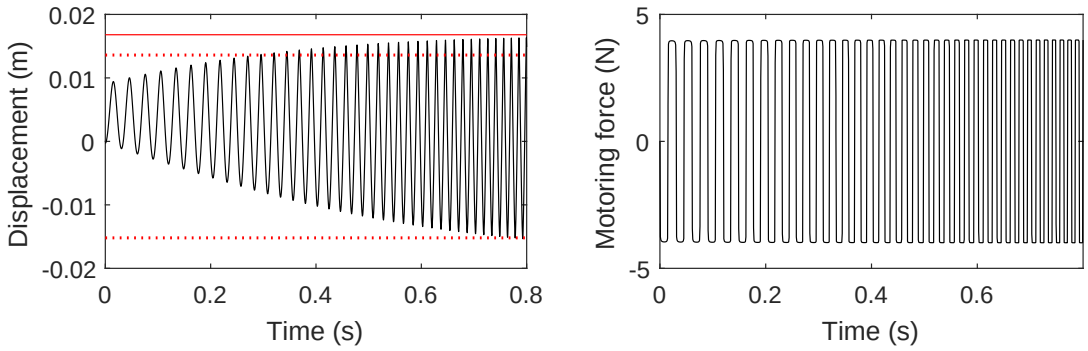

Figure 5.3: FPE start by mechanical resonance with bounce chamber as rebound device.

in this sense. This approach is to be contrasted to the previous section where a (relatively) small motoring force was sought that yields large piston oscillation amplitudes, for a start duration that is not imposed a priori.

To emphasize why a minimal motoring force is desirable, consider the power equivalence between an FPE's mechanical and electrical systems given by

$$F_m \dot{x}_0 = \eta i_m e_m \tag{5.19}$$

Here i_m is the motor armature current, e_m is the armature voltage and η is the power conversion efficiency of the FPE from electrical to mechanical power. From (5.19) it is noted that

$$F_m \propto i_m \tag{5.20}$$

Thus, by minimizing the motoring force, the armature current is minimized. In turn, for a motor circuit resistance R_m, power losses attributed to $i_m^2 R_m$ are also minimized. And, if i_m is a battery discharge current, then minimizing it also prevents fast battery charge decline and hence longer battery usage cycles.

5.4.1 Mechanical Spring as rebound device

5.4.1.1 Main Developments

With a spring as the rebound device, the proposed starting procedure involves first driving the piston from its rest state to the nominal bottom dead centre position (where the spring is fully compressed). When the driving/motoring force is removed, the combustion chamber closed and generation mode activated, the spring then goes into tension, pushing the piston to the nominal top dead centre position within a compression stroke (assuming the spring is of correctly designed stiffness as per Section 4.4.1.2). Piston transition from nominal bottom dead centre to nominal top dead centre ensures that a nominal compression ratio has been achieved, allowing combustion to start.

Assuming the combustion chamber remains open during motoring, then $F_c = 0$. And as before, neglect friction but consider a damper with force (5.5) introduced to limit the piston oscillations within the cylinder ends. Defining x_1 as piston position and x_2 as piston speed, the state equations for (5.1) are in fact linear, i.e.

$$\begin{aligned} \dot{x}_1 &= x_2 \\ \dot{x}_2 &= -\frac{k_s}{m}x_1 - \frac{b}{m}x_2 - \frac{1}{m}F_m \end{aligned} \tag{5.21}$$

The task is to find motoring force $F_m(t)$ that drives state $(x_1(t), x_2(t))$ from the rest state $(0, 0)$ at time $t = 0$ to a final state $(x_B, 0)$ at time $t = t_f$; where x_B is the nominal bottom dead centre position, while minimizing the performance index

$$J(F_m) = \int_0^{t_f} rF_m(t)^2 dt \tag{5.22}$$

where r is a positive constant. The choice of (5.22) is motivated by the discussion provided for the relations (5.19) and (5.20). Optimal control problems with a perfor-

mance index (5.22) involving the integral of the square of a system input variable are generally known as minimum-energy problems [61].

Let only smooth functions for $F_m(t)$ be admissible. Following the variational approach to optimal control [61], by defining a Hamiltonian function

$$H = rF_m(t)^2 + p_1(t)x_2(t) + p_2(t)\left(-\frac{k_s}{m}x_1 - \frac{b}{m}x_2 - \frac{1}{m}F_m\right) \tag{5.23}$$

where $p_1(t)$ and $p_2(t)$ are costate variables, necessary conditions for an optimal solution comprising the optimal control, state, and costate variables respectively denoted $F_m^*(t)$, $(x_1^*(t), x_2^*(t))$, and $(p_1^*(t), p_2^*(t))$ are found as

$$\begin{aligned}
\dot{x}_1^*(t) &= \left.\frac{\partial H}{\partial p_1}\right|_* &&= x_2^*(t) \\
\dot{x}_2^*(t) &= \left.\frac{\partial H}{\partial p_2}\right|_* &&= -\frac{k_s}{m}x_1^*(t) - \frac{b}{m}x_2^*(t) - \frac{1}{m}F_m^*(t) \\
\dot{p}_1^*(t) &= -\left.\frac{\partial H}{\partial x_1}\right|_* &&= \frac{k}{m}p_2^*(t) \\
\dot{p}_2^*(t) &= -\left.\frac{\partial H}{\partial x_2}\right|_* &&= -p_1^*(t) + \frac{b}{m}p_2^*(t) \\
0 &= \left.\frac{\partial H}{\partial F_m}\right|_* &&= 2rF_m^*(t) - \frac{p_2^*(t)}{m}
\end{aligned} \tag{5.24}$$

where $t \in [0, t_f]$. The solutions to the necessary conditions (5.24) are derived in Appendix A. The optimal control $F_m^*(t)$ and optimal state trajectories $(x_1^*(t),\ x_2^*(t))$ are of interest here. They are respectively taken from (A.16), (A.21), and (A.22) as

$$\begin{aligned}
F_m^*(t) &= \frac{1}{2rk_s}\left(c_1\theta_1 e^{\theta_1 t} + c_2\theta_2 e^{\theta_2 t}\right) \\
x_1^*(t) &= \frac{c_1\theta_1 e^{\theta_1 t}}{2rk_s\left(\theta_1^2 m + \theta_1 b + k_s\right)} + \frac{c_2\theta_2 e^{\theta_2 t}}{2rk_s\left(\theta_2^2 m + \theta_2 b + k_s\right)} + c_3 e^{\theta_3 t} + c_4 e^{\theta_4 t} \\
x_2^*(t) &= \frac{c_1\theta_1^2 e^{\theta_1 t}}{2rk_s\left(\theta_1^2 m + \theta_1 b + k_s\right)} + \frac{c_2\theta_2^2 e^{\theta_2 t}}{2rk_s\left(\theta_2^2 m + \theta_2 b + k_s\right)} + c_3\theta_3 e^{\theta_3 t} + c_4\theta_4 e^{\theta_4 t}
\end{aligned} \tag{5.25}$$

where

$$\begin{aligned}\theta_{1,2} &= \frac{1}{2}\left(\frac{b}{m} \pm \sqrt{\left(\frac{b}{m}\right)^2 - 4\frac{k}{m}}\right) \\ \theta_{3,4} &= \frac{1}{2}\left(\frac{-b}{m} \pm \sqrt{\left(\frac{b}{m}\right)^2 - 4\frac{k}{m}}\right)\end{aligned} \tag{5.26}$$

and where c_1, c_2, c_3, and c_4 are integration constants. Applying the boundary conditions at $t = 0$ and $t = t_f$ to the second and third equations of (5.25) yields the system of algebraic equations

$$\begin{bmatrix} 0 \\ 0 \\ x_B \\ 0 \end{bmatrix} = \begin{bmatrix} \frac{\theta_1}{2rk_s\left(\theta_1^2 m+\theta_1 b+k_s\right)} & \frac{\theta_2}{2rk_s\left(\theta_2^2 m+\theta_2 b+k_s\right)} & 1 & 1 \\ \frac{\theta_1^2}{2rk_s\left(\theta_1^2 m+\theta_1 b+k_s\right)} & \frac{\theta_2^2}{2rk_s\left(\theta_2^2 m+\theta_2 b+k_s\right)} & \theta_3 & \theta_4 \\ \frac{\theta_1 e^{\theta_1 t_f}}{2rk_s\left(\theta_1^2 m+\theta_1 b+k_s\right)} & \frac{\theta_2 e^{\theta_2 t_f}}{2rk_s\left(\theta_2^2 m+\theta_2 b+k_s\right)} & e^{\theta_3 t_f} & e^{\theta_4 t_f} \\ \frac{\theta_1^2 e^{\theta_1 t_f}}{2rk_s\left(\theta_1^2 m+\theta_1 b+k_s\right)} & \frac{\theta_2^2 e^{\theta_2 t_f}}{2rk_s\left(\theta_2^2 m+\theta_2 b+k_s\right)} & \theta_3 e^{\theta_3 t_f} & \theta_4 e^{\theta_4 t_f} \end{bmatrix} \begin{bmatrix} c_1 \\ c_2 \\ c_3 \\ c_4 \end{bmatrix} \tag{5.27}$$

from which c_1, c_2, c_3, and c_4 can be obtained.

The optimal control $F_m^*(t)$ in the first equation of (5.25) has been derived from necessary conditions of optimality (5.24). It can however be verified that $F_m^*(t)$ is unique and that it does indeed minimize the performance index (5.22) [10].

5.4.1.2 Simulation Testing

The optimal control response is now simulated for an FPE, again with the parameters listed in Table 5.1. The spring is of stiffness $k_s = 170$ kN/m, the damping coefficient is set at $b = 10$, while $r = 2$ in (5.22) and $t_f = 0.4$ seconds—the same start time as in the case of mechanical resonance in Fig. 5.2. Figure 5.4 shows the piston response which, as expected, satisfies the boundary conditions in the required start time. The piston does not exceed the cylinder end (solid line), although it does exceed the nominal top dead centre position (upper dotted line). Table 5.4.1.2 shows the clear superiority of

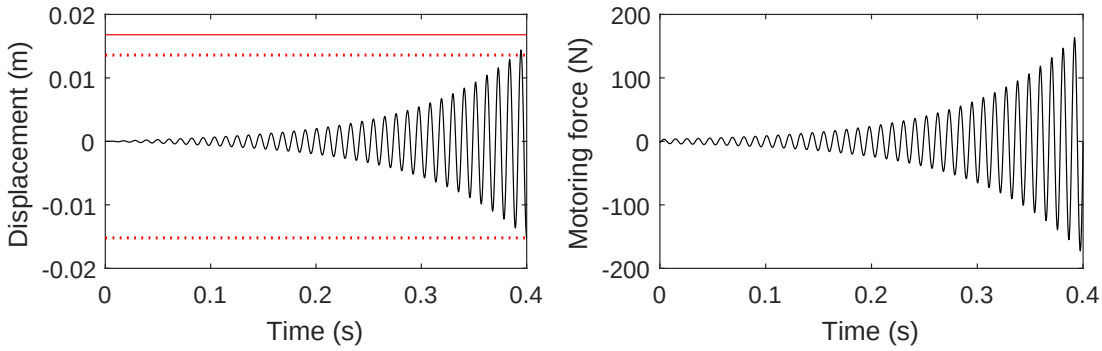

Figure 5.4: Optimal FPE start with spring as rebound device.

Table 5.2: Comparison of FPE Starting Strategies (Spring as Rebound Device)

	RMS force (N)	**Performance index**
Optimal strategy	44.3	1.57×10^3
Resonance strategy	62.7	1.26×10^4

optimal control compared to mechanical resonance: the optimal RMS force is lower by 29% while the optimal performance index J in (5.22) is less by a factor of 10.

5.4.2 Air bounce chamber as rebound device

5.4.2.1 Main Developments

Finally with a bounce chamber as rebound device, first consider both combustion and bounce chambers kept closed during start. Owing to alternate compression and expansion in the chambers, a driven piston (from a perturbed rest position) can be expected to oscillate about its rest position to new amplitudes. The task therefore is to optimally drive the piston until it acquires a large enough amplitude for combustion to begin.

However, as the dynamics are highly nonlinear, one cannot expect a closed-form solution for the optimal start problem and must instead rely on numerical approaches. To improve numerical tractability, a simplification is made where at least one of the gas chambers is open during start. This avoids the complication of having two polytropic

process nonlinearities (5.3) in the dynamics. The following starting procedure then applies:

Step 1. From the piston rest state; with an open bounce chamber (i.e. $F_{rd} = 0$) and open combustion chamber (i.e. $F_c = 0$), drive the piston to nominal top dead centre.

Step 2. Pressurize the bounce chamber i.e. fill it with air ($F_{rd} \neq 0$) and drive the piston to nominal bottom dead centre while keeping the combustion chamber open ($F_c = 0$).

At the nominal bottom dead centre position; when the motoring force is removed, the combustion chamber closed, and generation mode activated, the expanding air in the bounce chamber propels the piston to the nominal top dead centre position (assuming the bounce chamber is correctly pressurized) in a compression stroke towards the end of which combustion can start. The proposed starting procedure is relatively straight forward, but a price is paid with Step 2, where the motoring force must do work to compress the bounce chamber air *in a single stroke*. Consequently one can expect large motoring force amplitudes even with an optimal approach.

5.4.2.2 Simulation Testing

A numerical simulation is undertaken using optimisation software package GPOPS-II [90] to generate the response in Figure 5.5. Again, the chosen FPE parameters are those in Table 5.1 for a bounce chamber of compression ratio 12 and the performance index is (5.22) with $r = 2$. In GPOPS-II, the piston is constrained not to exceed the nominal bottom and top dead centre positions. The motoring force magnitude is also saturated at 500 N. The simulation encounters numerical tractability problems for many of the test cases attempted, for example in testing different final times t_f. Nonetheless the result produced in Figure 5.5 is achieved, although it may not

be globally optimal or even unique [61, 10]. Compared with the 4 N required for starting the FPE by mechanical resonance in 0.8 seconds in Fig. 5.3 (under frictionless assumptions), starting by mechanical resonance is the more practical approach for the case of a bounce chamber as rebound device.

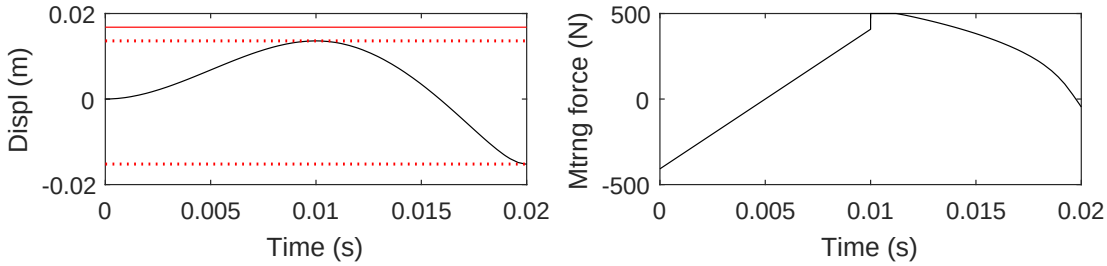

Figure 5.5: Optimal FPE start with bounce chamber as rebound device.

5.5 Chapter Conclusions

Two strategies for starting FPEs have been studied; these are with mechanical resonance and by optimal start. Readily implementable closed-form motoring force functions have been developed and tested where none had been previously advanced in the literature. For an FPE whose rebound device is a mechanical spring, the optimal strategy has been verified as superior with a significantly less root-mean-square motoring force and performance index than the resonance strategy. For an FPE whose rebound device is a bounce chamber, the optimal strategy should be better in principle, but can face numerical tractability hurdles. Here, a designed mechanical resonance strategy has been found adequate.

Chapter 6

Strategies for Misfire Mitigation and Compression Ratio Control using In-Stroke Motoring

6.1 Introduction

The failure of combustion to occur at or towards the end of a compression stroke—also known as misfire—is an undesirable but typical occurrence in free-piston engine (FPE) operation that can lead to instability in the form of stall [54, 53, 55]. Misfire stems from various causes and may be difficult to predict or completely prevent in practice. Accordingly, this chapter proposes strategies that ensure continued engine operation in spite of misfire; that is, misfire mitigation strategies. The strategies involve externally driving the piston within its stroke (the FPE electric machine being operated as a motor), a process referred to here as *in-stroke motoring*. This chapter also examines another use of in-stroke motoring: the control of compression ratio. The need for in-stroke motoring can therefore be viewed as an effort in the quest for stable and repeatable FPE cycles.

To achieve stable and indefinite FPE operation, the literature on FPE piston control has largely focused on the use of energy-based approaches [56, 57, 80, 81, 52, 39, 113] in ensuring the piston reaches target top and bottom dead-centre positions—thereby also controlling compression ratio (Chapter 4 provides a model-based method). With an energy-based approach, injected fuel mass introduced in the cylinder is regulated to ensure the piston reaches the bottom dead-centre (BDC) position, while the energy in a rebound device is regulated to ensure the piston subsequently reaches the top dead-centre (TDC) position. The rebound device energy is regulated either by varying gas mass (for the case of a bounce chamber rebound device) or by varying fuel supply (for the case of a combustion chamber rebound device). In the case of a mechanical spring rebound device, active energy regulation is avoided at the price of ensuring correct spring stiffness design for a given compression ratio and load (Section 4.4.1.2).

Despite the apparent success of energy-based compression ratio control strategies (i.e. via fuel and rebound-device energy regulation) in practice, supplementary or alternative control strategies may still be required to ensure stable and repeatable engine cycles [53, 54, 62]. Indeed, achieving stable operation is problematic for energy-based strategies when trying to achieve:

i) Sustained operation in the event of abnormal combustion such as misfire.

ii) Compression ratio control when faced with actuator precision limitations.

iii) Tracking of a desired piston trajectory.

These requirements can be addressed by exploiting the concept of in-stroke motoring, which refers to externally driving a piston whilst it traverses a stroke; implemented by operating the FPE's electrical machine as a motor rather than a generator.

In-stroke motoring has recently been verified under experimental conditions. Highly robust operation of an FPE has been demonstrated using a trajectory tracking strategy implemented with in-stroke motoring [63, 42]. It is reported in this study, that

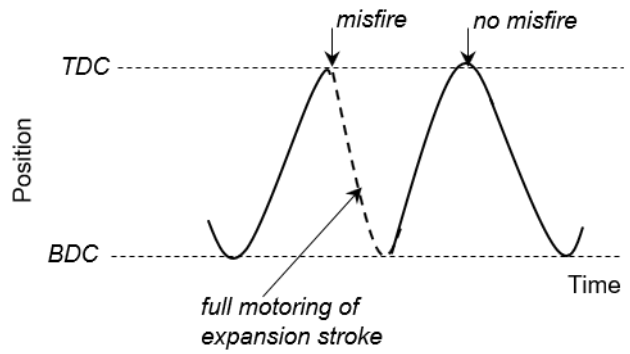

Figure 6.1: Illustration of in-stroke motoring where the entire expansion stroke is motored following a misfire. The piston is returned to BDC, allowing a full-length subsequent compression stroke. The engine does not stall provided energy is available for motoring.

the FPE maintains stable operation for several hours despite the occurrence of abnormal combustion events. More recently, stable compression ratio control has been demonstrated by partial motoring of the piston strokes towards BDC and TDC respectively [84]. The authors' motivation for the approach in [84] is to have power generation only take place in the high-piston-speed zone where generation efficiency is highest. Conversely, the low-piston-speed zone near BDC and TDC is left to compression ratio control with in-stroke motoring action.

Figures 6.1 and 6.2 illustrate the main idea behind in-stroke motoring as a control strategy. In Figure 6.1, the expansion stroke of the engine is fully motored following a misfire event, allowing subsequent operation to continue. By contrast, in an energy-based strategy, it would not be feasible to drive the piston back to BDC over an entire stroke with mere regulation of rebound device energy. In Figure 6.2, partially motoring the compression and expansion strokes towards their end ensures that a steady piston oscillation amplitude is maintained, and therefore also a steady compression ratio.

The ideas of in-stroke motoring reported in [63, 42, 84] have sound physical basis and are quite intuitive. But, they do not yet have general analytical grounding. In the

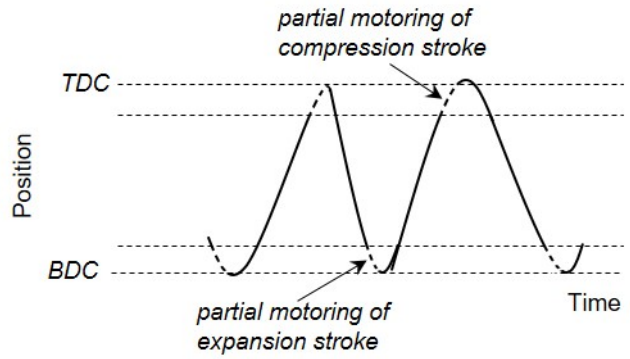

Figure 6.2: Illustration of in-stroke motoring where the expansion and compression strokes are partially motored. Steady piston amplitude and compression ratio are maintained.

current form, the ideas have limited scope for generalization.

In this chapter, in-stroke motoring as a control strategy for FPEs is put on a sound analytical footing. This is achieved by developing a model-based analytical approach which yields directly usable motoring force functions or profiles in addressing two control problems:

i) control to ensure sustained engine operation following a misfire event i.e. control for misfire mitigation, and,

ii) control of compression ratio during normal engine operation.

Accordingly, the objectives of the chapter are to demonstrate that in-stroke motoring can be developed under general conditions to provide a strategy for FPE misfire mitigation and compression ratio control. Towards this end, constant and dynamic in-stroke motoring forces are separately examined.

The analysis considers FPEs of two different rebound device types, namely a mechanical spring, and a bounce chamber. The main analytical results are verified by simulation.

6.2 Modelling

This section revisits an appropriate mathematical model of an FPE, which is used to construct the required control solutions. Figure 6.3 is used to show an idealized representation of a single piston two-stroke FPE. The engine comprises three major parts: a piston-translator assembly, known as the moving or active mass; a rebound device to return the piston to top-dead-centre from bottom-dead-centre; and an integrated electric machine for power generation or motoring function.

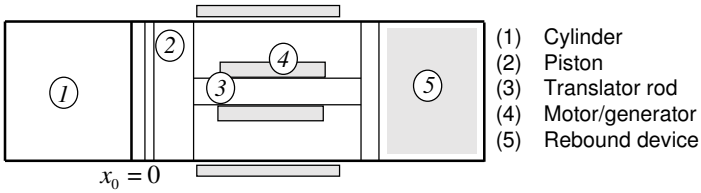

Figure 6.3: Idealized FPE generator schematic.

Defining the direction of the compression stroke as positive for piston displacement x_0, application of Newton's second law to the piston-translator mass m gives

$$-mx_0 = F_c + F_{rd} + F_{em} + F_f \tag{6.1}$$

where F_c is the force due to cylinder gas pressure in the combustion chamber, F_{rd} is the rebound device force, and F_f is the friction force. The instantaneous force created by the electric machine F_{em} is either an opposing or driving force, depending on the mode of operation, and is typically assumed to satisfy the equation

$$F_{em} = \begin{cases} \mu_g \dot{x}_0 & \text{generator mode} \\ F_m & \text{motor mode} \end{cases} \tag{6.2}$$

In generator mode, the force is assumed to be proportional to piston speed with constant parameter $\mu_g > 0$ dependent on the physical properties of the electric machine.

In motor mode, the driving force is denoted by F_m. The general control problem is to design F_m that ensures stable continuous engine operation following a misfire event (as depicted in Fig. 6.1), or that achieves a target compression ratio (as depicted in Fig. 6.2).

The cylinder gas pressure force is given by

$$F_c = A_p P_c \tag{6.3}$$

where A_p is the piston crown area, and P_c is the instantaneous cylinder pressure. Two models are adopted to describe the behavior of P_c. In all analytical work, P_c is assumed to vary as an adiabatic process, i.e.

$$P_c = \frac{K_c}{V_c^{\gamma_c}} \tag{6.4}$$

where K_c is a constant determined by the stroke (compression or expansion), $V_c = V_c(x_0)$ is the instantaneous cylinder volume which varies with piston position, and γ_c is the ratio of the specific heat capacities of the (gaseous) contents of the cylinder volume. In all simulations however, the model for P_c takes into account heat transfer exploiting the single-zone thermodynamic model [47]

$$\frac{dP_c}{dt} + \frac{\gamma_c}{V_c}\frac{dV_c}{dt}P_c = \frac{\gamma_c - 1}{V_c}\left(\frac{dQ_{ch}}{dt} - \frac{dQ_{ht}}{dt}\right) \tag{6.5}$$

where Q_{ch} is the gross heat release from the fuel burned, and Q_{ht} is the heat transfer through the cylinder walls. The heat transfer rates on the right-hand side of (6.5) are modelled by the equations

$$\frac{dQ_{ch}}{dt} = \eta_c Q_{LHV}\ m_f \frac{dx_\beta}{dt} \tag{6.6a}$$

$$\frac{dQ_{ht}}{dt} = hA_s(T_c - T_w) \tag{6.6b}$$

where the variables and parameters in (6.6) take on their usual meanings as stated in Section 2.3. The gas exchange process pressure involving scavenging, is assumed to be the instantaneous value at known pressure, obtained for example, from a scavenge pump.

The rebound device force takes different forms depending on the rebound device type, i.e. a mechanical spring or bounce chamber. Accordingly, the force is modelled as

$$F_{rd} = \begin{cases} k_s x_0 & \text{mechanical spring} \\ -A_{rd} P_{rd} & \text{bounce chamber} \end{cases} \tag{6.7}$$

where k_s is the spring stiffness, A_{rd} is the area of the translator surface interfacing with the bounce chamber, and P_{rd} is the bounce chamber pressure that varies in general according to a polytropic process

$$P_{rd} = \frac{K_{rd}}{V_{rd}^{\gamma_{rd}}} \tag{6.8}$$

where K_{rd} is a constant, $V_{rd} = V_{rd}(x_0)$ is the rebound device volume (dependent on piston position), and γ_{rd} is the polytropic process index for air.

The friction force is assumed to have a Coulomb friction and viscous friction component in the form

$$F_f = a_f \text{sgn}(\dot{x}_0) + b_f \dot{x}_0 \tag{6.9}$$

where a_f and b_f are empirical parameters obtained by measurement.

With a model in place, the task of designing a motoring force for misfire mitigation and compression ratio control is now addressed. Two strategies are examined: i) a simple approach involving the construction of a constant motoring force, and ii) a more involved task of finding a dynamic motoring force. These approaches are developed in the subsequent sections starting with constant force motoring. In both

cases the ability of the proposed motoring profile to meet the requirement is checked by simulation.

6.3 Constant Force In-Stroke Motoring

The motivation to find a constant in-stroke motoring force stems from practical considerations where it is expected that a constant motoring force (with constant armature current) will be much easier to implement than a dynamic motoring force. The use of a constant force will address both requirements for misfire mitigation and compression ratio control; culminating in a boundary value problem (BVP). To begin with, some analytical generalities of constant force motoring are outlined. This is followed by respective subsections addressing misfire mitigation and compression ratio control.

6.3.1 Main Developments of Constant Force In-Stroke Motoring

When the electric machine is in motoring mode, the force in (6.2) is

$$F_{em} = F_m \tag{6.10}$$

where F_m is a *constant* to be found. The analysis can be much simplified by linearizing the cylinder gas and rebound device forces about a point along the piston stroke. This is achieved by taking the first two terms in a Taylor series expansion of (6.3) and (6.7) about $x_0 = 0$ producing the linear forms

$$F_c \approx A_p K_c \left(\alpha_c + \beta_c x_0\right) \tag{6.11a}$$

$$F_{rd} \approx \alpha_{rd} + \beta_{rd} x_0 \tag{6.11b}$$

where α_i, β_i $(i = c, rd)$ are constants. In (6.11a), $\alpha_c = V_c^{\gamma_c}(0)$, $\beta_c = \partial V_c^{\gamma_c}(0)/\partial x_0$ and in (6.11b), $\alpha_{rd} = 0$, $\beta_{rd} = k_s$ if the rebound device is a mechanical spring, or $\alpha_{rd} = -A_p K_{rd} V_{rd}^{\gamma_{rd}}(0)$, $\beta_{rd} = -A_p K_{rd} \partial V_{rd}^{\gamma_{rd}}(0)/\partial x_0$ if the rebound device is a bounce chamber.

By using (6.9)–(6.11), the FPE dynamics simplify to

$$\ddot{x}_0 + \gamma \dot{x}_0 + \omega_0 x_0 = F_0 \tag{6.12}$$

where

$$F_0 = -\frac{F_m + A_p K_c \alpha_c + \alpha_{rd} + a_f \text{sgn}(\dot{x}_0)}{m} \tag{6.13a}$$

$$\omega_0^2 = \frac{A_p K_c \beta_c + \beta_{rd}}{m} \tag{6.13b}$$

$$\gamma = \frac{b_f}{m} \tag{6.13c}$$

Equation (6.13a) can easily be rearranged to give an expression for F_m as follows

$$F_m = -\left(mF_0 + A_p K_c \alpha_c + \alpha_{rd} + a_f \text{sgn}(\dot{x}_0)\right) \tag{6.14}$$

such that by considering dynamics (6.12), determination of F_0 required to meet a given control objective for dynamics (6.12) is done first, after which the motoring force F_m is calculated from (6.14).

Both control objectives of interest (i.e. misfire mitigation and compression ratio control) both pose the following question: With (6.12) representing the simplified FPE dynamics within a given stroke, what value of F_0 is required to drive the piston from some initial state (x_i, v_i) within a stroke, to a terminal state $(x_f, v_f = 0)$ at the end of the stroke? The goal here is to find a parameter which satisfies this boundary value problem. Finding the solution exploits (6.12); a linear second-order equation

with constant forcing, and with a general solution [94]

$$x_0(t) = e^{-\frac{\gamma}{2}t}\left(A_1\cos(\omega_u t) + A_2\sin(\omega_u t)\right) + \bar{F}_0 \tag{6.15}$$

where

$$\bar{F}_0 = \frac{F_0}{\omega_0^2} \tag{6.16a}$$

$$\omega_u = \omega_0\sqrt{1 - \left(\frac{\gamma}{2\omega_0}\right)^2} \tag{6.16b}$$

and where A_1 and A_2 are constants determined by the initial conditions (x_i, v_i), with dependence on $\bar{F}_0$ as

$$A_1(\bar{F}_0) = x_i - \bar{F}_0 \tag{6.17a}$$

$$A_2(\bar{F}_0) = \frac{v_i + \frac{\gamma}{2}\left(x_i - \bar{F}_0\right)}{\omega_u} \tag{6.17b}$$

At the boundary $(x_f, v_f = 0)$, the first derivative of $x_0(t = t_f)$ is

$$\dot{x}_0(t_f) = 0 \tag{6.18}$$

where t_f is the time taken from (x_i, v_i) at $t = 0$ to $(x_f, v_f = 0)$. Applying the general solution given by (6.15)–(6.17) to (6.18) yields

$$-\frac{\gamma}{2}e^{-\frac{\gamma}{2}t}\left(A_1\cos(\omega_u t_f) + A_2\sin(\omega_u t_f)\right) + e^{-\frac{\gamma}{2}t}\left(-A_1\omega_u\sin(\omega_u t_f) + A_2\omega_u\cos(\omega_u t_f)\right) = 0 \tag{6.19}$$

which can be simplified to

$$e^{-\frac{\gamma}{2}t}B\sin(\omega_u t_f + \phi) = 0, \tag{6.20}$$

which when expanded and manipulated with the substitutions

$$B\sin(\phi) = \omega_u A_2 - \frac{\gamma}{2} A_1 \tag{6.21a}$$

$$B\cos(\phi) = -\omega_u A_1 - \frac{\gamma}{2} A_2 \tag{6.21b}$$

recovers the original equation (6.19). Dividing (6.21a) by (6.21b) gives

$$\phi(\bar{F}_0) = \tan^{-1}\left\{ \frac{\omega_u A_2(\bar{F}_0) - \frac{\gamma}{2} A_1(\bar{F}_0)}{-\left(\omega_u A_1(\bar{F}_0) + \frac{\gamma}{2} A_2(\bar{F}_0)\right)} \right\} \tag{6.22}$$

where dependence on $\bar{F}_0$ follows from (6.17). Returning to (6.20), one finds

$$\omega_u t_f + \phi = \sin^{-1}(0) = n\pi \qquad n = 1, 2, 3, \ldots \tag{6.23}$$

Since the motion of interest occurs between the boundary conditions within one stroke, setting $n = 1$ in (6.23) gives t_f as

$$t_f(\bar{F}_0) = \frac{\pi - \phi(\bar{F}_0)}{\omega_u} \tag{6.24}$$

Three unknowns in the problem have thus far been solved, namely A_1, A_2, and t_f in (6.17a), (6.17b), and (6.24) respectively—all of which depend on $\bar{F}_0$. The remaining unknown,$\bar{F}_0$, is solved from (6.15) at $t = t_f$; i.e. from the equation

$$x_f = A(\bar{F}_0) e^{-\frac{\gamma}{2} t_f(\bar{F}_0)} \sin\left(\omega_u t_f(\bar{F}_0) + \theta(\bar{F}_0)\right) + \bar{F}_0 \tag{6.25}$$

where

$$A(\bar{F}_0) = \sqrt{A_1(\bar{F}_0^2 + A_1(\bar{F}_0^2))} \tag{6.26a}$$

$$\theta(\bar{F}_0) = \tan^{-1}\left(\frac{A_1(\bar{F}_0)}{A_2(\bar{F}_0)}\right) \tag{6.26b}$$

Equation (6.25) is a highly nonlinear equation from which $\bar{F}_0$ is calculated. The solution is used in (6.16a) to compute parameter F_0 in (6.12). The required motoring force F_m is then calculated from (6.14), thereby completing the analysis.

6.3.2 Misfire Mitigation with Constant Force In-Stroke Motoring

The first application of the above analysis is now demonstrated as one of ensuring sustained engine operation after misfire, i.e. misfire mitigation. Misfire is to be considered as a failure of the air-fuel mixture to ignite at the end of a compression stroke. There are several causes of misfire which are determined by thermodynamic conditions in the cylinder [100, 47]. Without intervention, misfire in an FPE results in engine stall because the expansion stroke following a misfire does not compress the rebound device sufficiently to achieve adequate piston return.

The proposed mitigation here is to motor the piston from the point of misfire to BDC. This so-called 'full-stroke' motoring of the expansion stroke is illustrated in Figure 6.1, and ensures no stall provided motoring energy is available. Accordingly, assuming misfire occurs at TDC, the initial and final piston states for in-stroke motoring are expressed as

$$x_i = x_T, \quad v_i = 0 \tag{6.27a}$$

$$x_f = x_B, \quad v_f = 0 \tag{6.27b}$$

where x_T and x_B denote the piston displacement at TDC and BDC respectively. And for simplicity, assume friction is negligible, i.e. $a_f = 0$, $b_f = 0$ in (6.9), therefore from (6.13c)

$$\gamma = 0 \tag{6.28}$$

When assumptions (6.27) and (6.28) hold, Equations (6.12)–(6.24) yield the following conditions:

$$A_1 = x_T - \bar{F}_0,\ A_2 = 0,\ \omega_u = \omega_0,\ \phi = 0,\ t_f = \frac{\pi}{\omega_0},\ \theta = \frac{\pi}{2} \tag{6.29}$$

which, when applied to (6.25), generate the simple equation

$$x_B = -(x_T - \bar{F}_0) + \bar{F}_0 \tag{6.30}$$

And with the use of (6.16a), gives the expression for F_0, i.e.

$$F_0 = \frac{1}{2}\omega_0^2(x_T + x_B) \tag{6.31}$$

The use of (6.31) in (6.14) gives the required motoring force F_m for the relevant type of rebound device.

6.3.2.1 Simulation Testing

Numerical simulation is now used to assess the effectiveness of the proposed analysis in (6.10)–(6.31) in finding a constant motoring force to mitigate against misfire. Two different types of rebound device are examined: first a mechanical spring, and second, a bounce chamber. Parameter details for the FPE and the simulations are given in Table 6.1. A misfire is simulated as a no-combustion event at which point the generator is switched to operate as a motor. The constant motoring force needed to drive the piston towards nominal BDC is computed from (6.31) and (6.14).

Mechanical Spring as Rebound Device With a mechanical spring as the rebound device, Fig. 6.4a shows the piston position as a function of time, with a misfire triggered between 0.33 and 0.34 seconds. The broken line section of the response

Table 6.1: Simulation Parameters

Parameter	**Value**	**Parameter**	**Value**
bore	86 mm	m	9 kg
stroke(nominal)	86 mm	a_f	10
cylinder comp. ratio (nominal)	10.44	b_f	0
bounce chamber comp. ratio (nominal)	10	k_s	5.1 kN/m
ambient pressure	1 bar	μ_g(expansion)	0.1 kg/s
ambient temperature	25 °C	μ_g(compression)	0 kg/s

corresponds to the piston being driven by the constant motoring force. It can be seen that the piston is returned to a position very near to the nominal BDC as expected. This creates a subsequent compression stroke of acceptable length to allow continued engine operation in generation mode. Had the motoring force been some way above or below the computed level, the piston would have missed the BDC target, potentially leading to component damage or stall. Figure 6.4b shows the in-cylinder pressure trace over a longer time period showing two minima peaks corresponding to two misfire events, where for convenience of scaling, the second minimum (which occurs just before 0.7 seconds) is not corresponded to in Fig. 6.4a. It is evident that the engine exhibits sustained operation with consistent pressure peaks despite intermittent misfiring. Figure 6.4c shows the electrical machine force profile over the same duration as shown in Figure 6.4b. The negative section of the machine force corresponds to power generation while the positive section corresponds to constant force motoring.

Bounce Chamber as Rebound Device With a bounce chamber as rebound device, Figure 6.5 shows the simulated piston position as a function of time, with a misfire triggered between 0.38 and 0.39 seconds. It can be seen that the motoring force applied in this instance is not sufficient to drive the piston back to nominal BDC. This is an indication that the linearization approach developed in (6.16)–(6.31) to compute the motoring force has broken down. The problem stems from use of a

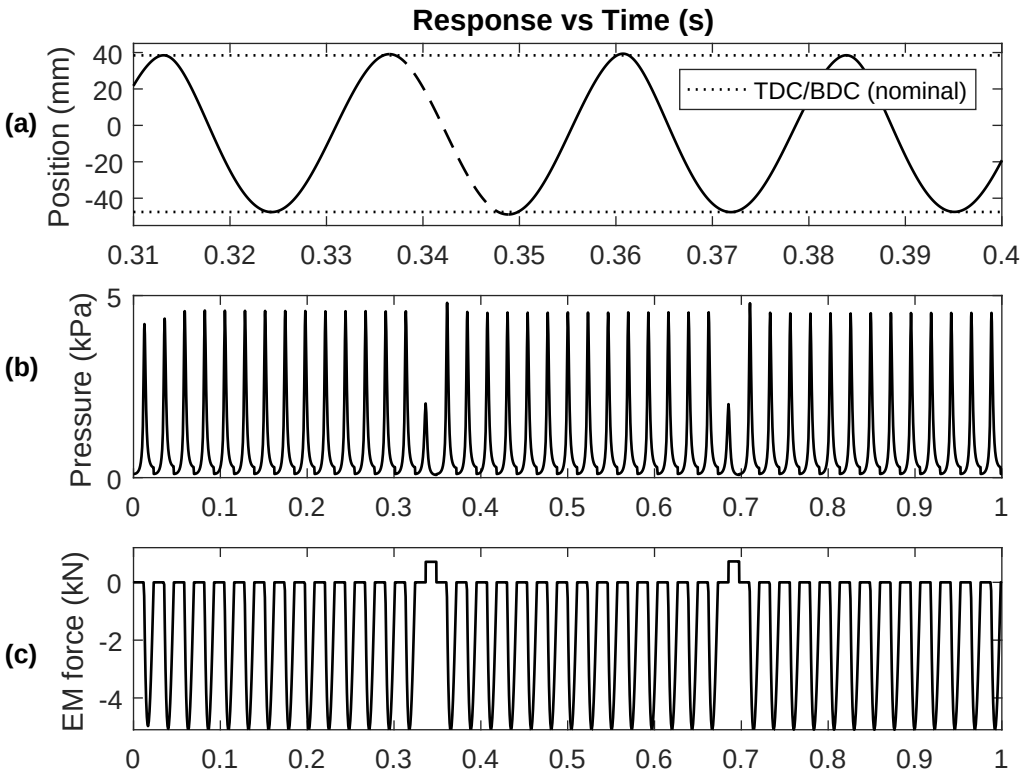

Figure 6.4: Time responses of piston position in (a), in-cylinder pressure in (b), and electric machine force in (c) where FPE rebound device is a mechanical spring. The FPE sustains operation after two misfire events owing to motoring of the entire expansion stroke following a misfire.

bounce chamber as rebound device which results in the FPE dynamics containing two strong nonlinearities which appear respectively in the cylinder pressure (6.4) and bounce chamber pressure (6.8). To address the shortcoming of linearization, a more direct approach is examined to compute the motoring force F_m numerically by solving the BVP associated with FPE nonlinear dynamics (6.1) and boundary conditions (6.27), using the Matlab BVP solver with the bvp4c function. Here, F_m takes the form

$$F_m = \bar{F}_m \text{sgn}(\dot{x}_0) \tag{6.32}$$

where $\bar{F}_m$ is a constant parameter to be found as a solution to the BVP. Using the solution obtained, the piston response is shown in Figure 6.6a, showing a good

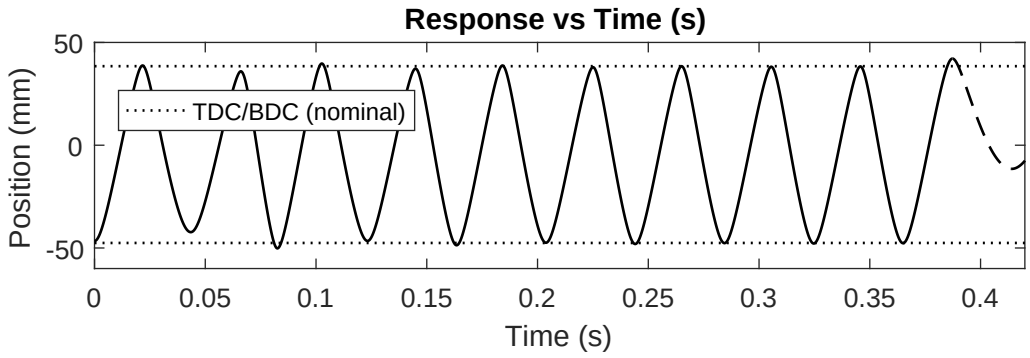

Figure 6.5: Time response of piston position where FPE rebound device is a bounce chamber. A sufficiently large force was not produced to motor the piston to nominal BDC following a misfire.

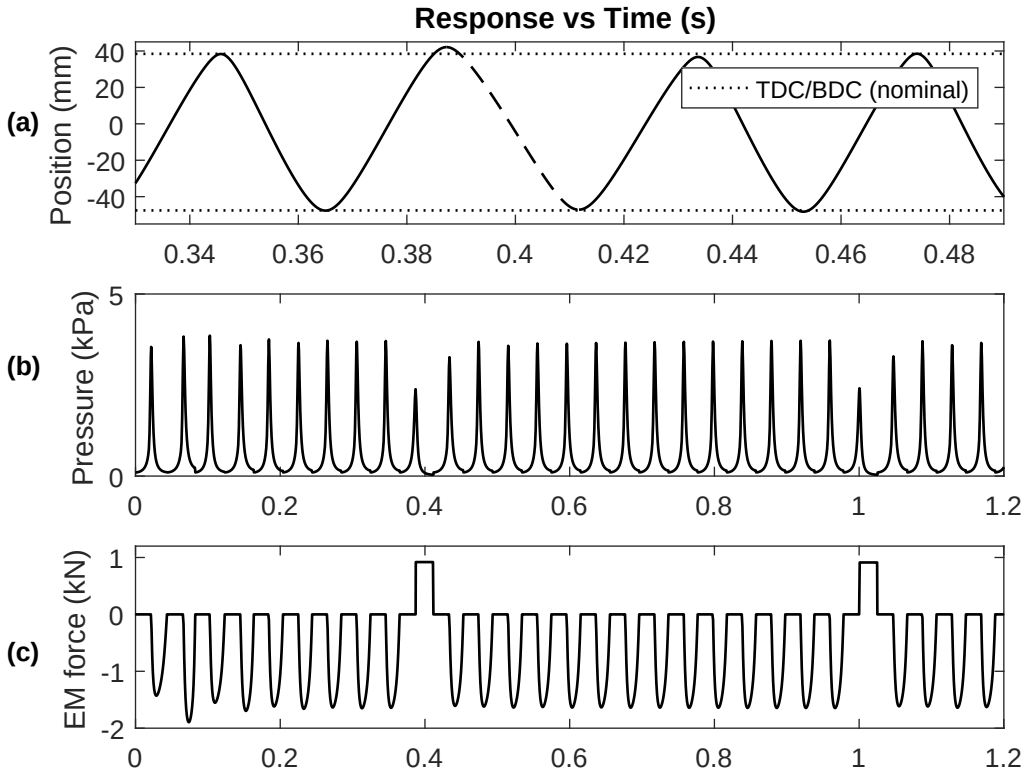

Figure 6.6: Time responses of piston position in (a), in-cylinder pressure in (b), and electric machine force in (c) where FPE rebound device is a bounce chamber. The FPE sustains operation after two misfire events owing to motoring of the entire expansion stroke following a misfire.

recovery from misfire. Figures 6.6b and 6.6c show the corresponding pressure and electric machine force histories, similar to Figures 6.4b and 6.4c. Overall, following

a misfire event, the simulations confirm that a constant force in-stroke motoring strategy results in sustained engine operation.

6.3.3 Compression Ratio Control with Constant Force In-Stroke Motoring

Compression ratio control using in-stroke motoring involves motoring the piston only towards the end of a stroke (i.e. partial motoring, as compared to full motoring seen earlier) so as to achieve a desired stroke and therefore also a desired compression ratio (Figure 6.2). The piston is guided to reach either target BDC or TDC at the end of the respective expansion or compression stroke. The basis of this control strategy was proposed in [84] where experimental success was reported but without any supporting analytical development. The strategy is an alternative to the energy-based compression ratio control strategies where fuel and rebound device energy are regulated to achieve a compression ratio target.

Here, for demonstration purposes, only the expansion stroke is partially motored. It is assumed that by assisting the piston to reach nominal BDC at the end of the expansion stroke, the rebound device has acquired sufficient energy to return the piston to nominal TDC in the subsequent compression stroke. Accordingly, denoting ($x_b \neq 0$,$v_b \neq 0$) as the piston state at which motoring begins within the expansion stroke, gives piston motion boundary conditions

$$x_i = x_b, \quad v_i = v_b \tag{6.33a}$$

$$x_f = x_B, \quad v_f = 0 \tag{6.33b}$$

However, even assuming negligible friction, the boundary conditions defined by (6.33) do not lead to simplification of (6.25) (as was the case for misfire mitigation where $(x_i, v_i) = (x_T, 0)$). Equation (6.25) must therefore be solved numerically for $\bar{F}_0$,

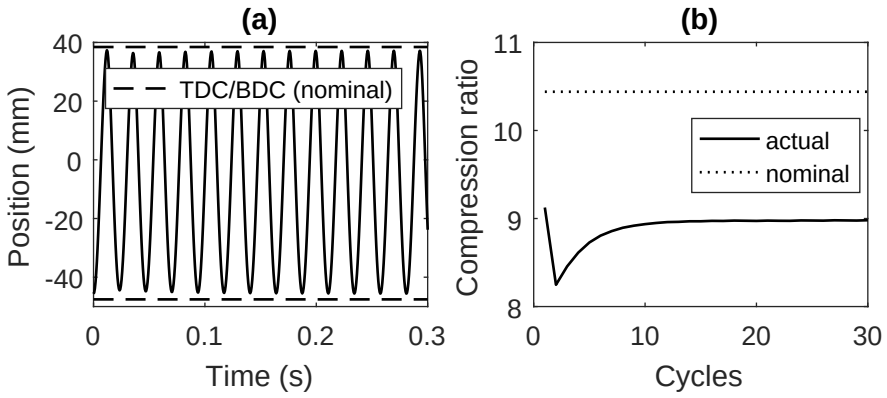

Figure 6.7: Unassisted piston response where the piston does not reach nominal BDC or nominal TDC in (a). Correspondingly, the compression ratio is below nominal in (b). FPE rebound device is a mechanical spring.

for example using a root-finding algorithm such as the bisection method [26]. The solution is then used in (6.16a) to compute F_0 in (6.12), from which the required motoring force F_m is computed from (6.14).

6.3.3.1 Simulation Testing

A simulation is now conducted to assess compression ratio control with constant force motoring using the analysis described below Equation (6.33). Again, two types of rebound device are considered, namely a mechanical spring and a bounce chamber. Simulation parameter details remain as in Table 6.1.

Mechanical Spring as Rebound Device Where a mechanical spring is the rebound device, Fig. 6.7a shows a piston response without in-stroke motoring. It is evident that neither the compression nor expansion strokes reach the target TDC or BDC positions. The result, as shown in Figure 6.7b, is that the compression ratio falls well short of the nominal value of 10.44. By contrast, the outcome is successful when, for the last portion of its journey towards BDC, the piston expansion stroke is partially motored with a constant force computed via Equation (6.14). By commencing motoring at a point corresponding to the dotted horizontal line in Figure 6.8a, it

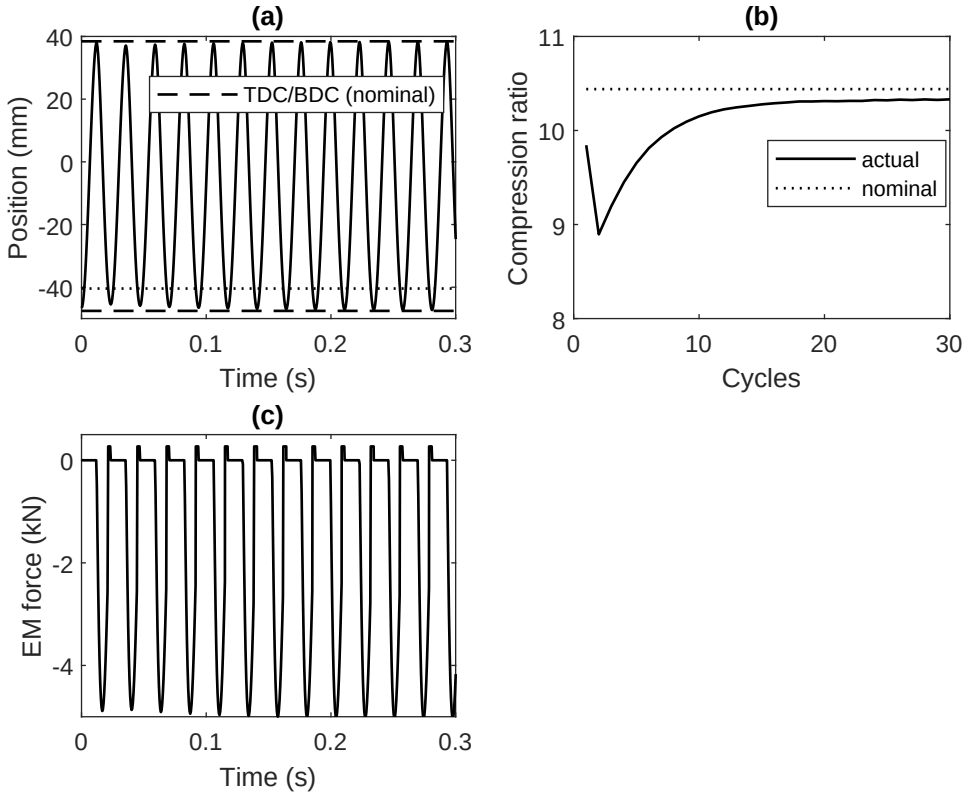

Figure 6.8: Assisted, or partially motored piston response towards nominal BDC (a). Compression ratio response accordingly converges close to nominal (b). Electric machine force (c). FPE rebound device is a mechanical spring.

is evident that a full-length expansion stroke is achieved. A corresponding full-length compression stroke is also achieved, owing to the correctly selected spring stiffness (Section 4.4.1.2). And as shown in Figure 6.8b, the compression ratio converges towards the target value of 10.44.

Bounce Chamber as Rebound Device Where a bounce chamber is the rebound device, an unassisted piston response (without in-stroke motoring) is shown in Figure 6.9a, where the expansion stroke does not reach nominal BDC. Accordingly, in Figure 6.9b, the compression ratio is well below the nominal value 10.44. A constant motoring force is then modelled as (6.32) and obtained by numerical solution of the BVP defined by nonlinear dynamics in (6.1) and boundary conditions (6.33). Applica-

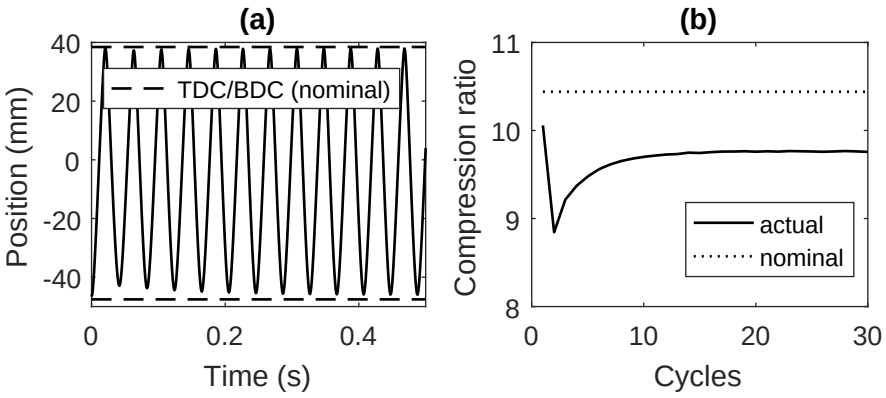

Figure 6.9: Unassisted piston response where the piston does not reach nominal BDC or nominal TDC in (a). Correspondingly, the compression ratio is below nominal in (b). FPE rebound device is a bounce chamber.

tion of the force obtained, results in successful piston progress towards nominal BDC, which is confirmed in Figure 6.10a (the force is applied starting from the horizontal dotted line). Full-length expansion stroke is achieved, as is the corresponding full-length compression stroke, again owing to assignment of the correct bounce chamber air mass (analogous to assignment of correct spring stiffness in Section 4.4.1.2). Figure 6.10b, in contrast to Figure 6.9b, shows the compression ratio converging closer to target compression ratio.

6.4 Dynamic Force In-Stroke Motoring

In-stroke motoring is now considered with a dynamic motoring force rather than a constant force investigated in Section 6.3. Constructing a dynamic motoring force makes it possible to adopt advanced motoring schemes, for example piston trajectory tracking. Whereas experimental investigation of piston trajectory tracking using various approaches can be found in the literature [63, 42, 70], the novelty here is the development of a piston trajectory tracking scheme based on sliding mode control, with misfire mitigation as the control objective in focus. Sliding mode control is chosen here for its robustness to modelling uncertainty [91].

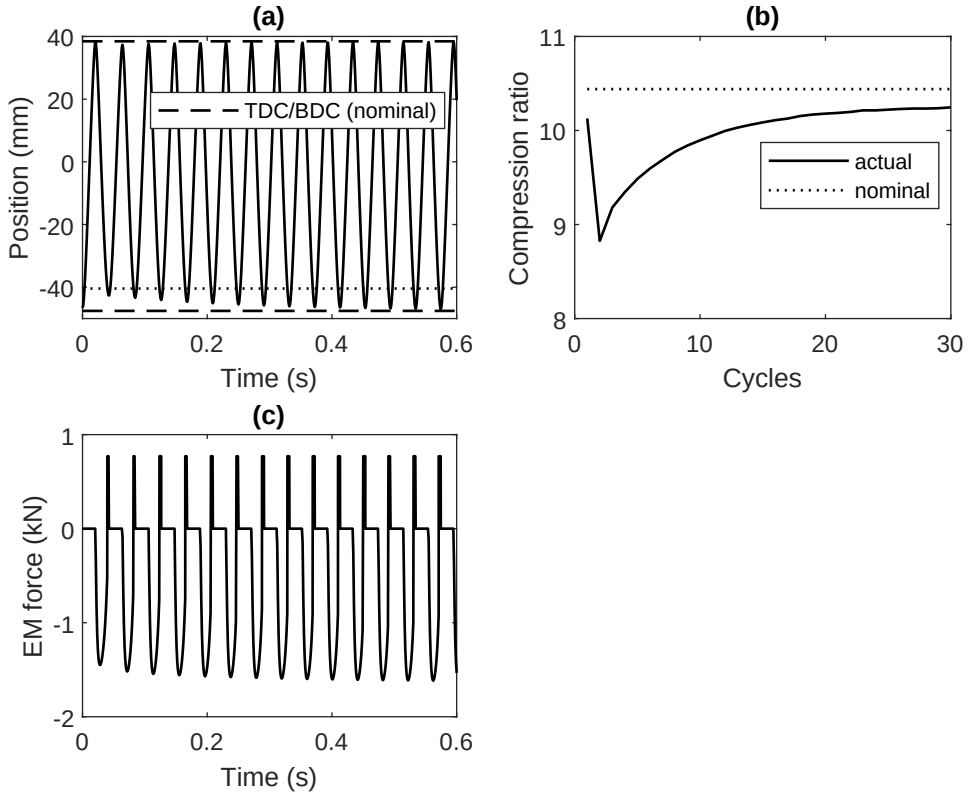

Figure 6.10: Assisted, or partially motored piston response towards nominal BDC in (a). Compression ratio response accordingly converges close to nominal in (b). Electric machine force (c). FPE rebound device is a bounce chamber.

It is acknowledged that the idea of controlling the entire piston trajectory (i.e. the entire cycle) is also appealing, such as investigated by Li et al. [68, 70] where an FPE is designed to follow a conventional engine piston profile. However, trajectory tracking constitutes *active* piston motion control—a necessarily energy demanding proposition. Accordingly, the benefits (such as controlled emissions formation [82, 79]) must be carefully weighed with the costs in a given application.

In what follows, the general ideas of dynamic motoring for trajectory tracking are developed and applied to misfire mitigation. Testing by numerical simulation is then performed.

6.4.1 Main Developments of Dynamic Force In-Stroke Motoring

To begin, the electrical machine of the FPE is set to motor mode as in (6.2), and the state variables are defines to be $x_1 = x_0$, $x_2 = \dot{x}_1$ with the selected output as $y = x_0$. From (6.1), the state and output equations of an FPE for a given stroke are

$$\dot{x}_1 = x_2 \tag{6.34a}$$

$$\dot{x}_2 = f(x) + gF_m + \Delta(x,t) \tag{6.34b}$$

$$y = x_1 \tag{6.34c}$$

where $x = \begin{bmatrix} x_1 & x_2 \end{bmatrix}$,

$$f(x) = -\frac{1}{m}\left(F_c + F_{rd} + F_f\right) \tag{6.35a}$$

$$g = -\frac{1}{m} \tag{6.35b}$$

and where $\Delta(x,t)$ in (6.34) represents a bounded uncertainty that may vary with the state and time, i.e. $|\Delta(x,t)| < \Delta_{max}$.

Given a desired output trajectory $y_d(t)$, the objective is to design a dynamic motoring force F_m, so that $y(t)$ tracks $y_d(t)$. A sliding mode controller is designed to satisfy this objective owing to its well-known robustness properties [91]. To start the controller design, define the tracking error as

$$e_0(t) = y(t) - y_d(t) \tag{6.36}$$

such that when $y = y_d$ the trajectory tracking error $e_0 = 0$. Accordingly, the next

step is to define a so-called sliding surface

$$s_0(e_0) = 0 \tag{6.37}$$

on which e_0 diminishes , i.e. 'slides' to zero. It is common to define the left-hand side of (6.37) (i.e. the so-called switching function) in the general form

$$s_0(e_0) = \dot{e}_0 + p_0(e_0) \tag{6.38}$$

which, by choice of p_0, determines the nature of the convergence of e_0 to zero. For example, if p_0 is selected as

$$p_0(e_0) = \alpha_0 |e_0|^{\rho_0} \text{sgn}(e_0), \qquad \alpha_0 > 0,\ 0 < \rho_0 < 1 \tag{6.39}$$

e_0 converges to zero in finite time (as opposed to asymptotic convergence). It is apparent therefore that in order to achieve trajectory tracking, the sliding surface constraint given by (6.37) must be enforced. A controller that enforces (6.37) is a sliding mode controller. Indeed, consider the controller

$$F_m = -\frac{1}{g}\left(f(x) - \ddot{y}_d + \dot{p}_0(e_0) + K\text{sgn}(s_0)\right) \tag{6.40}$$

where K is a positive parameter. From the output equation (6.34c), $\ddot{y} = \dot{x}_2$. Thus, putting (6.40) into (6.34c) yields

$$\ddot{y} = \ddot{y}_d - \dot{p}(e_0) - K\text{sgn}(s_0) + \Delta \tag{6.41}$$

Equation (6.41) can be re-arranged and used with (6.36) to give

$$\ddot{e}_0 + \dot{p}_0(e_0) = -K\text{sgn}(s_0) + \Delta \tag{6.42}$$

And using (6.38) in (6.42) produces the equation

$$\dot{s}_0 = -K\text{sgn}(s_0) + \Delta \tag{6.43}$$

from which it follows that $s_0(e_0)$ converges to zero in finite time provided $K > \Delta_{max}$. The controller defined by (6.40) is notably discontinuous at $s_0 = 0$ owing to the sign term. Therefore, when implemented, this controller will unfortunately exhibit the well-known and undesirable 'chattering' phenomenon (i.e. high frequency switching behaviour in the control signal) [67]. A common way to avoid chattering is to replace the sign term with a continuous approximation. This method is simple but undermines controller robustness [98]. An alternative method, using high-order sliding modes, has been proposed [64]. The idea is to design a controller that is discontinuous, not in the control, but in the control derivative. More involved approaches for second and higher order sliding mode controllers can be found in [65, 66].

A simple approach to realizing high order sliding mode controllers is developed here similar to the Wu, Yu and Man [110] second order sliding mode controller approach. This approach considers a second sliding surface

$$s_1(s_0) = 0 \tag{6.44}$$

on which s_0 is required to decay to zero in finite time. Accordingly, similar to (6.38), the left hand-side of (6.44) takes the general form

$$s_1(s_0) = \dot{s}_0 + p_1(s_0) \tag{6.45}$$

where p_1 can be selected as

$$p_1(s_0) = \alpha_1 |s_0|^{\rho_1} \text{sgn}(s_0), \qquad \alpha_1 > 0,\ 0 < \rho_1 < 1 \tag{6.46}$$

to ensure finite time convergence of s_0 in (6.44). The controller is now proposed in the form

$$\dot{F}_m = -\frac{1}{g}\left(\dot{f}(x) - \dddot{y}_d + \ddot{p}_0(e_0) + \dot{p}_1(s_0) + K\text{sgn}(s_1)\right) \tag{6.47}$$

where K is a sufficiently large positive parameter. The controller defined by (6.47) is in the form of a discontinuous time-derivative of the control. The actual control, realized by time integration of (6.47), is time-continuous and therefore does not exhibit chattering. To show that the controller enforces the sliding mode constraint equation (6.44), consider the second time derivative of $s_0(e_0)$, in (6.37), i.e.

$$\ddot{s}_0(e_0) = \dddot{e}_0 + \ddot{p}_0(e_0) \tag{6.48}$$

which, by using (6.36), evaluates as

$$\ddot{s}_0(e_0) = \dot{f}(x) + g\dot{F}_m - \dddot{y}_d + \ddot{p}_0(e_0) \tag{6.49}$$

Applying the control (6.47) in (6.49) gives

$$\ddot{s}_0(e_0) = -\dot{p}_1(s_0) - K\text{sgn}(s_1) + \dot{\Delta} \tag{6.50}$$

which can be rewritten as

$$\frac{d}{dt}\left\{\dot{s}_0(e_0) + p_1(s_0)\right\} = -K\text{sgn}(s_1) + \dot{\Delta} \tag{6.51}$$

or equivalently, using (6.45), as

$$\dot{s}_1 = -K\text{sgn}(s_1) + \dot{\Delta} \tag{6.52}$$

in which s_1 decays to zero in finite time provided $K > \dot{\Delta}_{max}$, where $|\dot{\Delta}| < \dot{\Delta}_{max}$. This completes the general development of a trajectory tracking controller for dynamic in-

stroke motoring.

6.4.2 Misfire Mitigation with Dynamic Force In-Stroke Motoring

The trajectory tracking controller developed in Section 6.4.1 is now specialized to misfire mitigation. This involves motoring the piston from the point of misfire to BDC, so that the piston follows a desired trajectory. The choice of trajectory can be based on the following guidelines:

i) For a trajectory to be admissible, it must be a physically viable path for a piston to track.

ii) In following an admissible trajectory, the path tracked by the piston is such that the piston experiences only minor departure from its nominal operating frequency.

Both requirements above are fulfilled if a desired trajectory $y_d(t)$ is generated by an FPE reference model generated from the FPE dynamics in (6.1), i.e.

$$-m\ddot{y}_d = F_{c_d} + F_{rd_d} + F_{f_d} + F_{em_d} \tag{6.53}$$

where subscript d denotes 'desired'. When following a trajectory generated by (6.53), the piston tracks a virtual piston path corresponding to a piston with identical physical properties. Thus, path planning based on (6.53) can be such that it yields a trajectory $y_d(t)$ that the piston would have followed had no misfire occurred.

6.4.3 Simulation Testing

A simulation is now conducted to assess performance of the developed trajectory tracking controller in the event of a misfire. The rebound device is a mechanical spring, and Table 6.1 remains as the reference for FPE simulation parameters. Two misfire events are to be triggered, and, upon misfire detection, the proposed second order sliding mode trajectory tracking scheme (6.47) is to be activated for returning the piston to BDC. The desired trajectory to be tracked is to be generated from (6.53) as one which the piston would have traversed had the misfire not occurred. For finite-time trajectory tracking, (6.39) and (6.46) are respectively selected for (6.38) and (6.45). Figure 6.11a shows the piston position response with two misfire cycles.

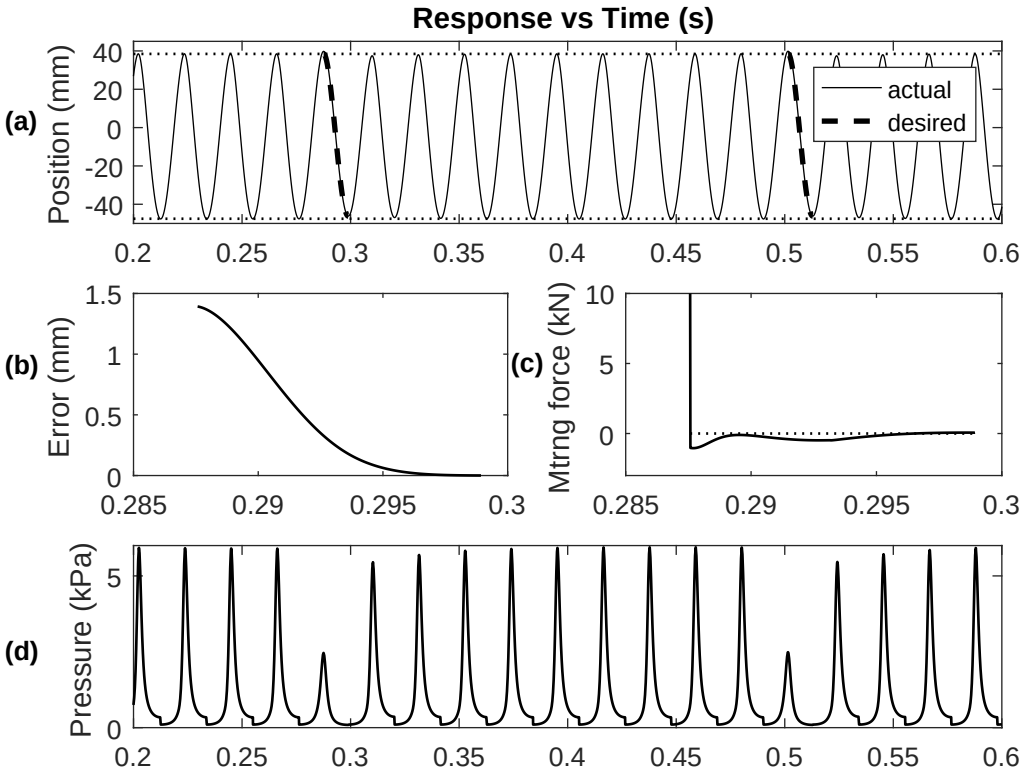

Figure 6.11: Time response of piston position in (a), trajectory tracking error in expansion stroke following misfire in (b), motoring force in expansion stroke following misfire in (c) and in-cylinder pressure in (d). FPE rebound device is a mechanical spring.

It is seen that engine operation remains virtually uninterrupted despite the misfire events just before 0.3 and 0.55 seconds. The piston tracks the desired trajectory almost exactly, thereby maintaining the engine operating frequency. Figure 6.11b is the trajectory tracking error, which is seen to converge to zero in finite time. The corresponding motoring force is shown in Figure 6.11c. The force is continuous as expected, although it exhibits an initial spike to ensure good tracking performance. In practice, the motoring force must be saturated to a level in line with the maximum current rating of the motor. Here, the motoring force was saturated at 10kN. An in-cylinder pressure trace is finally provided in Fig. 6.11d to clearly show the two misfire events at the trace's minima peaks, and pressure peak recovery following the misfire events. The simulation results were qualitatively no different when the FPE was simulated with a bounce chamber rebound device.

6.5 Chapter Conclusions

The concept of in-stroke motoring in free-piston engines has been analytically developed for applications in misfire mitigation and compression ratio control. The developments have been motivated not only by the limitations of energy-based control strategies, but also by the need to build an analytical basis for recent experimental work involving in-stroke motoring. Accordingly, formal concept development has been added to what has been available as promising test results in the broader area of free-piston engine control. The strategies presented are well-suited to take advantage of already existing highly developed motor control technology when implemented in practice.

Chapter 7

Estimation of In-Cylinder Pressure and Piston Speed

7.1 Introduction

Engine performance optimization and diagnostics requires knowledge of key operational variables such as engine speed and combustion pressure [95]. This information is usually supplied by sensors. However, the number of sensors that may be placed on an engine is constrained by cost and technical limitations. Pressure sensors in particular are notoriously costly and for this reason not installed on production engines, even though a pressure feedback signal would be useful for applications such as closed-loop combustion control and detection of faults such as misfire.

Accordingly, reconstruction of engine in-cylinder pressure in conventional reciprocating engines has been addressed by several authors. A myriad of approaches including model-based observer design [5, 24], neural networks [103, 14], and bespoke algorithms [43, 44] have been investigated. However, the subject remains unaddressed for FPEs in the literature.

This chapter develops an in-cylinder pressure and piston speed observer for FPEs. The observer reconstructs in-cylinder pressure and piston speed from measured piston position and net heat release rate. This process of reconstruction of the FPE state (i.e. in-cylinder pressure and piston speed) is more generally known as *state estimation*.

Starting by examining a *high gain* observer and revealing its limitations in a numerical study, a newly-developed sliding mode observer is proposed. The sliding mode observer features finite-time observer error convergence and is particularly useful for applications requiring accurate real-time pressure estimation—for example high engine frequency operation.

Effectiveness of the observer is analytically proven with Lyapunov theory and verified by simulation. A generalization of the observer structure into a large family of sliding mode observers is also provided, facilitating further work in the area.

7.2 Modelling

This section provides the FPE model for which an observer is developed. It is remarked that no further simplifications to the model in Section 2.3 are made. The model is restated here only for convenience. Also for convenience, an idealized schematic of a single piston two-stroke FPE generator is shown again in Fig. 7.1. The engine comprises three major parts, namely: a piston-translator assembly (the moving mass), a rebound device (for returning the piston), and an integrated generator (for power generation or motoring).

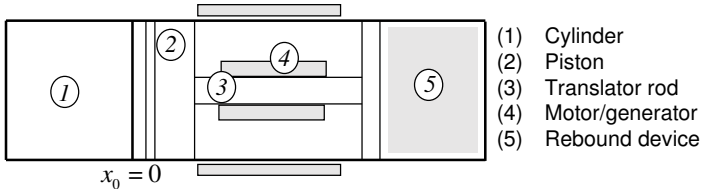

Figure 7.1: Idealized FPE generator schematic.

Considering the compression stroke as the positive direction for piston displacement x_0, piston motion is described by Newton's second law as

$$-mx_0 = F_c + F_{rd} + F_g + F_f \tag{7.1}$$

where m is the mass of the piston-translator assembly, F_c is the cylinder gas force on the piston, F_{rd} is the rebound device force, F_g is the generator force and F_f is the friction force.

The forces on the right hand-side of (7.1) are typically modelled as

$$F_g = \mu_g \dot{x}_0 \tag{7.2}$$

$$F_f = a_f \text{sgn}(\dot{x}_0) + b_f \dot{x}_0 \tag{7.3}$$

$$F_c = A_p P_c \tag{7.4}$$

$$F_{rd} = \begin{cases} k_s x_0 & \text{if rebound device is a mechanical spring} \\ -A_{rd} P_{rd} & \text{if rebound device is a bounce chamber} \end{cases} \tag{7.5}$$

where μ_g is a constant known as the generator coefficient, a_f and b_f are Coulomb and viscous friction parameters determined empirically, A_p is the piston crown area, k_s is a spring stiffness, A_{rd} is the area of of the translator surface interfacing with the bounce chamber, and P_c and P_{rd} are combustion and bounce chamber pressures respectively.

Pressure P_{rd} is taken to be an adiabatic process

$$P_{rd} V_{rd}^{\gamma_{rd}} = \text{constant} \tag{7.6}$$

where $V_{rd} = V_{rd}(x_0)$ is the rebound device volume (which depends on piston position x_0) and γ_{rd} is the ratio of specific heats of the rebound device fluid, typically air. For the time segment of the engine cycle for which the cylinder volume is closed, pressure

P_c is obtained from the so-called single zone thermodynamics model [47] as

$$\frac{dP_c}{dt} + \frac{\gamma_c}{V_c}\frac{dV_c}{dt}P_c = \frac{\gamma_c - 1}{V_c}\left(\frac{dQ_{ch}}{dt} - \frac{dQ_{ht}}{dt}\right) \tag{7.7}$$

where $V_c = V_c(x_0)$ is the cylinder volume (which depends on piston position), γ_c is the ratio of specific heats of the cylinder contents, Q_{ch} is the gross heat release from fuel burned, and Q_{ht} is the heat transfer through the cylinder walls. The time segment of the engine cycle where the cylinder volume is open constitutes the gas exchange process known as scavenging. In this study, scavenging is approximated as instantaneous and occurs at a known scavenging pressure.

The heat transfer rates on the right-hand side of (7.7) are modelled as

$$\frac{dQ_{ch}}{dt} = \eta_c Q_{LHV}\ m_f \frac{dx_\beta}{dt} \tag{7.8a}$$

$$\frac{dQ_{ht}}{dt} = hA_s(T_c - T_w) \tag{7.8b}$$

where in (7.8a), η_c is the combustion efficiency, Q_{LHV} is the fuel's lower heating value, m_f is the fuel mass available in the cylinder, and x_β is the fuel mass fraction burned given by a time-based Wiebe function [47]. In (7.8b), h is a heat transfer coefficient for example given by Hohenberg [48], A_s is the surface area enclosing the combustion volume, T_c is the combustion chamber temperature (available by sensor or estimated with ideal gas law computations) and T_w is the cylinder wall temperature.

7.3 Observer Development

To begin observer construction, let an input u to the FPE system developed in (7.1)–(7.7) be the net heat release rate, taken from (7.7) as

$$u = \frac{dQ_{ch}}{dt} - \frac{dQ_{ht}}{dt} \tag{7.9}$$

Note that u is available following the computations in (7.8). Next, let the piston position be the measured output y, i.e.

$$y = x_0 \tag{7.10}$$

The FPE system (7.1)–(7.7) will now be transformed into a suitable state space form. To this end, define the state variables x_1, x_2, and x_3 as

$$\begin{aligned} x_1 &= x_0 \\ x_2 &= \dot{x}_1 \\ x_3 &= -\frac{A_p}{m} P_c \end{aligned} \tag{7.11}$$

Using (7.11), (7.9) and (7.10), the FPE system (7.1)–(7.7) is transformed into a single input, single output (SISO) state space system of the general form

$$\begin{aligned} \dot{x}_1 &= x_2 + g_1(x_1, u) \\ \dot{x}_2 &= x_3 + g_2(x_1, x_2, u) \\ \dot{x}_3 &= f_3(x_1, x_2, x_3) + g_3(x_1, x_2, x_3, u) \\ y &= x_1 \end{aligned} \tag{7.12}$$

where

$$\begin{aligned} g_1 &= 0 \\ g_2 &= -\frac{1}{m} F_{rd} - \frac{1}{m} F_g - \frac{1}{m} F_f \\ f_3 &= -\frac{\gamma_c}{V_c} \dot{V}_c \; x_3 \\ g_3 &= -\frac{A_p}{m} \left(\frac{\gamma_c - 1}{V_c} \right) u \end{aligned} \tag{7.13}$$

It is easily checked from the original FPE system (7.1)–(7.7) that the functions on the right hand-side of (7.13), i.e. F_{rd}, F_g, F_f, V_c, and $\dot{V}_c$, are all state-dependent as

follows: $F_{rd} = F_{rd}(x_1)$, $F_g = F_g(x_2)$, $F_f = F_f(x_2)$, $V_c = V_c(x_1)$, and $\dot{V}_c = \dot{V}_c(x_2)$.

The system structure (7.12) constitutes both a linear part and a nonlinear part where the nonlinear part is an *additive triangular nonlinearity.* It is shown in [15] that system (7.12) is *uniformly observable* i.e. all states can be reconstructed for any input to the system. Having established this fact, the search for a suitable observer commences.

A commonly applied observer type for nonlinear systems known as a high gain observer [15, 60, 36] is first implemented. Its limitations under high frequency FPE operation are pointed out with a numerical example, after which a newly-developed sliding mode observer overcoming the limitations of the high gain observer is proposed. The Extended Kalman Filter—although commonly applied for nonlinear system state estimation—is not investigated in this chapter owing to its reliance on linearized dynamics of the observed system, a reliance which may or may not produce successful results.

7.3.1 High Gain Observer

Here, a high gain observer for system (7.12) is briefly introduced and tested in simulation.

7.3.1.1 Main Developments

System (7.12) may be compactly written as

$$\begin{aligned} \dot{x} &= A_0 x + \varphi(x, u) \\ y &= C_0 x \end{aligned} \tag{7.14}$$

where $x = \begin{bmatrix} x_1 & x_2 & x_3 \end{bmatrix}^T$ and

$$A_0 = \begin{bmatrix} 0 & 1 & 0 \\ 0 & 0 & 1 \\ 0 & 0 & 0 \end{bmatrix}, \quad C_0 = \begin{bmatrix} 1 & 0 & 0 \end{bmatrix}, \quad \varphi = \begin{bmatrix} g_1 \\ g_2 \\ f_3 + g_3 \end{bmatrix}$$

Let φ in (7.14) be globally Lipschitz continuous with respect to x (achieved if the Coulomb friction component a_f in (7.3) is negligible). Taking $\hat{x}$ as an estimate of state x, the system (7.14) admits an observer [15]

$$\dot{\hat{x}}_0 = A_0\hat{x} + \varphi(\hat{x}, u) - \lambda_0 K_0(C_0\hat{x} - y) \tag{7.15}$$

with

$$\lambda_0 = \begin{bmatrix} \lambda & 0 & 0 \\ 0 & \lambda^2 & 0 \\ 0 & 0 & \lambda^3 \end{bmatrix}, \qquad K_0 = \begin{bmatrix} k_1 \\ k_2 \\ k_3 \end{bmatrix}$$

where K_0 is chosen such that the matrix $A_0 - K_0C_0$ is Hurwitz, and $\lambda > 0$. The observer error $(\hat{x} - x)$ converges to zero *asymptotically* provided the high gain parameter λ is sufficiently large [21]. For this reason, observer (7.15) is referred to as a high gain observer.

7.3.1.2 Simulation Testing

High gain observer (7.15) is now tested on simulated engine data where an FPE runs at 86 Hz frequency (approximately 0.01s cycle duration). Note that high frequency FPE operation is quite typical, and in fact desirable for high power generation. Table 7.1 details the engine parameters considered for the simulation, in which the FPE's rebound device is taken as a mechanical spring. A plot of the estimated and actual in-cylinder pressures for two engine cycles using a gain of $\lambda = 1 \times 10^4$ is shown in

Table 7.1: Simulation Parameters

Parameter	**Value**	**Parameter**	**Value**
bore	86 mm	m	2 kg
stroke	86 mm	k_s	490 kN/m
comp. ratio	10.44	μ_g	0.1 kg/s
ambient press.	1 bar	a_f	0
ambient temp.	25 °C	b_f	5

Fig. 7.2. Clearly, the estimated pressure does not converge to the actual pressure fast enough. A further increase in the gain λ should in theory increase the convergence rate, but doing so results in numerical computation difficulties. Furthermore, addition of measurement noise renders the observer completely ineffective. This is not surprising, as it is well-known that presence of measurement noise placed an upper limit on the choice of λ [60]. No suitable value of λ is found to give an acceptable observer response for both in-cylinder pressure and piston speed.

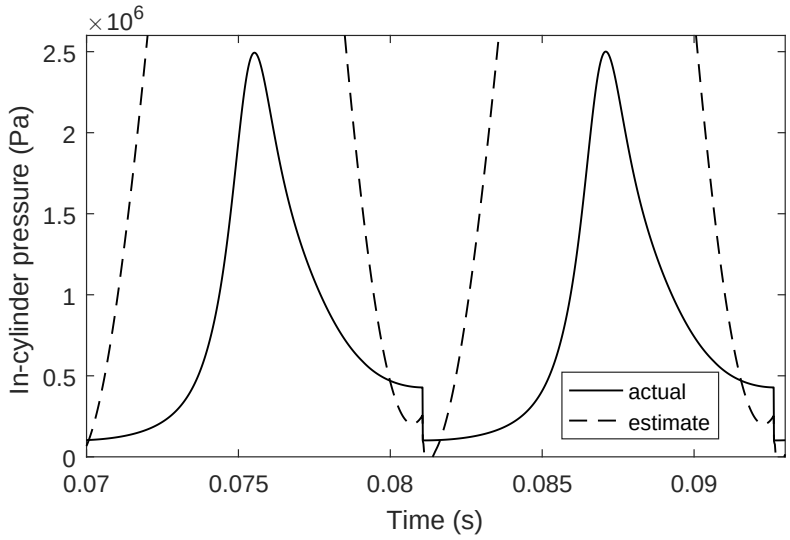

Figure 7.2: High gain observer response. The estimated in-cylinder pressure does not converge fast enough to the actual pressure.

7.3.2 Sliding Mode Observer

The failure of the high gain observer motivates investigations into a different type of observer, namely the sliding mode observer. In this section, a newly-developed sliding mode observer is proposed and tested.

7.3.2.1 Main Developments

In a sliding mode observer, the observer error $e = \hat{x} - x$ is constrained to lie on a so-called sliding surface $e = 0$. On this surface, it is trivial that $\hat{x} = x$; i.e. the state estimate exactly matches the true state. Thus, necessarily, the key idea of a sliding mode observer is to enforce the constraint $e = 0$ in finite time (as opposed to asymptotically with high gain observers). Finite time convergence is essential for fast and accurate state estimation, as required in this chapter.

A survey of sliding mode observer development for linear and nonlinear systems is found in [99]. For nonlinear systems of interest in the form (7.12), a sliding mode observer has been proposed by Barbot and Boukhobza [12]. Similar to many sliding mode observer designs, the observer is implemented with the discontinuous sign function. The problem with the sign function is, however, well-known; it is the function's high frequency switching output when evaluated with an argument that is not perfectly at zero but rapidly fluctuating about zero—say due to uncertainties in the system or limited computational precision. These fluctuations are amplified by the gains in the observer and can ultimately be propagated into the observed signals, impacting accuracy and even stability. The usual mitigation of this undesirable effect has been with implementation of low pass filters within the observer to get an *equivalent output* of the sign function [12, 27]. But, this intervention slows down the observer convergence time and may therefore not be suitable for time-critical real-time applications.

A modified form of Barbot and Boukhobza's sliding mode observer [12] that does not implement the discontinuous sign function is now proposed. The observer is continuous, and therefore does not require low pass filtering in achieving the constraint $e = 0$. The proposed observer is constructed as

$$\begin{aligned}
\dot{\hat{x}}_1 &= \hat{x}_2 + g_1(x_1, u) + \lambda_1 \left(x_1 - \hat{x}_1\right)^{q/p} \\
\dot{\hat{x}}_2 &= \hat{x}_3 + g_2(x_1, \tilde{x}_2, u) + E_1\lambda_2 \left(\tilde{x}_2 - \hat{x}_2\right)^{q/p} \\
\dot{\hat{x}}_3 &= f_3(x_1, \tilde{x}_2, \tilde{x}_3) + g_3(x_1, \tilde{x}_2, \tilde{x}_3, u) + E_2\lambda_2 \left(\tilde{x}_3 - \hat{x}_3\right)^{q/p}
\end{aligned} \tag{7.16}$$

where λ_1, λ_2, λ_3 are positive tuning parameters (high values result in short convergence times), p, q (with $p > q$) are positive odd integers such that for a real number a, only the real solution of $a^{q/p}$ is considered, and

$$\begin{aligned}
\tilde{x}_2 &= \hat{x}_2 + E_1\lambda_1 \left(x_1 - \hat{x}_1\right)^{q/p} \\
\tilde{x}_3 &= \hat{x}_3 + E_2\lambda_2 \left(\tilde{x}_2 - \hat{x}_2\right)^{q/p}
\end{aligned} \tag{7.17}$$

with

$$\begin{aligned}
E_1 &= \begin{cases} 1 & \text{if } \hat{x}_1 = x_1 \\ 0 & \text{otherwise} \end{cases} \\
E_2 &= \begin{cases} 1 & \text{if } E_1 = 0 \text{ and } \hat{x}_2 = \tilde{x}_2 \\ 0 & \text{otherwise} \end{cases}
\end{aligned} \tag{7.18}$$

Let it be the case that for a bounded input u, the state in (7.12) does not go to infinity in finite time, i.e. (7.12) is Bounded Input Bounded State (BIBS) in finite time. Then, the following theorem states the effectiveness of the observer:

Theorem 1 (Sliding Mode Observer). *Considering system* (7.12) *and the observer* (7.16)–(7.18)*, for any initial observer state* $\hat{x}(0) \neq x(0)$ *and any bounded input* u*, there exists* λ_1*,* λ_2*, and* λ_3 *such that* $\hat{x}$ *converges in finite time to* x*.*

Proof.

Since $\hat{x}(0) \neq x(0)$ as per the statement of the Theorem, $E_1 = 0$ and $E_2 = 0$ according to (7.18). The observer error being $e_i = x_i - \hat{x}_i$ $(i = 1, 2, 3)$, the observer error dynamics from (7.16) and (7.17) are

$$\begin{aligned}
\dot{e}_1 =& e_2 - \lambda_1 (x_1 - \hat{x}_1)^{q/p} \\
\dot{e}_2 =& e_3 + g_2(x_1, x_2, u) - g_2(x_1, \hat{x}_2, u) \\
\dot{e}_3 =& f_3(x_1, x_2, x_3) - f_3(x_1, \hat{x}_2, \hat{x}_3) \\
& + g_3(x_1, x_2, x_3, u) - g_3(x_1, \hat{x}_2, \hat{x}_3, u)
\end{aligned} \tag{7.19}$$

Recall that by assumption, the state x does not go to infinity in finite time for a bounded input u. Accordingly, neither does the observer error (7.19). By setting a candidate Lyapunov function $V_1 = (1/2)e_1^2$ for the first error equation of (7.19), one finds

$$\dot{V}_1 = -e_1^{(q+p)/p} \left(\lambda_1 - e_2 e_1^{q/p} \right) \tag{7.20}$$

Since q and p are odd, $q + p$ is even. Hence, $e_1^{(q+p)/p} > 0$ in (7.20). If λ_1 is greater than the maximum of $|e_2 e_1^{q/p}|$ (in subsequent notation: $\lambda_1 > |e_2 e_1^{q/p}|_{\max}$) then $\dot{V}_1 < 0$. As $\dot{V}_1$ is negative definite, e_1 converges towards zero. Moreover, the convergence is in finite time—since, with $\lambda_1 > |e_2 e_1^{q/p}|_{\max}$ in the first equation of (7.19), the dominant error dynamics $\dot{e}_1 = -\lambda_1 e_1^{q/p}$ are finite time converging, as can be verified by direct integration. It then follows, that after some finite time t_1, $\dot{e}_1 = 0$. In the first equation of (7.19) this implies that $e_2 = \lambda_1 (x_1 - \hat{x}_1)^{q/p}$. Consequently, according to the first equation in (7.17), $\tilde{x}_2 = x_2$.

Also after time t_1, $E_1 = 1$ and $E_2 = 0$ in (7.18). The observer error dynamics therefore

become

$$\begin{aligned}\dot{e}_1 =& e_2 - \lambda_1(x_1 - \hat{x}_1)^{q/p} = 0 \\ \dot{e}_2 =& e_3 - \lambda_2(x_2 - \hat{x}_2)^{q/p} \\ \dot{e}_3 =& f_3(x_1, x_2, x_3) - f_3(x_1, \hat{x}_2, \hat{x}_3) \\ & + g_3(x_1, x_2, x_3, u) - g_3(x_1, \hat{x}_2, \hat{x}_3, u)\end{aligned} \tag{7.21}$$

Setting a candidate Lyapunov function for the first two error equations of (7.21) as $V_2 = (1/2)e_1^2 + (1/2)e_2^2$, one finds

$$\dot{V}_2 = -e_1^{(q+p)/p}\left(\lambda_1 - e_2 e_1^{q/p}\right) - e_2^{(q+p)/p}\left(\lambda_2 - e_3 e_2^{q/p}\right) \tag{7.22}$$

But, it was established that $\lambda_1 > |e_2 e_1^{q/p}|_{\max}$ implies $e_1 \to 0$ in time t_1. Hence $\dot{V}_2 = -e_2^{(q+p)/p}(\lambda_2 - e_3 e_2^{q/p})$, which is negative definite if $\lambda_2 > |e_3 e_2^{q/p}|_{\max}$. For this λ_2, the dominant dynamics in the second equation of (7.21) are $\dot{e}_2 = -\lambda_2 e_2^{q/p}$, in which e_2 can be shown to converge to zero in finite time by direct integration. It then follows, that after some finite time $t_2 > t_1$, $\dot{e}_2 = 0$. In the second equation of (7.21) this implies that $e_3 = \lambda_2(x_2 - \hat{x}_2)^{q/p}$. Consequently, according to the second equation in (7.17), $\tilde{x}_3 = x_3$.

Also after time t_2, $E_1 = 1$ and $E_2 = 1$ in (7.18). The observer error dynamics therefore become

$$\begin{aligned}\dot{e}_1 =& e_2 - \lambda_1(x_1 - \hat{x}_1)^{q/p} = 0 \\ \dot{e}_2 =& e_3 - \lambda_2(x_2 - \hat{x}_2)^{q/p} = 0 \\ \dot{e}_3 =& -\lambda_3(x_3 - \hat{x}_3)^{q/p}\end{aligned} \tag{7.23}$$

Setting a candidate Lyapunov function for the entire observer dynamics (7.23) as $V_3 = (1/2)e_1^2 + (1/2)e_2^2 + (1/2)e_3^2$, it can be shown with similar arguments as in the previous discussions that $e_3 \to 0$ in a finite time $t_3 > t_2$ if $\lambda_1 > |e_2 e_1^{q/p}|_{\max}$,

$\lambda_2 > |e_3 e_2^{q/p}|_{\max}$, and $\lambda_3 > 0$. This ends the proof. □

7.3.2.2 Simulation Testing

Observer (7.16)–(7.18) is now tested in simulation (experimental testing is to be discussed in Chapter 8). Noisy input and output data was generated from an FPE operating at 86 Hz with the parameters in Table 7.1. The observer is simulated to be of the same step size as the sampling period used to generate the input and output data. To avoid observing the engine's scavenging inlet pressure (assumed as known), the observer's initial conditions are reset on every new engine cycle. The constant parameters are set as $\lambda_1 = 40$, $\lambda_2 = 20$, $\lambda_3 = 20$, $q = 3$ and $p = 5$.

Figure 7.3 shows a good match between actual and estimated in-cylinder pressure. It is seen from the error plot in Fig. 7.4 that the largest mismatch between the two pressures is observed in the region around top dead centre (interestingly, as is the case in conventional engines [24]). The estimated and actual piston speeds are shown in Fig. 7.5, where they can be seen to match very closely. Clearly, the sliding mode observer response is superior to the high gain observer response in terms of

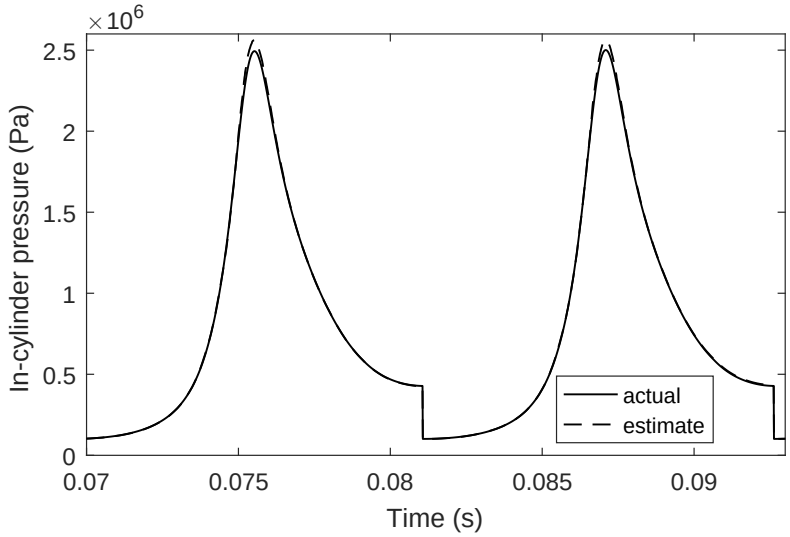

Figure 7.3: Sliding mode observer response. The estimated in-cylinder pressure converges quickly and accurately to the actual pressure.

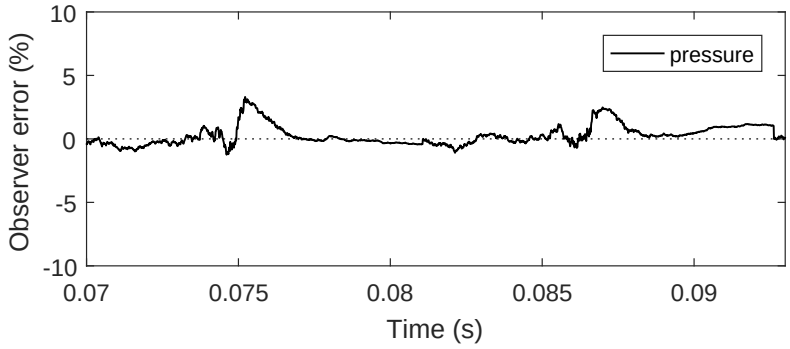

Figure 7.4: Sliding mode observer error. The largest error between actual and estimated in-cylinder pressure is in the peak pressure region around top dead centre.

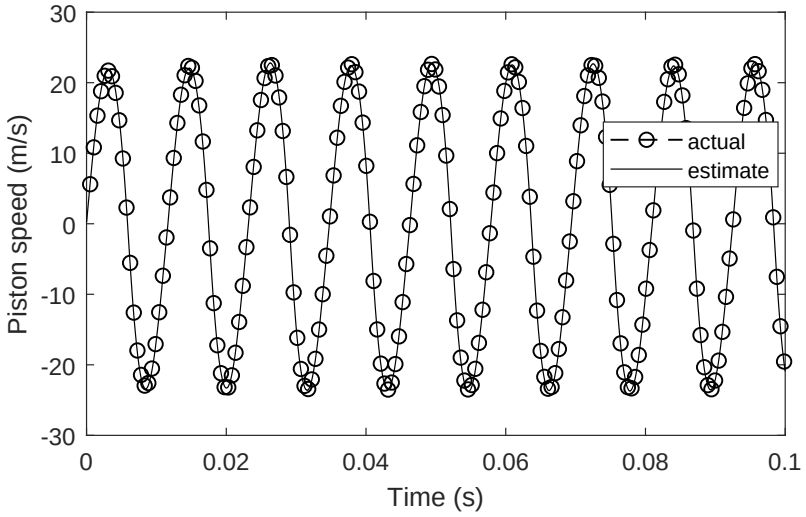

Figure 7.5: Sliding mode observer response. The actual and estimated piston speed match very closely.

convergence rate and robustness to noise.

7.4 Generalized Sliding Mode Observer

Observer (7.16)–(7.18) can be generalized into a family of sliding mode observers, allowing versatility to the engineer in its construction. The generalization is achieved when the error terms raised to the power q/p—terms known as the *output error injection*—are replaced by a general function. This general function, i.e. the general output error injection, represents a class of functions for which the observer error e reaches the manifold, or surface, $e = 0$ in finite time.

Denoting a general output error injection as function υ, a general sliding mode observer is constructed from observer (7.16)–(7.18) as

$$\begin{aligned}
\dot{\hat{x}}_1 &= \hat{x}_2 + g_1(x_1, u) + \upsilon\left(x_1 - \hat{x}_1\right) \\
\dot{\hat{x}}_2 &= \hat{x}_3 + g_2(x_1, \tilde{x}_2, u) + E_1\upsilon\left(\tilde{x}_2 - \hat{x}_2\right) \\
\dot{\hat{x}}_3 &= f_3(x_1, \tilde{x}_2, \tilde{x}_3) + g_3(x_1, \tilde{x}_2, \tilde{x}_3, u) + E_2\upsilon\left(\tilde{x}_3 - \hat{x}_3\right)
\end{aligned} \tag{7.24}$$

where

$$\begin{aligned}
\tilde{x}_2 &= \hat{x}_2 + E_1\upsilon\left(x_1 - \hat{x}_1\right) \\
\tilde{x}_3 &= \hat{x}_3 + E_2\upsilon\left(\tilde{x}_2 - \hat{x}_2\right)
\end{aligned} \tag{7.25}$$

with E_1 and E_2 as in (7.18). To ensure finite time convergence of the observer error, function $\upsilon(\cdot)$ is selected according to the following criterion: when $\upsilon(\cdot)$ is implemented in the scalar dynamic equation

$$\dot{s} + \upsilon(s) = 0 \qquad s(0) \neq 0 \tag{7.26}$$

the variable s reaches zero in finite time. This requirement on $\upsilon(\cdot)$ is derived from the

Table 7.2: Examples of Injection Functions

Type	**No.**	**Function***
Discontinuous	1	$\upsilon(s) = \lambda_s \text{sgn}(s)$
Continuous	2	$\upsilon(s) = \lambda_s s^{q/p}$
	3	$\upsilon(s) = \lambda_s \lvert s \rvert^{\alpha} \text{sign}(s)$
High order (continuous)	4	$\upsilon(s) = \phi(s) + \lambda_s \lvert s \rvert^{1/2} \text{sgn}(s)$ $\dot{\phi}(s) = \alpha_s \text{sign}(s)$
*Where used, $\lambda_s, \alpha_s > 0$, (p, q) are odd with $p > q$, and $0 < \alpha < 1$.		

fact that the observer achieves the sliding mode $e = \begin{bmatrix} e_1 & e_2 & e_3 \end{bmatrix} = 0$ sequentially in the order $e_1 = 0$, $e_2 = 0$, $e_3 = 0$ (see proof of Theorem 1). As such, (7.26) is a general representation of the so called *reaching dynamics* towards any one of the three sliding modes $e_i = 0$ ($i = 1, 2, 3$).

Table 7.2 provides some example choices of function $\upsilon(\cdot)$ available to the engineer. The provided function examples are categorized as discontinuous, continuous, and high order. Note that all function examples ensure that (7.26) satisfies the finite time convergence requirement. Also observe that function example 2 is what was used in observer (7.16)–(7.18). For function examples 1, 2 and 3, finite time convergence of (7.26) can be checked by direct integration, yielding the respective convergence times

$$T_1 = \frac{1}{\lambda_s} \lvert s(0) \rvert \tag{7.27}$$

$$T_2 = \frac{p}{\lambda_s (p - q)} s(0)^{\frac{p-q}{q}} \tag{7.28}$$

$$T_3 = \frac{1}{\lambda_s (1 - \alpha_s) \lvert s(0) \rvert^{1-\alpha}} \tag{7.29}$$

Verification of finite time convergence of (7.26) when function example 4 is used is not trivial. The verification can be found in [64].

As has been explained in Section 7.3.2.1, implementation of the discontinuous version of $\upsilon(\cdot)$ (for example in [12, 27]) usually requires use of low pass filters which inherently

slows down observer convergence time. For time-critical applications such as real-time estimation of FPE in-cylinder pressure, continuous or high order implementations of $v(\cdot)$ must be preferred.

7.5 Chapter Conclusions

This chapter has developed an observer for both in-cylinder pressure and piston speed for free piston engines. The observer has been successfully tested with simulated engine data (testing with experimental data follows in the following chapter). Accordingly, the chapter makes an important stride in addressing a gap in the engine's development literature. The proposed observer is suitable for robust real-time pressure estimation at high engine frequencies owing to finite time observer error convergence. Indeed, the observer's finite-time convergence property grants it a distinct advantage over asymptotically converging observers; such as the high gain observer (as the chapter shows) and Extended Kalman Filter (where linearization of FPE dynamics is an acceptable modelling compromise). A generalization of the proposed observer has been developed, allowing the engineer to select from various observer implementations while assessing any performance differences.

Chapter 8

Experimental Work on Model Validation, State Estimation, and Stability

8.1 Introduction

An FPE generator model, developed in Chapter 2, has thus far been used to successfully verify the proposed methods on stability, control, and state estimation developed in Chapters 3–7. Groundwork has accordingly been laid for experimental testing on a physical FPE system.

To this end, a test FPE generator has been developed at the University of Sussex. This test FPE generator is subsequently referred to simply as a 'test FPE'.

This chapter details the experimental work undertaken on the test FPE hardware rig; in particular covering three important aspects, namely free-piston engine model validation, state estimation, and stability. The chapter will:

i) Describe the features of the test FPE. (It is remarked that although the author

was involved in the team-based FPE design process, no credit is claimed for detailed mechanical design, as the author's designated role was Control.)

ii) Validate the test FPE dynamics with measured data. Here, a tailored parameter identification scheme is developed; one that does not require 'persistent excitation' of the system under parameter identification.

iii) Estimate in-cylinder pressure and piston speed (i.e. state estimation) from measurement data. The newly-developed sliding mode observer in Chapter 7 is tested here with measurement data for the first time.

iv) Diagnose the limitations of the FPE hardware rig, and take the opportunity to explain FPE stability using the energy-based concepts developed in Chapter 3.

The diagnosis in item (iv) will form the basis for future work recommendations in Chapter 9.

8.2 Description of the Test FPE

In the following subsections, the test FPE's technical specification is first described, followed by a description of the associated control hardware, and finally a description of the FPE's starting mechanism. High-level control architecture for the FPE has also been developed, and can be found in Appendix B.

8.2.1 Technical Specification

The test FPE is of linear opposed piston layout, with a helical mechanical spring as rebound device, and is designed to produce 300 W at 48 V. Table 8.1 describes further details of the FPE's technical specification.

A photograph of the test FPE is provided in Fig. 8.1, and a 3-D sectioned view

provided in Fig. 8.2. Piston and cylinder matching is adapted from a model aircraft engine. The piston has one ring. Under-piston scavenge supplies a volume of fresh charge through the transfer ports. Each translator rod is rigidly connected to an electric machine permanent magnet and supported on two linear bearings. The total power supplied is split equally between the two electric machines.

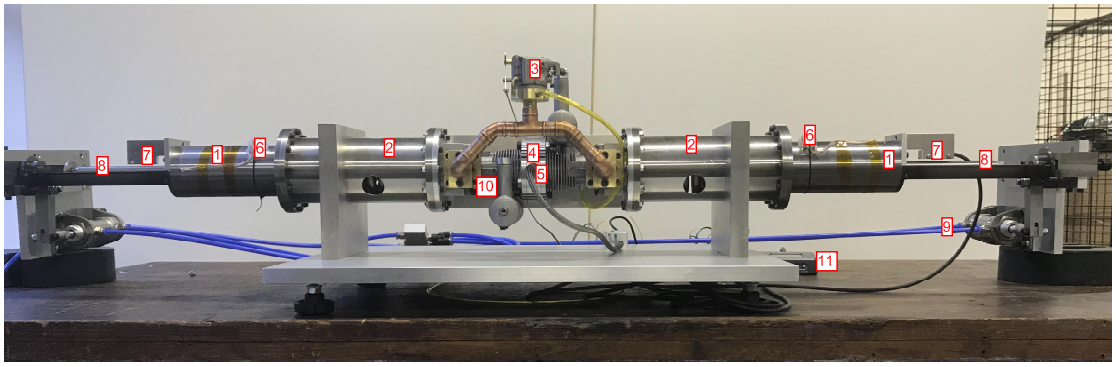

Figure 8.1: Photograph of test FPE generator. 1—Electric machine, 2—Spring case, 3—Carburetor, 4—Combustion chamber (cylinder), 5—Spark plug, 6—Electrical terminals, 7–Linear encoder, 8—Translator rod, 9—Compressed air supply line, 10—Scavenge case, and 11—Microcontroller.

Table 8.1: Technical Specifications of Test FPE Generator

Attribute	**Specification**
Layout	Linear opposed piston
Rebound device	Mechanical spring (stiffness: 170 kN/m)
Combustion	Spark ignited, two stroke
Geometry	Bore: 29 mm, Stroke (nominal): 25.6 mm, Compression ratio (nominal): 9
Mechanical	Loop scavenged, air cooled, piston-translator mass: 2.2 kg
Electrical	300 W, 48 V Parmanent Magnet (PM) electric machine (translator mounted PM)

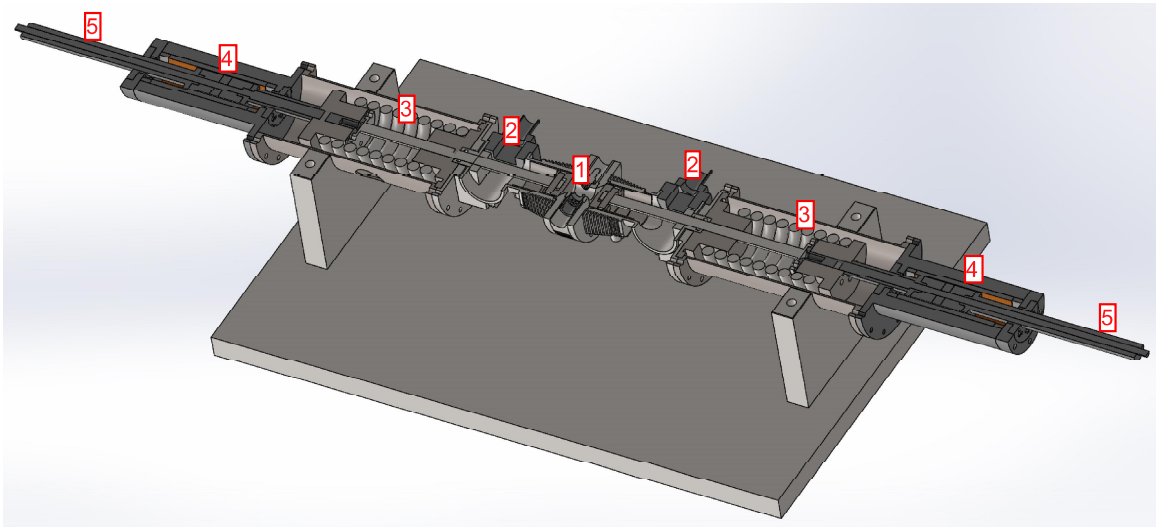

Figure 8.2: Sectioned view CAD render of test FPE generator. 1—Combustion chamber (cylinder), 2—Scavenge case, 3—Spring, 4—Electric machine, and 5—Translator rod.

8.2.2 Control Hardware

The control hardware deployed on the test FPE can be categorised as follows: Sensing, Data Acquisition (DAQ) & Control, and Actuation. Details of the deployed control hardware and associated function are provided in Table 8.2.

Table 8.2: Control Hardware and Assigned Function

Type	**Hardware**	**Assigned Function**
Sensing	Linear encoder	Piston position measurement.
	Pressure transducer	In-cylinder pressure measurement.
DAQ and Control	NI MyRIO	Encoder read and spark plug activation.
	Arduino Due	Carburetor throttle control.
Actuation	Spark plug	Ignition of fuel-air mixture.
	Servo motor linked throttle	Fuel supply adjustment.

8.2.3 Starting

In principle, the test FPE can be started electrically by operating the two electric machines as motors. Figure 8.3 is an electrical circuit schematic designed to implement a resonant starting scheme for the test FPE. In the Figure 8.3 a power source supplies a current to an electric machine coil. The direction of current is manipulated by power electronic switches operated by a microcontroller to ensure that the force produced by the coil always acts in the direction of the piston (picked up by the piston position sensor). If the force is sufficient to overcome friction, piston oscillation amplitude grows, until stopped at the required compression ratio.

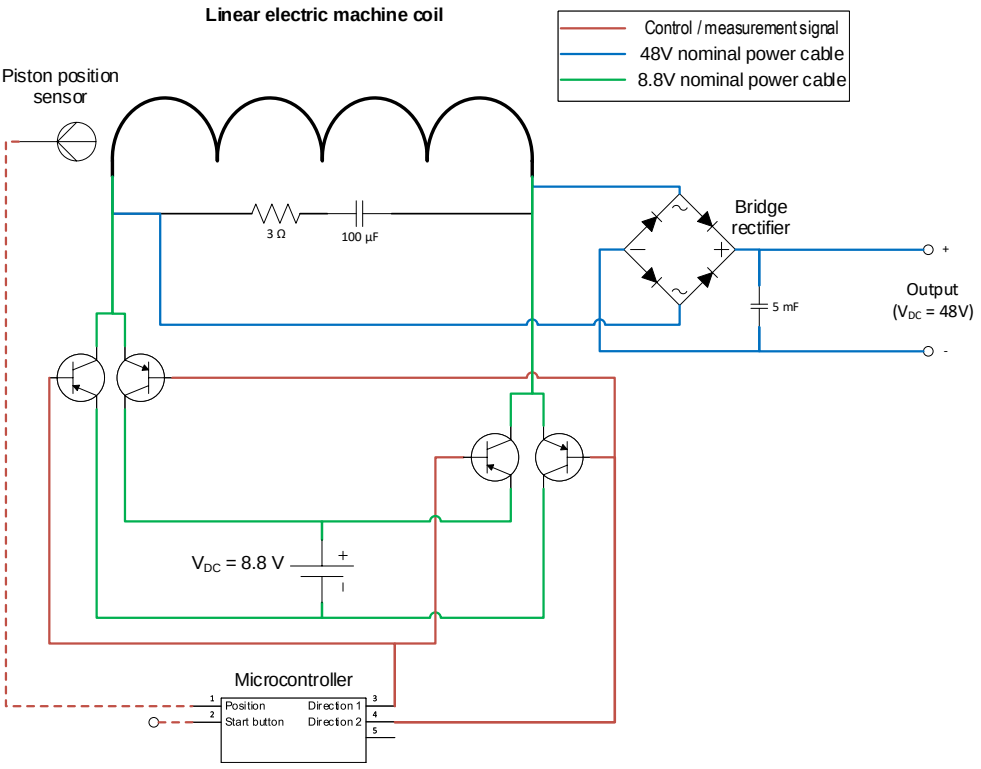

Figure 8.3: Electrical circuit schematic for starting the test FPE generator.

However, in the existing design iteration, the FPE is started mechanically. Here, the starting procedure is the following: a piston is manually driven from the rest position to TDC, in so doing tensioning the spring . The piston is then released at any decided moment. Piston release is activated by a trigger mechanism powered by a compressed

air supply at the end of the translator rod (see Fig. 8.1).

8.3 Experiment 1: Model Validation of Test FPE

A mathematical model of the test FPE is now to be validated. Successful validation of the model places confidence in model-based analysis (as has been pursued in Chapters 3–7). Here, model validation is to be achieved by identification of the FPE's physical parameters from measured data. Of special interest are the parameters describing friction, as they are completely unknown at this stage.

In the following subsections, a parameter identification scheme is first developed and tested with simulated FPE data. Then, a brief description of the experiment that produced the measured data for physical parameter identification is provided. A discussion of the parameter identification results lastly follows.

8.3.1 Parameter Identification Scheme

A vast number of well-established parameter identification algorithms—commonly used in system identification and adaptive parameter estimation [51]—require a 'persistent excitation' property of an input or other driving signal for the correct identification of a system's parameters from measured data. In physical terms, a persistently exciting input would be one of sufficient spectral richness to excite all the system modes, and in so-doing facilitate correct parameter identification.

For reasons that become clear later on (in Section 8.5), no persistently exciting input (in the form of successive combustion from one engine cycle to the next) could be generated to drive the test FPE system. Measurement data was from free-response tests and was therefore output-only. Effectiveness of conventional well-established parameter identification algorithms under these circumstances cannot be guaranteed—and,

as such, other identification methods were to be sought.

Parameter identification of the test FPE system is achieved here by casting the parameter identification task into a general optimisation problem. The term "general" is used to mean that the optimisation problem is both nonlinear and constrained. The solution to the problem, constituting the constant FPE parameters being sought, is numerically computed. Indeed, constrained nonlinear optimisation problems generally do not have closed-form analytic solutions.

Developed next is the optimal parameter identification procedure. (A recursive least squares parameter identification algorithm that requires persistent excitation is provided in Appendix C.) The procedure constitutes two steps; the first step is to formulate the parameter identification task into a continuous time optimisation problem, and the second step is to numerically solve the problem, after first transcribing (i.e. converting) it into a nonlinear program (NLP).

8.3.1.1 Technical Developments

Continuous time optimisation problem formulation

Modelling either side of the opposed piston test FPE follows the familiar FPE dynamics introduced in Chapter 2, i.e.

$$-m\ddot{x}_0 = F_c + F_{rd} + F_g + F_f \tag{8.1}$$

where x_0 is piston displacement, m is the moving mass, F_c is the force due to in-cylinder gas pressure in the combustion chamber, F_{rd} is the rebound device force, F_g is the generator force, and F_f is the friction force. Without loss of generality, it is assumed that the generator coefficient μ_g is such that no power generation takes

place in a parameter identification experiment, i.e.

$$\mu_g = 0 \tag{8.2a}$$

$$\therefore F_g = 0 \tag{8.2b}$$

Forces F_c, F_{rd}, and F_f are modelled as

$$F_c = A_p P_c(x_0), \tag{8.3a}$$

$$F_{rd} = k_s x_0 \tag{8.3b}$$

$$F_f = a_f \text{sgn}(\dot{x}_0) + b_f \dot{x}_0 \tag{8.3c}$$

where A_p is the piston crown area, $P_c(x_0)$ is the in-cylinder pressure that depends on piston position x_0 while following an isentropic process, k_s is the rebound device spring stiffness, and a_f, b_f are friction parameters.

Being of opposed piston layout, perfect symmetry about the FPE's centre line is assumed (see Fig. 4.10). The symmetry implies that the shared combustion chamber volume V_c is given by

$$V_c = 2V_{c_l} = 2V_{c_r} \tag{8.4}$$

where V_{c_l}, V_{c_r} is the respective left and right combustion chamber volume on either side of the centre line (as described in Section 4.4.4).

Now, let θ constitute a vector of the unknown parameters, i.e. one or more parameters from (m, k_s, a_f, b_f). System (8.1) can be written more generally in state space form as

$$\dot{x}(t) = f(x(t), \theta) \tag{8.5}$$

where $x(t)$ is a two-dimensional state vector and f is a vector function.

Denoting $x_m(t)$ as measurement data history collected from a time instant $t = 0$ to a

time instant $t = t_f$, the parameter identification problem is stated as follows: Find a *constant* vector θ that minimises the objective function

$$J = \int_0^{t_f} \left(x(t) - x_m(t)\right)^T Q \left(x(t) - x_m(t)\right) dt \tag{8.6}$$

where Q is a nonzero positive semidefinite weighting matrix, under the dynamic constraint (8.5), parameter constraints

$$\underline{\theta} \leq \theta \leq \overline{\theta} \tag{8.7}$$

and state constraints

$$\underline{x} \leq x(t) \leq \bar{x} \tag{8.8}$$

It is remarked that the dependence of J on θ in (8.6) is implicit, originating from $x(t)$ dependence on θ when (8.5) is solved.

This optimisation problem has no known general analytic solution but can be solved numerically. Key to finding a physically plausible numerical solution is using prior knowledge about the system to inform the setting of parameter constraints (8.7) and state constraints (8.8).

Problem transcription into a nonlinear program

Finding the solution to the optimisation problem could either be done *indirectly*, by solving the pertinent equations describing the necessary and sufficient conditions satisfied by the optimal solution (typically derived from Bellman's principle of optimality or Pontryagin's minimum principle) or *directly*, by transcribing the optimisation problem into a nonlinear program and solving it.

Whereas indirect methods generally yield globally optimal solutions, the construction and solving of necessary and sufficient conditions for optimality is generally difficult.

By contrast, direct methods yield optimal solutions that require checking for global optimality but after much easier problem construction and solution-finding.

For demonstration, the optimisation problem at hand is transcribed into a nonlinear program using the Trapezoidal collocation method. For other collocation methods, and a more detailed treatment on solving optimal control problems by direct methods, the reader is referred to Betts [16].

Constraints. Since the decision variable θ of the optimisation problem is required to be constant, the dynamic constraint (8.5) may be modified as follows

$$\dot{x} = f(x, \theta) \tag{8.9a}$$

$$\dot{\theta} = 0 \tag{8.9b}$$

For compactness, (8.9) is written as

$$\dot{z} = f_z(z) \tag{8.10}$$

where $z = \begin{bmatrix} x & \theta \end{bmatrix}$ and $f_z = \begin{bmatrix} f(x,\theta) \\ 0 \end{bmatrix}$. Next, consider the discretization of time and state into N so-called collocation points:

$$t \to t_0 \dots t_k \dots t_N$$

$$z \to z_0 \dots z_k \dots z_N$$

By integrating both sides of (8.10), the relationship between two successive collocation points z_k and z_{k+1} can be approximated by the trapezoidal rule as follows

$$\int_{t_k}^{t_{k+1}} \dot{z} \quad dt = \int_{t_k}^{t_{k+1}} f_z \quad dt \tag{8.11a}$$

$$z_{k+1} - z_k \approx \frac{1}{2} h_k \cdot (z_{k+1} + z_k) \tag{8.11b}$$

where $h_k = t_{k+1} - t_k$. This approximation is then applied to every pair of collocation points:

$$z_{k+1} - z_k = \frac{1}{2} h_k \cdot (z_{k+1} + z_k), \quad k \in 0, \ldots, (N-1). \tag{8.12}$$

Equation (8.12) represents what are known as collocation constraints, which serve to enforce the problem's dynamic constraint. The parameter and state constraints remain as in (8.7) and (8.8).

Objective function. Let $w(\cdot)$ be defined as the integrand on the right-hand side of the objective function (8.6). The objective function is, accordingly,

$$J = \int_0^{t_f} w\left(z(\tau)\right) d\tau \tag{8.13}$$

which can be approximated at each collocation point following the trapezoid rule to yield

$$J \approx \sum_{k=0}^{N-1} \frac{1}{2} h_k \cdot (w_k + w_{k+1}) \tag{8.14}$$

where $w_k = w(z(t_k))$.

Nonlinear program. The nonlinear programme is that of minimising (8.14), with z as the decission variable, subject to constraints (8.12), (8.7) and (8.8). Such a program can be solved by widely available nonlinear program solvers on a digital computer. The final step is usually an interpolation of the optimal solution at each collocation point.

This concludes the development of Trapezoidal collocation as an exemplar method for solving the continuous time optimisation problem defined in (8.5)–(8.8).

8.3.1.2 Simulation Testing

The proposed parameter identification scheme, constituting an optimisation problem defined in (8.5)–(8.8), is now tested on simulated FPE data, where the true solution

Table 8.3: Parameter Identification Results (Simulation)

Parameter	**Units**	**True Value**	**Estimated Value**	**Error**
m	kg	2.2	2.15	2.27 %
k_s	kN/m	170	165.78	2.48 %
a_f	N	5	5.10	2.00 %
b_f	Ns/m	0	0.00	0.00 %

to the problem (i.e. the parameter vector θ) is known *a priori*. The problem is implemented in the general purpose optimal control software package GPOPS-II [90] to find a numerical solution. The software package uses adaptive direct collocation methods, together with sparse nonlinear programming, in order to numerically solve optimal control problems.

The measurement data $x_m(t)$ is piston displacement and piston speed, generated from the dynamics (8.1) when parameterised with Table 8.1. The unknown parameter vector θ constitutes the four parameters m, k_s, a_f, and b_f. The weighting matrix Q is set as $500I$, where I is the identity matrix. A starting 'guess' for the numerical scheme is implemented as $\frac{1}{2}(\underline{\theta} + \bar{\theta})$ for the unknown parameter vector θ and as $x_m(t)$ for the state $x(t)$.

Table 8.3 contains the parameter identification results. It can be seen that the estimated parameters are very near the true parameters, with an estimation error of less than 2.5 %. Figure 8.4 is a plot of the original piston displacement response overlaid with a reconstructed response using the estimated parameters. The two plots are indistinguishable.

The simulation test has verified the effectiveness of the proposed parameter identification scheme on FPE dynamics. In what follows, the parameter identification scheme is applied to physical FPE measurement data.

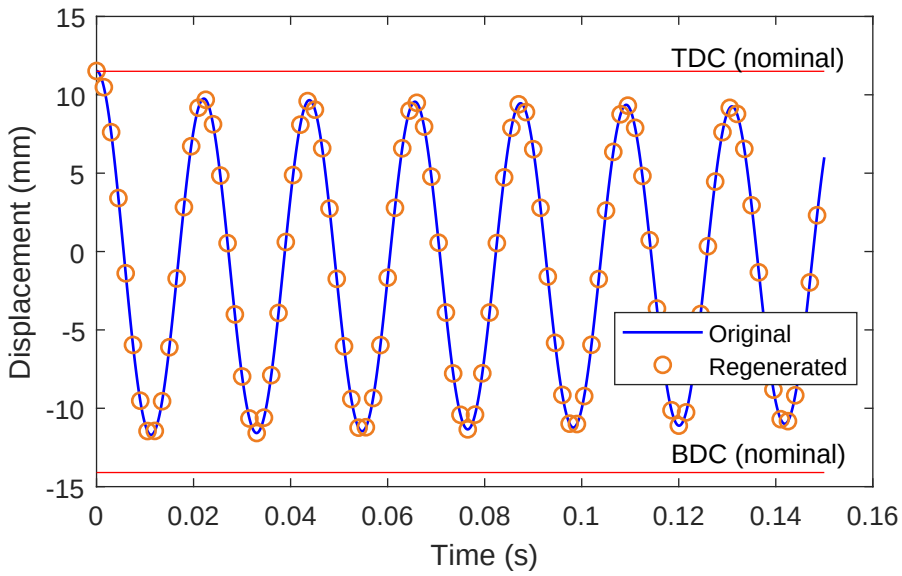

Figure 8.4: Original piston response versus reconstructed piston response following parameter identification (simulation).

8.3.2 Experiment Data Collection

Measured data of piston displacement used for parameter identification was taken from a free-response test; i.e. one where the test FPE system was not externally driven by combustion. The test was conducted by releasing the piston from TDC and recording the piston response with a high-resolution optical linear encoder. The encoder produced a virtually noise-free measurement from which piston speed was derived by numeric differentiation. The test FPE was kept unloaded.

8.3.3 Experiment Results and Discussion

First to be presented are are results where only the friction parameters (a_f, b_f) are identified. Following this are results where all the parameters, i.e. (m, k_s, a_f, b_f), are identified.

In both sets of results, the the weighting matrix Q in (8.6) is set as $500I$, where I is the identity matrix. A starting 'guess' for the numerical scheme is implemented as

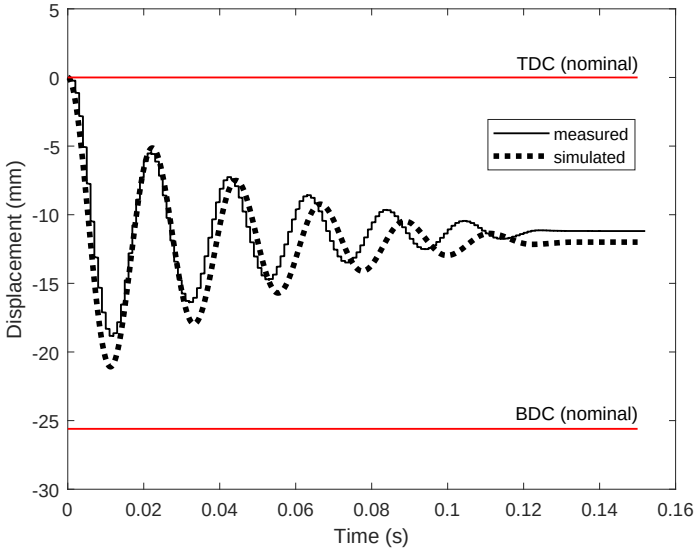

Figure 8.5: Measured versus simulated piston displacement where only friction parameters are estimated.

$\frac{1}{2}(\underline{\theta} + \bar{\theta})$ for the unknown parameter vector θ and as $x_m(t)$ for the state $x(t)$.

8.3.3.1 Friction-Only Parameter Identification

Table 8.4: Parameter Identification Results—Friction Parameters

Parameter	**Units**	**Estimated Value**
a_f	N	26.17
b_f	Ns/m	69.92

Table 8.4 contains the parameter identification results for the friction parameters a_f and b_f. Using these parameters, simulated piston displacement is plotted with the measured piston displacement in Fig. 8.5. The plot shows a close fit of the two graphs in the early high-amplitude part of the response. However, the two graphs progressively go out of phase in the latter low-amplitude part of the response.

In search of a closer-fitting response, a second parameter identification test is carried out where all parameters (m, k_s, a_f, b_f) are identified.

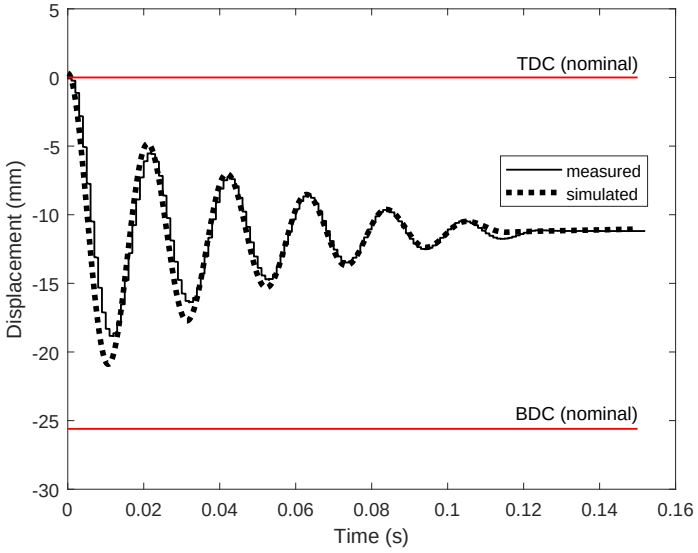

Figure 8.6: Measured versus simulated piston displacement where the entire parameter set is estimated.

8.3.3.2 Entire Parameter Set Identification

Table 8.5: Parameter Identification Results—Entire Parameter Set

Parameter	**Units**	**Estimated Value**	**Designed Value**
m	kg	1.59	2.2
k_s	kN/m	136.08	170
a_f	N	31.63	–
b_f	Ns/m	29.00	–

Table 8.5 contains the parameter identification results for the entire parameter set (m, k_s, a_f, b_f). Using these parameters, simulated piston displacement is plotted with the measured piston displacement in Fig. 8.6. It can be seen in Fig. 8.6 that a closer fit of the two graphs is achieved as compared to Fig.8.5. This parameter set therefore offers good predictive capability for the test FPE piston motion.

It is also interesting to note from Table 8.5 that the estimated parameter values for m and k_s are less than their designed values. This discrepancy could be due to

manufacturing tolerance and other sources of design inaccuracies. But, of greater significance from Table 8.5 (and Table 8.4) is that friction parameters a_f and b_f, while desired to be as small as possible, are in fact large. This indicates high levels of friction in the test FPE system.

On investigating the test FPE, one contributor to the friction was determined as the radial magnetic pull of the translator rod to a magnet pole in the electric machine, resulting in strong contact between the translator rod and linear bearings. This radial magnetic pull between electric machine parts is in fact well-known in electric machine construction [50]; and is due to an unbalanced magnetic field distribution around the translator rod that causes a net resultant attractive force towards a pole. Another possible source of friction was identified as translator rod misalignment, owing to the multiple flanges that link the cylinder, spring case, and electric machine.

This completes the validation of the test FPE dynamics (8.1), which has concluded with high friction levels owing to large Coulomb and viscous friction parameters a_f and b_f (Table 8.5). Model validation has been done here with no combustion. In combustion conditions, the method is still successful, as depicted later in Fig. 8.11.

8.4 Experiment 2: State Estimation of Test FPE

With a validated test FPE model in place, state estimation of the test FPE using measurement data can now be conducted. Towards this end, Chapter 7 provided detailed development of a newly-developed observer for FPE dynamics that culminated into Theorem 1. Having been successfully tested in simulation, the observer—a sliding mode observer—is now to be tested with FPE measurement data for the reconstruction of in-cylinder pressure and piston speed. As in the previous model validation section, measurement data is collected from a free response test.

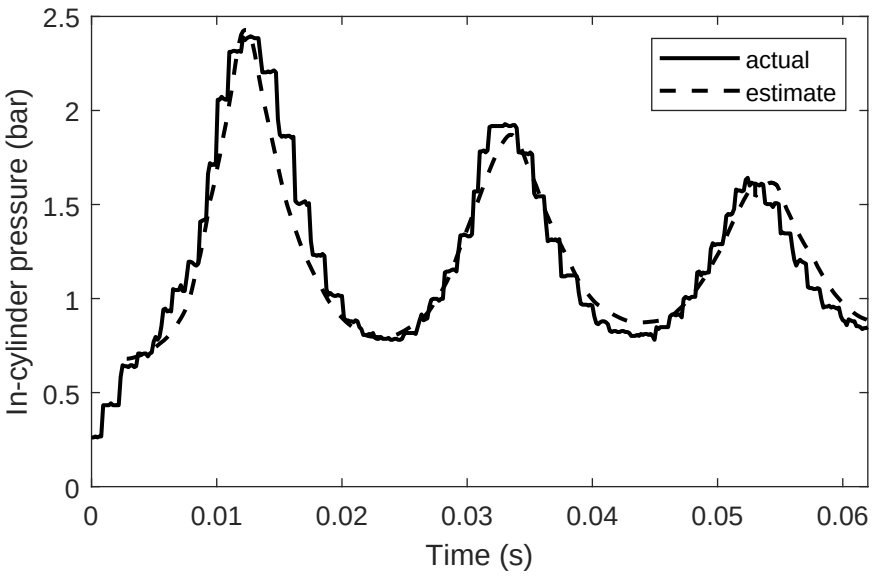

Figure 8.7: Actual versus estimated in-cylinder pressure. The estimated pressure converges quickly and accurately to the actual pressure.

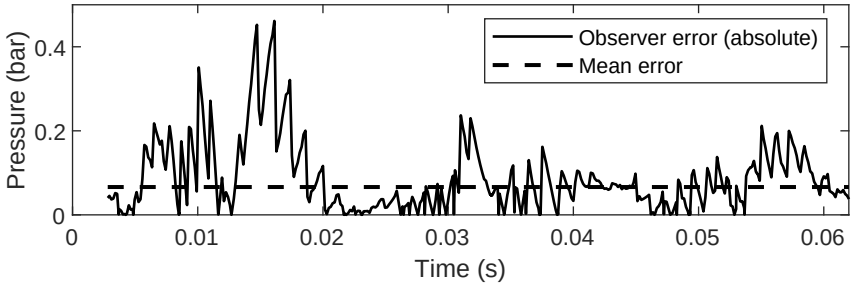

Figure 8.8: Observer error—in-cylinder pressure estimation.

8.4.1 Observer Set Up

The observer input is the net heat release rate, as described in (7.9) and (7.8). The measured output of the FPE is the piston position, as described in (7.10). The applied observer structure is that provided in (7.16)–(7.18).

8.4.2 Experiment Results and Discussion

Figure 8.7 is a plot of the actual versus estimated in-cylinder pressure for three cycles. It can be seen that the estimated in-cylinder pressure trace aligns very closely with

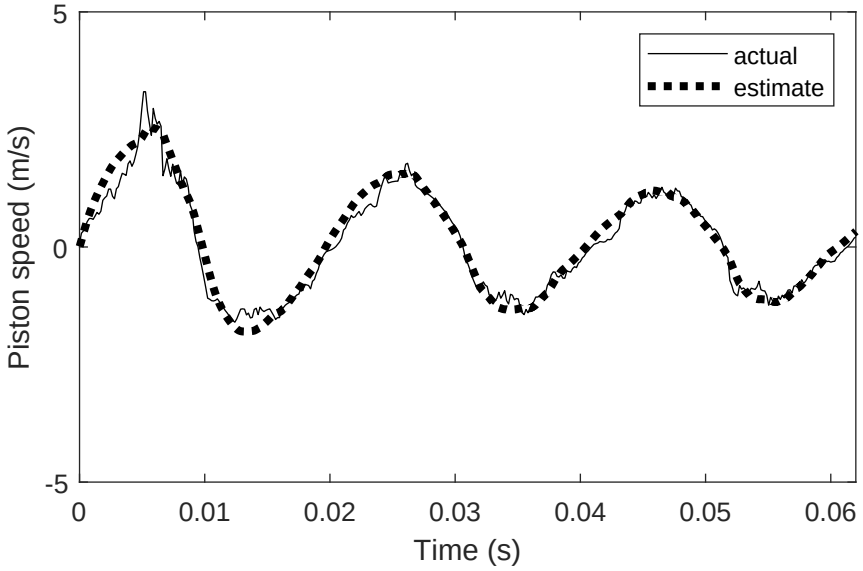

Figure 8.9: Actual versus estimated piston speed.

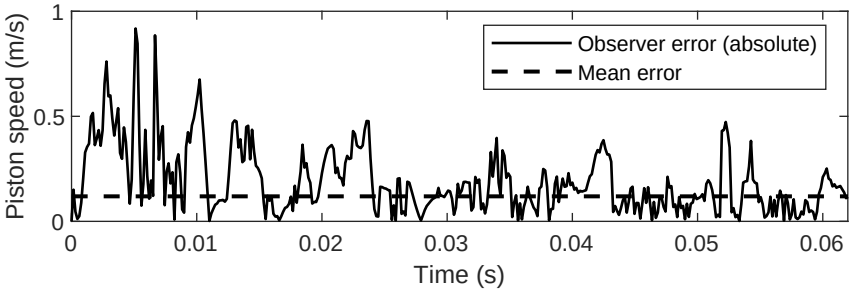

Figure 8.10: Observer error—piston speed estimation.

that of the actual in-cylinder pressure. Indeed, the mean observer error is found to be very small; approximately 0.05 bar as shown in Fig. 8.8. This very close alignment shows high effectiveness of the proposed observer, consistent with simulation results in Fig. 7.3. Also consistent with simulation results is the fact that the largest observer error is seen to occur in the neighbourhood of TDC.

Figure 8.9 is a plot of the actual versus estimated piston speed. The two plots match very closely, with the mean observer error at approximately 0.1 m/s as seen in Fig. 8.10. The observer's effectiveness for piston speed estimation is accordingly demonstrated, consistent with simulation results in Fig. 7.5.

One may observe that the piston speed estimation in Fig. 8.9 is a much closer fit to its actual value than is the in-cylinder pressure estimation in Fig. 8.7. The same observation can be made with the simulation results in Fig. 8.10 and Fig. 7.3 respectively. The difference in observer estimation accuracy can be explained by two reasons. The first is that piston speed is a directly estimated state whereas in-cylinder pressure is an indirectly estimated state, as per the state transformation (7.11). Accordingly, an extra transformation inversion stage is required in the reconstruction of in-cylinder pressure, a computation which may introduce some error owing to uncertainties in the parameters of the transformation. The second reason is that the relationship between piston speed and piston position is much simpler than that between in-cylinder pressure and piston position.

8.5 Stability Remarks on Test FPE

The next and final item of this Chapter is to discuss stability of the test FPE. First, however, a general diagnosis of the operational state of the hardware rig is provided.

8.5.1 Diagnosis Remarks

In these diagnosis remarks, it is first noted that the model validation exercise (Section 8.3) allowed successful state estimation of the test FPE hardware. The model validation exercise did also reveal high Coulomb and viscous friction parameters (a_f and b_f respectively) as per Table 8.5 and Table 8.4. These high friction levels presented limitations to further hardware testing, rectifiable only with significant hardware design modification.

To explain, high friction levels lead to shorter-than-nominal piston stroke (as seen in Fig. 8.5 and Fig. 8.6). Short piston stroke implies weak compression of the scavenge case. A weakly compressed scavenge case in turn prevents effective delivery of fresh fuel-air mixture into the combustion chamber, constituting ineffective scavenging. The engine is then starved of its energy input, fuel, and consequently stalls.

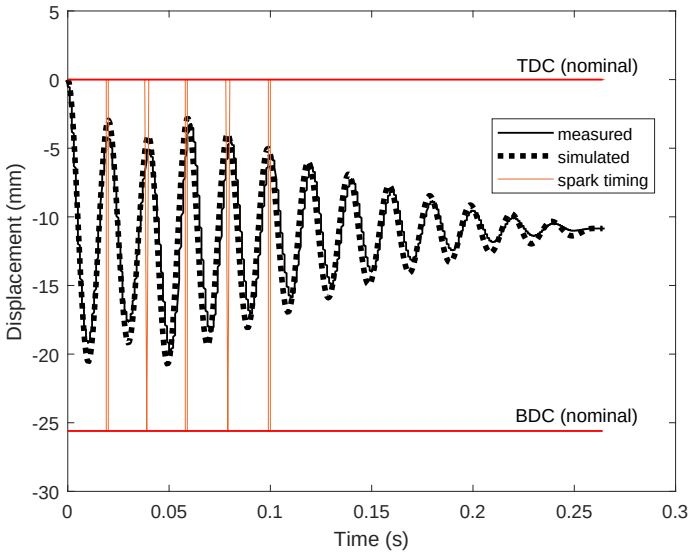

Figure 8.11: Combustion in test FPE.

Additionally, when combustion occurs, successive combustion from one cycle to the next may not take place, as the scavenging process is ineffective. For example, Fig. 8.11 shows test FPE measurement data *with* combustion (a simulation trace is included to emphasize the predictive capability of the validated FPE model (8.5)).

Combustion occurs at the second spark event, evidenced by the rise in piston amplitude in the following cycle. However, due to an ineffective scavenging process, the combusted fuel is not replenished, starving the cylinder of fuel and consequently leading to stall.

It is nonetheless re-stated that despite hardware limitations, significant pieces of experimental work were successfully undertaken on the rig; namely model validation and estimation of in-cylinder pressure and piston speed.

8.5.2 Stability Remarks

Chapter 3 provided an energy-based framework in which FPE stability can be understood. This framework is now used to explain FPE stability using the piston response in Fig. 8.11.

It can be observed in Fig. 8.11 that piston oscillation amplitude decays to zero. The FPE is therefore *unstable*, as per Definition 1.

In Fig. 8.11, one combustion event occurs. This is at the second spark, as evidenced by the subsequent rise in piston amplitude. Let the combusted fuel mass be the nominal fuel mass for which a nominal spring stiffness in Table 8.1 and a nominal generator coefficient in Equation (8.2a) produce the nominal stroke in Table 8.1. (These associations can be asserted following Fact 3.)

If the nominal fuel mass were to be applied on every cycle, Proposition 1 stipulates that the FPE stroke would converge to the nominal stroke, having started away from it. Indeed, in Fig. 8.11, the piston stroke changes (by rising) following the combustion, but does not reach the nominal stroke because application of the nominal fuel mass is not sustained. Instead, for the reasons elaborated in Section 8.5.1, misfire occurs and the FPE becomes unstable by stalling.

The occurrence of misfire can be interpreted as a perturbation on the nominal fuel

mass from the actual value to zero. Proposition 2 stipulates that such a perturbation on the fuel will cause the FPE to find a new operating point. An operating point at which the fuel combusted is zero, i.e. where there is no energy supplied to the FPE, can be expected to have zero stroke, as observed in Fig. 8.11.

8.6 Chapter Conclusions

This chapter has first described the features of a test FPE in hardware and thereafter described three aspects of experimental work; namely (i) model validation, following a parameter identification procedure that has been cast as a general optimisation problem, (ii) state estimation of in-cylinder pressure and piston speed, and (iii) stability assessment of the test FPE within an energy-based framework developed in Chapter 3. Model validation showed a simulation response predicting measurement to a very close fit. State estimation demonstrated strong effectiveness of the proposed sliding mode observer developed in Chapter 7. It was found here that the estimated in-cylinder pressure and piston speed traces were closely aligned to their actual traces, with mean errors of 0.05 bar and 0.1 m/s respectively. The chapter has also discussed the limitations of the test FPE hardware rig, the addressing of which entails significant hardware design modification and accordingly forms part of future work in Chapter 9.

Chapter 9

Conclusions and Future Work

9.1 Conclusions

Free-Piston Engines (FPEs) are appealing for their compactness, mechanical simplicity, and variable compression ratio. But, absence of a crank mechanism leaves the piston mechanically unconstrained, in turn introducing a stability and control problem associated with piston motion. The overall aim of this thesis has been to provide model-based approaches in the analysis of FPEs; to cover stability, control, and state estimation, whilst placing emphasis on FPEs as power generators. This objective has been met, as elaborated next.

A unified modelling approach that accommodates any rebound device (such as a mechanical spring, a bounce chamber, or another combustion chamber) has been taken. This unification has allowed development of a general analytical approach throughout the thesis aimed at encompassing multiple rebound device types. For simplicity, the FPE configuration of choice has been the single piston FPE configuration.

A framework for understanding FPE stability has been developed with the energy conservation principle. The framework includes definitions of stability, as well as

technical facts and propositions that relate key physical FPE parameters. The key developments in this area have been the energy-based conditions under which a nominal piston stroke is achieved, and conditions under which a nominal piston stroke is lost. It was noted that a more rigorous stability analysis based on Lyapunov theory could possibly be constructed if the FPE system is treated as a hybrid dynamical system.

The first and most important control problem of an FPE was stated as that of the control of compression ratio. In this thesis, a model-based procedure for control of BDC and TDC in a free-piston engine has been developed, thereby achieving analytically guided compression ratio control. The control was demonstrated with both a simple control scheme in the form of a PI controller, and more advanced control scheme in the form of the optimal LQR controller. Stability conditions in terms of the PI controller parameters were given. The performance difference between the two controllers was in the transient piston response; the LQR response generally being slower to reach steady state due to fuel input minimisation.

The second control problem considered was that of starting an FPE, where two strategies have been studied; these are with mechanical resonance and by optimal start. Readily implementable, closed-form motoring force functions have been developed and tested where none had been previously advanced in the literature. For an FPE whose rebound device is a mechanical spring, the optimal strategy has been verified as superior—with a significantly less root-mean-square motoring force and performance index compared to the resonance strategy. For an FPE whose rebound device is a bounce chamber, the optimal strategy should be better in principle, but can face numerical tractability hurdles . Here, a designed mechanical resonance strategy has been found adequate.

The third control problem involved mitigating against misfire, and the need for alternative approaches (to energy-based approaches) in the control of compression ratio.

For these two problems, the concept of in-stroke motoring was introduced, which refers to externally driving a piston whilst it traverses a stroke; achieved by operating the FPE's generator as a motor. This thesis puts in-stroke motoring on sound analytical footing following recent experimental work involving the strategy. Methods for development of both constant and dynamic in-stroke motoring forces are presented and successfully tested.

On state estimation, the thesis developed an observer for both in-cylinder pressure and piston speed for free piston engines. The proposed observer is suitable for robust real-time pressure estimation at high engine frequencies owing to finite time observer error convergence. Indeed, the observer's finite-time convergence property grants it a distinct advantage over asymptotically converging observers; such as the high gain observer (as the thesis shows) and Extended Kalman Filter (where linearization of FPE dynamics is an acceptable modelling compromise). A generalization of the proposed observer has also been developed, allowing the engineer to select from various observer implementations while assessing any performance differences.

Finally, the thesis has described experimental work on a free-piston engine developed at the University of Sussex. The experimental work covered three aspects, namely:

i) Model validation,

ii) Estimation of in-cylinder pressure and piston speed, and

iii) Stability assessment

The model validation exercise was carried out using a parameter identification approach that did not require the property of persistent excitation, yielding simulation results that predicted measurement to a very close fit. State estimation of in-cylinder pressure and piston speed was successfully demonstrated using the sliding mode observer developed in Chapter 7. The observer yielded closely-fitting estimated-versus-actual traces, with very small mean observer error; 0.05 bar and 0.1 m/s for in-cylinder

pressure and piston speed estimation respectively. Finally, the stability of the test FPE was assessed within the energy-based framework proposed by the thesis in Chapter 3.

9.2 Future Work

Some aspects of this work have been identified for further research. They are categorised into the three areas described below:

- **Modelling.** An assumption has been made that different commonly occurring FPE configurations can be approximated by one or more single piston FPE configurations. Arguments can be made to defend this assumption, and accordingly, the thesis has focused on the single piston FPE configuration. However, further research may explore developing multi-input multi-output (MIMO) techniques for which FPE configurations that are not of single piston type would directly be suitable for.

- **Stability.** Stability of FPE piston motion has been explained with energy-based arguments starting with the energy conservation principle. This approach is helpful for an intuitive understanding of FPE stability, and has been attempted by a number of authors [69, 109, 115] (and further developed in this thesis). However, further research may involve more rigorous stability analysis of FPE piston motion, say with Lyapunov theory. This thesis points to work by Goebel, Sanfelice, and Teel [38] on hybrid dynamical systems.

- **Testing in hardware.** All model-based methods developed in this thesis have been successfully tested against a mathematical FPE model validated in the literature. Indeed, the thesis validates the same mathematical model against a physical test FPE, and uses this model to experimentally verify the proposed sliding mode observer in a state estimation exercise for in-cylinder pressure and

piston speed.

The built test FPE hardware rig did, however, have limitations owing to friction; limitations that strongly impacted the scavenging process, thereby only allowing *some* hardware testing. Future work here involves significant hardware design modification, involving a detailed examination and subsequent removal of high friction sources, such as an unbalanced electric machine field distribution, translator rod misalignment, and overall improved mechanical design. Additionally, alternative charge delivery schemes such as direct injection may be considered in order to facilitate decoupling of the friction problem from the scavenging problem.

Overall, the experimentally successful model validation and state estimation results coupled with the extensive simulation have not only ensured that the thesis objectives have been met, but also provide confidence that the proposed model-based methods are directly implementable in practice.

References

[1] Overview of lithium ion batteries. Technical report, Panasonic, January 2007.

[2] P. A. J. Achten. A review of free piston engine concepts. *SAE Paper 941776*, 1994.

[3] P. A. J. Achten, J. P. J. Van den Oever, J. Potma, and G. Vael. Horsepower with brains: The design of the chiron free piston engine. *SAE Paper 2000-01-2545*, 2000.

[4] Hans Thomas Aichlmay. *Design Considerations, Modeling, and Analysis of Micro-Homogeneous Charge Compression Ignition Combustion Free-Piston Engines*. PhD thesis, University of Minnesota, 2002.

[5] A. Al-Durra., M. Canova, and S. Yurkovich. A model based methodology for on-line estimation of diesel engine cylinder pressure. *ASME Journal of Dynamic Systems, Measurement, and Control*, **133**:031005, 2011.

[6] B. D. O. Anderson and J. B. Moore. *Optimal Control, Linear Quadratic Methods*. Prentice Hall, 1989.

[7] Kurt D. Annen, David B. Stickler, and Paul L. Kebabian. Miniature generator. *US Patent No 6,349,683 B1*, February 2002.

[8] Kurt D. Annen, David B. Stickler, and Jim Woodroffe. Miniature internal combusti on engine-generator for high energy density portable power. In

Proceedings of the Army Science Conference, December 2008. Held in Orlando, Florida.

[9] Kurt D. Annen, Jaime Woodroffe, Michael Agnese, and David B. Stickler. Power generating system. *US Patent No 7,485,977 B2*, February 2009.

[10] Michael Athans and Peter L. Falb. *Optimal Control: An Introduction to the Theory and Its Applications*. Dover Publications, 2007.

[11] Christopher M. Atkinson, Sorin Petreanu, Nigel N. Clark, Richard J. Atkinson, Thomas I. McDaniel, Subhash Nandkumar, and Parviz Famouri. Numerical simulation of a two-stroke linear engine-alternator combination. *SAE Technical Paper 1999-01-0921*, 1999.

[12] J. P. Barbot and T. Boukhobza. Sliding mode observer for triangular input form. In *Proceedings of the 35th Conference on Decission and Control*, pages 1489–1490, 1996.

[13] Carl M. Bender and Steven A. Orszag. *Advanced Mathematical Methods for Scientists and Engineers I Asymptotic Methods and Perturbation Theory*. Springer, 1999.

[14] C. Bennett, J. F. Dunne, S. Trimby, and D. Richardson. Engine cylinder pressure reconstruction using crank kinematics and recurrently-trained neural networks. *Mechanical Systems and Signal Processing*, **85**:126–145, 2017.

[15] G. Besancon. *Nonlinear Observers and Applications*, chapter 1. Springer, 2007.

[16] John T. Betts. *Practical Methods for Optimal Control and Estimation Using Nonlinear Programming*. Society for Industrial and Applied Mathematics, 2010.

[17] G. P. Blair. *Design and Simulation of Two-Stroke Engines*. Society of Automotive Engineers, 1996.

[18] P. Van Blarigan, N. Paradiso, and S. Goldsborough. Homogeneous charge compression ignition with a free piston: A new approach to ideal otto cycle performance. *SAE Technical Paper 982484*, 1998.

[19] I. Boldea and S. A. Nasar. *Linear Electric Actuators and Generators*. Cambridge University Press, 1997.

[20] G. Borman and K. Nishiwaki. Internal-combustion engine heat transfer. *Progress in Energy Combustion Science*, **13**:1–46, 1987.

[21] G. Bornard, F. Celle-Couenne, and G. Gilles. *Nonlinear Systems - Modeling and Estimation*, chapter Observability and Observers, pages 173–216. Chapman & Hall, London, 1995.

[22] A. Cameron. *Basic Lubrication Theory*. Ellis Horwood, 2 edition, 1981.

[23] F. Caresana, G. Comodi, and L. Pelagalli. Design approach for a two stroke free piston engine for electric power generation. *SAE Technical Paper 2004-32-0037*, 2004.

[24] S. Chen and J. Moskwa. Application of nonlinear sliding mode observers for cylinder pressure reconstruction. *Control Engineering Practice*, **14**:1115–1121, 1997.

[25] M. Contestabile, G. Offer, and R. North. Electric vehicles: A synthesis of the current literature with a focus on economic and environmental viability. Technical report, LCAworks, 2012.

[26] G. Corliss. Which root does the bisection algorithm find? *SIAM Review*, **19**(2):325–327, 1977.

[27] S. V. Drakunov. Sliding-mode observers based on equivalent control method. In *Proceedings of the 31st Conference on Decission and Control*, pages 2368–2369, 1991.

[28] J. F. Dunne. Dynamic modelling and control of semifree-piston motion in a rotary diesel generator concept. *ASME Journal of Dynamic Systems, Measurement, and Control*, 2010.

[29] J. F. Dunne. Power supply systems. *US Patent No. 8519553 B2*, 2013.

[30] J. F. Dunne. Personal communication, 2017.

[31] Ulrich Eberle and Rittmar von Helmolt. Sustainable transportation based on electric vehicle concepts: a brief overview. *Energy & Environmental Science*, **3**:689–699, June 2010.

[32] L. Eriksson and L. Nielsen. *Modeling and Control of Engines and Drivelines*. Wiley, 2014.

[33] H. O. Farmer. Free-piston compressor-engines. *Proceedings of the Institution ofMechanical Engineers*, **156**:253–271, 1947.

[34] D. Foster. An overview of zero-dimensional thermodynamic models for IC engine data analysis. *SAE Technical Paper 852070*, 1986.

[35] Linda Gaines. The future of automotive lithium-ion battery recycling: Charting a sustainable course. *Sustainable Materials and Technologies*, **1-2**:2–7, December 2014.

[36] J. P. Gauthier and A. K. Kupka. *Deterministic Observation Theory and Applications*. Cambridge University Press, 1997.

[37] R. J. Gilmore and M. B. Steer. Nonlinear circuit analysis using the method of harmonic balance–A review of the art. Part I. Introductory concepts. *Int. J. Microw. Mill.-Wave Comput.-Aided Eng.*, **1**:22–27, 1991.

[38] Rafal Goebel, Ricardo G. Sanfelice, and Andrew R. Teel. *Hybrid Dynamical Systems, Modeling, Stability, and Robustness*. Princeton University Press, 2012.

[39] X. Gong, K. Zaseck, I. Kolmanovsky, and H. Chen. Modeling and predictive control of free piston engine generator. In *Proceedings of the 2015 American Control Conference*, pages 4735–4740, 2015. Chicago, IL.

[40] Graham C. Goodwin, Stefan F. Graebe, and Mario E. Salgado. *Control System Design*. Prentice Hall, 2001.

[41] V. Gopalakrishnan, P. M. P. Najt, and R. P. Durrett. Free piston linear alternator utilizing opposed pistons with spring return. *US Patent 8,714,117 B2*, 2014.

[42] S. Goto, K. Moriya, H. Kosaka, T. Akita, Y. Hotta, T. Umeno, and K. Nakakita. Development of free piston engine linear generator system Part 2 - Investigation of control system for generator. *SAE Technical Paper 2014-01-1193*, 2014.

[43] Y. Guezennec and P. Gyan. A novel approach to real-time estimation of the individual cylinder combustion pressure for S.I. engine control. *SAE Paper 1999-01-0209*, 1999.

[44] H. Hamedovic, F. Raichle, J. Breuninger, W. Fischer, W. Dieterle, and M. Klenk. IMEP-estimation and in-cylinder pressure reconstruction for multicylinder SI-engine by combined precessing of engine speed and one cylinder pressure. *SAE Paper 2005-01-0053*, 2005.

[45] M. R. Hanipah, R. Mikalsen, and A. P. Roskilly. Recent commercial free-piston engine developments for automotive applications. *Applied Thermal Engineering*, **75**(22):493–503, 2015.

[46] A. Hbi and T. Ito. Fundamental test results of a hydraulic free piston internal combustion engine. *Proceedings of Institute of Mechanical Engineering*, **218**(10):1149–1157, 2004.

[47] J. B. Heywood. *Internal Combustion Engine Fundamentals*. McGraw-Hill, 1988.

[48] G. Hohenberg. Advanced approaches for heat transfer calculations. *SAE Paper 790825*, 1979.

[49] K. V. Hoose and E. E. Shorey. The high performance toroidal engine concept (hipertec). In *Proceedings of the ASME 2011 Internal Combustion Engine Division Fall Technical Conference*, 2011. Morgantown, West Virginia.

[50] Austin Hughes and Bill Drury. *Electric Motors and Drives: Fundamentals, Types, and Applications*. Elsevier, fourth edition, 2013.

[51] Petros Ioannou and Baris Fridan. *Adaptive Control Tutorial*. Society for Industrial and Applied Mathematics, 2006.

[52] B. Jia, R. Mikalsen, A. Smallbone, Z. Zuo, and H. Feng. Piston motion control of a free-piston engine generator: A new approach. *Applied Energy*, **179**:1166–1175, 2016.

[53] B. Jia, Z. Zuo, H. Feng, G. Tian, and A. P. Roskilly. Development approach of a spark-ignited free-piston engine generator. *SAE Technical Paper 2014-01-2894*, 2014.

[54] B. Jia, Z. Zuo, H. Feng, G. Tian, and A. P. Roskilly. An experimental investigation into the starting process of free-piston engine generator. *Applied Energy*, **157**:798–804, 2015.

[55] B. Jia, Z. Zuo, G. Tian, H. Feng, and A. P. Roskilly. Development and validation of a free-piston engine generator numeric model. *Energy Conversion and Management*, **91**:333–341, 2015.

[56] T. A. Johansen, O. Egeland, E. A. Johannessen, and R. Kvamsdal. Free-piston diesel engine dynamics and control. In *Proceedings of the American Control Conference*, pages 4579–4584, 2001. Arlington, VA.

[57] T. A. Johansen, O. Egeland, E. A. Johannessen, and R. Kvamsdal. Free-piston diesel engine timing and control-toward electronic cam and crankshaft. *IEEE Trans. Control Syst. Technol.*, **10**(2):177–190, 2002.

[58] E. Kartashova. *Nonlinear Resonance: Analysis, Theory, Computation, Applications*. Cambridge University Press, New York, 2010.

[59] J. Kevorkian and J. D. Cole. *Perturbation Methods in Applied Mathematics*. Springer-Verlag, 1981.

[60] H. K. Khalil. *Nonlinear Systems*. Prentice Hall, 2002.

[61] D. Kirk. *Optimal Control Theory: An Introduction*. Dover Publications, 1998.

[62] F. Kock, J. Haag, and H. E. Friederich. The free piston linear generator-development of an innovative,compact, highly efficient range-extender module. *SAE Paper 2013-01-1727*, 2013.

[63] H. Kosaka, T. Akita, K. Moriya, S. Goto, Y. Hotta, T. Umeno, and K. Nakakita. Development of free piston engine linear generator system Part 1 - Investigation of fundamental characteristics. *SAE Technical Paper 2014-01-1203*, 2014.

[64] A. Levant. Sliding order and sliding accuracy in sliding mode control. *International Journal of Control*, **58**:1247–1263, 1993.

[65] A. Levant. Homogeneity approach to high-order sliding mode design. *Automatica*, **41**:823–830, 2005.

[66] A. Levant. Principles of 2-sliding mode design. *Automatica*, **43**:576–586, 2006.

[67] A. Levant. Chattering analysis. *IEEE Transactions on Automatic Control*, **55**(6):1380–1389, 2010.

[68] K. Li, A. Sadighi, and Z. Sun. Active motion control of a hydraulic free piston engine. *IEEE/ASME Transactions on Mechatronics*, 2014.

[69] K. Li and Z. Sun. Stability analysis of a hydraulic free piston engine with HCCI combustion. In *Proceedings of the ASME 2011 Dynamic Systems and Control Conference and Bath/ASME Symposium on Fluid Power and Motion Control*, **2**, pages 655–662, 2011.

[70] K. Li, C. Zhang, and Z. Sun. Precise piston trajectory control for a free piston engine. *Control Engineering Practice*, **34**:30–38, 2015.

[71] Ke Li. *Modelling and Control of Free Piston Engine*. PhD thesis, University of Minnessota, December 2014.

[72] J. M. Lin, Z. P. Xu, S. Q. Chang, and N. X. Yin. Thermodynamic simulation and prototype testing of a four-stroke free piston engine. *ASME Journal of Engineering for Gas Turbines and Power*, **136**:1–8, 2014.

[73] A. L. London and A. K. Oppenheim. The free-piston engine development - present status. *Transactions of the ASME*, **74**(2):1349–1361, 1952.

[74] J. Mao, Z. Zuo, and H. Feng. Parameters coupling designation of diesel free-piston linear alternator. *Applied Energy*, **88**:4577–4589, 2011.

[75] G. P. Merker and M. Gerstle. Evaluation of two stroke engines scavenging models. *SAE Technical Paper 970358*, 1997.

[76] R. Mikalsen and A. Roskilly. Performance simulation of a spark ignited free-piston engine generator. *Applied Thermal Engineering*, **28**:1726–33, 2008.

[77] R. Mikalsen and A. P. Roskilly. A review of free-piston engine history and applications. *Applied Thermal Engineering*, **27**:2339–52, 2007.

[78] R. Mikalsen and A. P. Roskilly. The design and simulation of a two-stroke free-piston compression ignition engine for electrical power generation. *Applied Thermal Engineering*, **28**:589–600, 2008.

[79] R. Mikalsen and A. P. Roskilly. The fuel efficiency and exhaust gas emissions of a low heat rejection free-piston diesel engine. *Proceedings of the Institution of Mechanical Engineers, Part A: Journal of Power and Energy*, **223**(4):379–386, 2009.

[80] R. Mikalsen and A. P. Roskilly. The control of a free-piston engine generator–Part 1: Fundamental analyses. *Applied Energy*, **87**(4):1273–1280, 2010.

[81] R. Mikalsen and A. P. Roskilly. The control of a free-piston engine generator–Part 2: Engine dynamics and piston motion control. *Applied Energy*, **87**(4):1281–1287, 2010.

[82] R. Mikalsen and A.P. Roskilly. A computational study of free-piston diesel engine combustion. *Applied Energy*, pages 1136–1143, 2009.

[83] John M. Miller. *Propulsion Systems for Hybrid Vehicles*. Institution of Engineering and Technology, illustrated edition, 2010.

[84] K. Moriya, S. Goto, T. Akita, H. Kosaka, Y. Hotta, and K. Nakakita. Development of free piston engine linear generator system part3 - novel control method of linear generator for to improve efficiency and stability. *SAE Technical Paper 2016-01-0685*, 2016.

[85] M. A. Mueller. Electrical generators for direct drive wave energy converters. In *IEE Proceedings - Generation, Transmission and Distribution*, 2002.

[86] James A. Murdock. *Perturbations: Theory and Methods*. Society for Industrial and Applied Mathematics, 1999.

[87] Fujio Nagao and Yuzuru Shimamoto. The effect of crankcase volume and the inlet system on the delivery ratio of two-stroke cycle engines. *SAE Technical Paper 670030*, 1967.

[88] Ali Hasan Nayfeh. *Perturbation Methods*. Wiley-VCH, 2004.

[89] O. B. Noren and R. L. Erwin. The future of the free-piston engine in commercial vehicles. *SAE Transactions*, **66**:305–314, 1958.

[90] M. A. Patterson and A. V. Rao. GPOPS - II Version 1.0: A general purpose MATLAB toolbox for solving optimal control problems using the radau pseudospectral method. University of Florida, 2013.

[91] W. Perruquetti and J. P. Barbot. *Sliding Mode Control in Engineering*. Marcel Dekker, 2002.

[92] R. P. Pescara. Motor compressor apparatus. *US Patent No. 1,657,641*, 1928.

[93] L.A. Pipes and L. R. Harvill. *Applied Mathematics for Engineers and Physicists*. McGraw-Hill, 1970.

[94] A. D. Polyanin and V. F. Zaitsev. *Handbook of Exact Solutions for Ordinary Differential Equations (2nd edition)*. Boca Raton: Chapman & Hall/CRC Press, 2003.

[95] J. Powell. Engine control using cylinder pressure: past, present, and future. *ASME Journal of Dynamic Systems, Measurement, and Control*, 1993.

[96] Mulukutla S. Sarma R. Sastry Vedam. *Power Quality: VAR Compensation in Power Systems*. CRC Press, 2017.

[97] S. F. Rezeka and N. A. Henein. A new approach to evaluate instantaneous friction and its components in internal combustion engines. *SAE Paper 840179*, 1984.

[98] J. Slotine and W. Li. *Applied Nonlinear Control*. Prentice-Hall, 1991.

[99] S. K. Spurgeon. Sliding mode observers: A survey. *International Journal of Systems Science*, **39**:751–764, 2008.

[100] R. Stone. *Introduction to Internal Combustion Engines*. Palgrave, fourth edition, 2012.

[101] S. Tikkanen and M. Vilenius. Hydraulic free piston engine–challenge for control. In *Proceedings of the European Control Conference*, pages 2943–2948, 1999. Aug. 31-Sept. 3, Karlsruhe, Germany.

[102] C. Toth-Nagy and N. N. Clark. The linear engine in 2004. *SAE Paper 2005-01-2140*, 2005.

[103] S. Trimby, J.F. Dunne, C. Bennett, and D. Richardson. Unified approach to engine cylinder pressure reconstruction using time-delay neural networks with crank kinematics or block vibration measurements. *International Journal of Engine Research*, **18**:256–272, 2017.

[104] G. E. M. Vael and P. A. J. Achten. The Innas fork lift truck, working under constant pressure. In *Proceedings of 1st IFK, IFAS/RWTH*, 1998. Aachen, Germany.

[105] Ferdinand Verhulst. *Nonlinear Differential Equations and Dynamical Systems*. Springer-Verlag, 1990.

[106] J. Wang and D. Howe. A linear permanent magnet generator for a free-piston energy converter. In *IEEE International Conference on Electric Machines and Drives*, 2005. San Antonio, TX.

[107] D. D. Weiner and J. E. Spiner. *Sinusoidal Analysis and Modeling of Weakly Nonlinear Circuits*. Van Nostrand Reinhold Company, 1980.

[108] G. Woschni. A universally applicable equation for the instantaneous heat transfer coefficient in the internal combustion engine. *SAE Technical Paper 670931*, 1967.

[109] W. Wu, J. Hu, and S. Yuan. Semi-analytical modelling of a hydraulic free-piston engine. *Applied Energy*, **120**:75–84, 2014.

[110] Y. Wu, X. Yu, and Z. Man. Terminal sliding mode control design for uncertain dynamic systems. *Systems & Control Letters*, **34**:281–287, 1998.

[111] Wei Yang, Ulrich Bonne, and Burgess R. Johnson. Microcombustion engine/generator. *US Patent No. 2001/0029911 A1*, 2001.

[112] Chenheng Yuan, Haigen Ren, and Jing Xu. Comparison of the gas exchange of a loop scavenged free-piston engine alternator and the conventional engine. *Applied Thermal Engineering*, **127**:638–649, 2017.

[113] K. Zaseck, M. Brusstar, and I. Kolmanovsky. Stability, control, and constraint enforcement of piston motion in a hydraulic free-piston engine. *IEEE Transactions on Control Systems Technology*, **25**(4):1284 – 1296, 2017.

[114] C. Zhang and Z. Sun. Using variable piston trajectory to reduce engine-out emissions. *Applied Energy*, **170**:403–414, 2016.

[115] S. Zhang, C. Zhao, and Z. Zhao. Stability analysis of hydraulic free piston engine. *Applied Energy*, 2015.

[116] Fuquan Zhao, Thomas W. Asmus, Dennis N. Assanis, John E. Dec, James A. Eng, and Paul M Najt. *Homogeneous Charge Compression Ignition (HCCI) Engines: Key Research and Development Issues*. SAE International, 2003.

[117] Zhenfeng Zhao, Fujun Zhang, Ying Huang, Changlu Zhao, and Feng Guo. An experimental study of the hydraulic free piston engine. *Applied Energy*, **99**:226–233, 2012.

[118] Saiful A. Zulkifli, Mohd N. Karsiti, and A. Rashid A. Aziz. Starting of a free-piston linear engine-generator by mechanical resonance and rectangular current commutation. In *Vehicle Power and Propulsion Conference*, 2008. Held in Harbin, China.

[119] Y. H. Zweiri, J. F. Whidborne, and L. D. Seneviratne. Instantaneous friction components model for transient engine operation. *Proc. Inst. Mech. Eng. D, J. Automobile Eng.*, **214**(7):809–824, 2000.

Appendix A

Minimum-Energy Optimal Control of a Linear Oscillator

Consider a system describing a linear oscillator with control input $u(t)$:

$$m\ddot{x}_0(t) + b\dot{x}_0(t) + kx_0(t) = u(t) \tag{A.1}$$

where m, b, and k are constant. Defining $x_1(t) = x_0(t)$ and $x_2(t) = \dot{x}_0(t)$, system (A.1) has the state space representation

$$\dot{x}_1(t) = x_2(t) \tag{A.2a}$$

$$\dot{x}_2(t) = -\frac{k}{m}x_1(t) - \frac{b}{m}x_2(t) - \frac{1}{m}u(t) \tag{A.2b}$$

The objective is to find a control input that minimizes a performance index

$$J(u) = \int_{t_0}^{t_f} ru(t)^2 dt \tag{A.3}$$

where $r > 0$ is constant, when driving the system state from an initial state $(x_1(0), x_2(0))$ at time $t = 0$ to a final state $(x_1(t_f), x_2(t_f))$ at time $t = t_f$. Optimal control problems

with a performance index (5.22) involving the integral of the square of a system input variable are generally known as minimum-energy problems [61].

Let only smooth control inputs $u(t)$ be admissible. Following the variational approach to optimal control [61], by defining a Hamiltonian function

$$H = ru(t)^2 + p_1(t)x_2(t) + p_2(t)\left(-\frac{k}{m}x_1 - \frac{b}{m}x_2 - \frac{1}{m}F_m\right) \tag{A.4}$$

where $p_1(t)$ and $p_2(t)$ are costate variables, necessary conditions for an optimal solution comprising the optimal control, state, and costate variables respectively denoted $u^*(t)$, $(x_1^*(t), x_2^*(t))$, and $(p_1^*(t), p_2^*(t))$ are found as

$$\dot{x}_1^*(t) = \left.\frac{\partial H}{\partial p_1}\right|_* = x_2^*(t) \tag{A.5}$$

$$\dot{x}_2^*(t) = \left.\frac{\partial H}{\partial p_2}\right|_* = -\frac{k}{m}x_1^*(t) - \frac{b}{m}x_2^*(t) - \frac{1}{m}u^*(t) \tag{A.6}$$

$$\dot{p}_1^*(t) = -\left.\frac{\partial H}{\partial x_1}\right|_* = \frac{k}{m}p_2^*(t) \tag{A.7}$$

$$\dot{p}_2^*(t) = -\left.\frac{\partial H}{\partial x_2}\right|_* = -p_1^*(t) + \frac{b}{m}p_2^*(t) \tag{A.8}$$

$$0 = \left.\frac{\partial H}{\partial F_m}\right|_* = 2ru(t)^*(t) - \frac{p_2^*(t)}{m} \tag{A.9}$$

where $t \in [0, t_f]$.

The next step in finding the solution to the optimal control problem is to solve the equations (A.5)–(A.9). First, equation (A.9) can directly be solved for the optimal control $u^*(t)$ as

$$u^*(t) = \frac{p_2^*(t)}{2rm} \tag{A.10}$$

Next, solving for the costate variables $p_1^*(t)$ and $p_2^*(t)$ proceeds as follows. Differenti-

ating equation (A.7) with respect to time gives

$$\ddot{p}_1^*(t) = \frac{k\dot{p}_2^*(t)}{m} \tag{A.11}$$

Using (A.8) in (A.1) yields a dynamic equation in $p_1^*(t)$ as

$$\ddot{p}_1^*(t) - \frac{b}{m}\dot{p}_1^*(t) + \frac{k}{m}p_1^*(t) = 0 \tag{A.12}$$

Equation (A.12) is a linear second order differential equation with the solution

$$p_1^*(t) = c_1 e^{\theta_1 t} + c_2 e^{\theta_2 t} \tag{A.13}$$

where

$$\theta_{1,2} = \frac{1}{2}\left(\frac{b}{m} \pm \sqrt{\left(\frac{b}{m}\right)^2 - 4\frac{k}{m}}\right) \tag{A.14}$$

and where $c_1$and c_2 are in general complex number constants dependent on boundary conditions. Using the solution for $p_1^*(t)$ in A.13, the solution for $p_2^*(t)$ is found as

$$p_2^*(t) = \frac{m}{k}\left(c_1\theta_1 e^{\theta_1 t} + c_2\theta_2 e^{\theta_2 t}\right) \tag{A.15}$$

The optimal control $u^*(t)$ is now found by substituting (A.15) in (A.10), giving

$$u^*(t) = \frac{1}{2rk}\left(c_1\theta_1 e^{\theta_1 t} + c_2\theta_2 e^{\theta_2 t}\right) \tag{A.16}$$

The constants $c_1$and c_2 are still undetermined. Solving for these constants requires application of boundary conditions to the problem. To do this, the optimal trajectories $x_1^*(t)$ and $x_2^*(t)$ must first be determined. Accordingly, when (A.16) is applied to (A.2), the the scalar differential equation describing $x_1^*(t)$ is realized as

$$\ddot{x}_1^*(t) + \frac{b}{m}\dot{x}_1^*(t) + \frac{k}{m}x_1^*(t) = \frac{1}{2rmk}\left(c_1\theta_1 e^{\theta_1 t} + c_2\theta_2 e^{\theta_2 t}\right) \tag{A.17}$$

Equation (A.17) is a forced second order linear differential equation whose complete solution constitutes the sum of the solution to the homogeneous equation and the so-called particular integral. The homogeneous solution is given by

$$x_{1h}^{*}(t) = c_3 e^{\theta_3 t} + c_4 e^{\theta_4 t} \tag{A.18}$$

where

$$\theta_{3,4} = \frac{1}{2}\left(-\frac{b}{m} \pm \sqrt{\left(\frac{b}{m}\right)^2 - 4\frac{k}{m}}\right) \tag{A.19}$$

while the particular integral given by

$$x_{1p}^{*}(t) = \frac{c_1\theta_1 e^{\theta_1 t}}{2rk\left(\theta_1^2 m + \theta_1 b + k\right)} + \frac{c_2\theta_2 e^{\theta_2 t}}{2rk\left(\theta_1^2 m + \theta_1 b + k\right)} \tag{A.20}$$

Parameters c_3 and c_4 in (A.18) are constants, generally complex numbers, dependent on boundary conditions. The complete solution to (A.17) is the sum of (A.18) and (A.20), written here as

$$x_1^{*}(t) = \frac{c_1\theta_1 e^{\theta_1 t}}{2rk\left(\theta_1^2 m + \theta_1 b + k\right)} + \frac{c_2\theta_2 e^{\theta_2 t}}{2rk\left(\theta_1^2 m + \theta_1 b + k\right)} + c_3 e^{\theta_3 t} + c_4 e^{\theta_4 t} \tag{A.21}$$

Using (A.2a), the optimal state variable $x_2^{*}(t)$ is found from (A.21) as

$$x_2^{*}(t) = \frac{c_1\theta_1^2 e^{\theta_1 t}}{2rk\left(\theta_1^2 m + \theta_1 b + k\right)} + \frac{c_2\theta_2^2 e^{\theta_2 t}}{2rk\left(\theta_1^2 m + \theta_1 b + k\right)} + c_3\theta_3 e^{\theta_3 t} + c_4\theta_4 e^{\theta_4 t} \tag{A.22}$$

Applying the boundary conditions at $t = 0$ and $t = t_f$ to the optimal trajectories (A.21) and (A.22) yields the system of algebraic equations

$$\begin{bmatrix} x_1(0) \\ x_2(0) \\ x_1(t_f) \\ x_2(t_f) \end{bmatrix} = \begin{bmatrix} \frac{\theta_1}{2rk\left(\theta_1^2 m+\theta_1 b+k\right)} & \frac{\theta_2}{2rk\left(\theta_2^2 m+\theta_2 b+k\right)} & 1 & 1 \\ \frac{\theta_1^2}{2rk\left(\theta_1^2 m+\theta_1 b+k\right)} & \frac{\theta_2^2}{2rk\left(\theta_2^2 m+\theta_2 b+k\right)} & \theta_3 & \theta_4 \\ \frac{\theta_1 e^{\theta_1 t_f}}{2rk\left(\theta_1^2 m+\theta_1 b+k\right)} & \frac{\theta_2 e^{\theta_2 t_f}}{2rk\left(\theta_2^2 m+\theta_2 b+k\right)} & e^{\theta_3 t_f} & e^{\theta_4 t_f} \\ \frac{\theta_1^2 e^{\theta_1 t_f}}{2rk\left(\theta_1^2 m+\theta_1 b+k\right)} & \frac{\theta_2^2 e^{\theta_2 t_f}}{2rk\left(\theta_2^2 m+\theta_2 b+k\right)} & \theta_3 e^{\theta_3 t_f} & \theta_4 e^{\theta_4 t_f} \end{bmatrix} \begin{bmatrix} c_1 \\ c_2 \\ c_3 \\ c_4 \end{bmatrix} \tag{A.23}$$

from which c_1, c_2, c_3, and c_4 can be obtained. The optimal control $u^*(t)$ in (A.16) has been derived from necessary conditions of optimality (A.5)–(A.9). It can however be verified that $u^*(t)$ is unique and that it does indeed minimize the performance index (A.3) [10].

Appendix B

High-Level Control Architecture

Figure B.1 is a flow chart detailing high level control architecture designed for a free-piston engine generator as implemented on a microcontroller, i.e. the engine control unit (ECU). Table B.1 remarks on the subsystems depicted in Fig. B.1.

Table B.1: Control Architecture Subsystems.

Subsystem	**Modes**	**Remarks**
Piston position feedback	ENABLED, DISABLED	Sensor: linear encoder mounted on translator rod.
Fuelling	ENABLED, DISABLED	Actuator 1: carburettor throttle with mechanical link to ECU-controlled servo motor. Actuator 2: Fuel supply valve closed/opened by ECU.
Ignition	ENABLED, DISABLED	Actuator: spark plug unit activated/deactivated by ECU.
Electric Machine	OFF, MOTOR, GENERATOR	Actuator: External transistors to set Electric Machine mode as required by ECU. OFF: open circuit, MOTOR: power is supplied to Electric Machine from onboard battery causing piston to oscillate, GENERATOR: By virtue of fuelling and ignition, piston moves and generates useful power.
Combustion chamber	OPEN, CLOSED	Actuator: Valve in combustion chamber closed/opened by ECU. Valve to remain open in Motoring stage (OPEN) but remain closed in Generation stage (CLOSED).

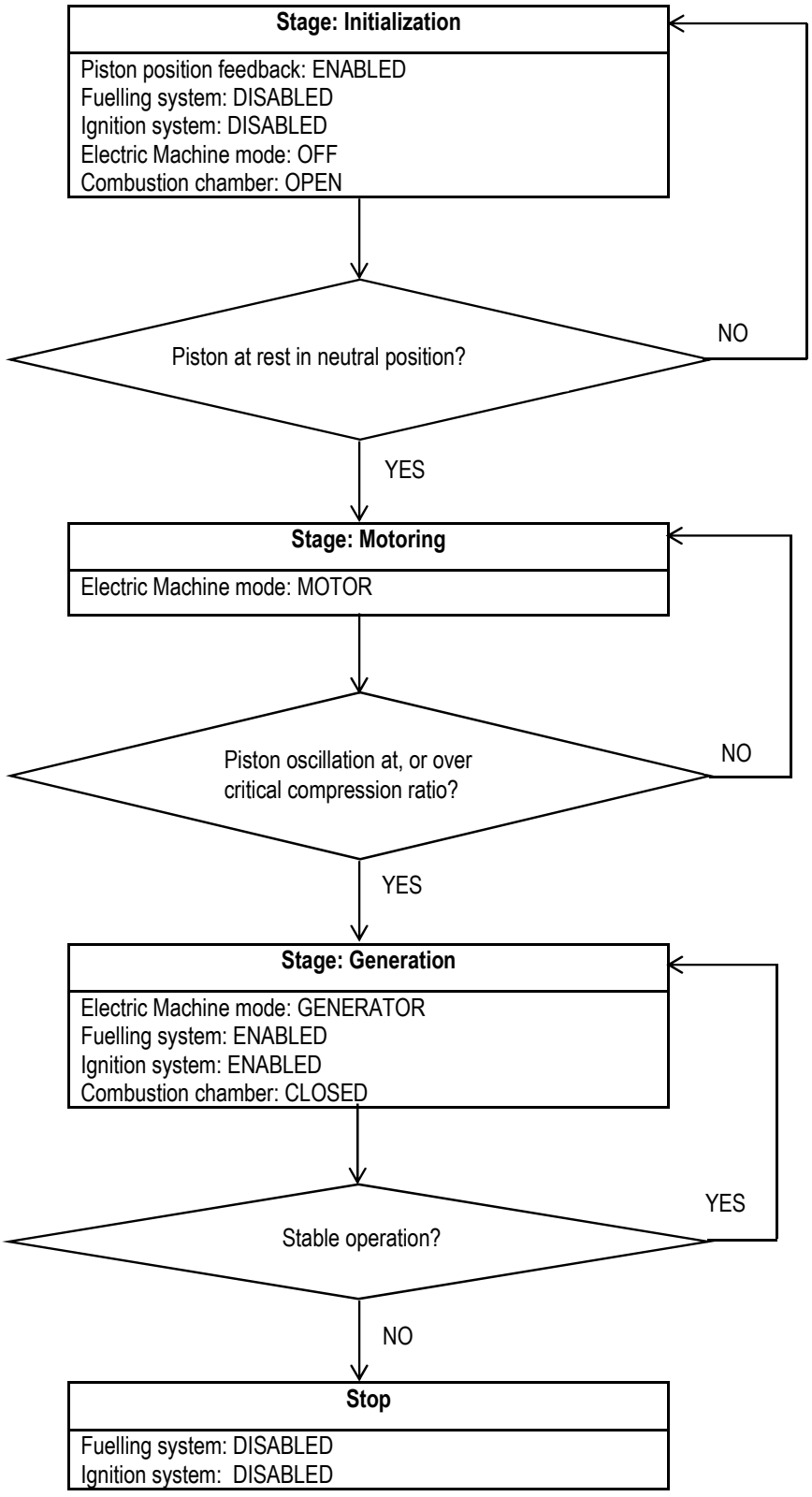

Figure B.1: High-level control architecture of FPE generator.

Appendix C

Adaptive Parameter Estimation Algorithm with Least Squares

FPE Model Preparation

An FPE generator whose rebound device is a mechanical spring has the dynamics

$$-m\ddot{x}_0 = A_p P_c(x_0) + \mu_g \dot{x}_0 + k_s x_0 + a_f \text{sgn}(\dot{x}_0) + b_f \dot{x}_0 \tag{C.1}$$

where P_c is the in-cylinder pressure, μ_g is the generator coefficient, k_s is the spring constant, and a_f, b_f are friction constants.

Assuming that only a measurement of x_0 is available, the filter $\frac{1}{(s+\lambda)^2}$, $\lambda > 0$ is applied to both sides of (C.1), and $\dot{x}_0$ in the fourth term of (C.1) realized with use of the derivative filter $\frac{Ns}{s+N}$ (where $N > 0$ is large), to yield a rearranged equation

$$-\frac{1}{(s+\lambda)^2} A_p P_c(x_0) - \frac{\mu_g}{s+\lambda} x_0 \approx \frac{ms^2}{(s+\lambda)^2} x_0 + \frac{k_s}{(s+\lambda)^2} x_0 + \frac{a_f}{(s+\lambda)^2} \text{sgn}\left(\frac{Ns}{s+N} x_0\right) + \frac{b_f s}{(s+\lambda)^2} x_0 \tag{C.2}$$

where it can be observed that the equation contains no derivatives of x_0, and is linear in all unknown parameters.

From (C.2), a so-called *static parameter model* is easily constructed as

$$z \approx \theta^{*T}\phi \tag{C.3}$$

where

$$z = -\frac{1}{(s+\lambda)^2}A_p P_c(x_0) - \frac{\mu_g}{s+\lambda}x_0 \tag{C.4a}$$

$$\theta^* = \begin{bmatrix} m & k_s & a_f & b_f \end{bmatrix}^T \tag{C.4b}$$

$$\phi = \begin{bmatrix} \frac{s^2}{(s+\lambda)^2}x_0 & \frac{1}{(s+\lambda)^2}x_0 & \frac{1}{(s+\lambda)^2}\mathrm{sgn}\left(\frac{sN}{s+N}x_0\right) & \frac{s}{(s+\lambda)^2}x_0 \end{bmatrix}^T \tag{C.4c}$$

Having constructed the static parameter model (C.3), the objective at hand is to algorithmically process the known signals $z(t)$ and $\phi(t)$ in order to generate an estimate of the unknown parameter vector θ^*. Following Ionnou and Fridan [51], an estimate $\hat{z}$ of z is generated by an estimation model that has the same form as the parametric model (C.3), i.e.

$$\hat{z} = \theta^T\phi \tag{C.5}$$

where $\theta(t)$ is an estimate of θ^* at time t. An estimation error ε can thus now be constructed as

$$\varepsilon = \frac{z - \hat{z}}{m_s^2} = \frac{z - \theta^T\phi}{m_s^2} \tag{C.6}$$

where $m_s^2 \geq 1$ is a normalising signal that is designed to guarantee that $\frac{\phi}{m_s}$ is bounded. It is common to construct this normalising signal as $m_s^2 = 1 + \alpha\phi^T\phi$, $\alpha > 0$.

The next task is to design a rule by which $\theta(t)$ must evolve in time, to not only ensure that ε converges to zero, but also to ensure that θ converges to θ^*. Such a rule is

commonly designed to depend on ε according to

$$\dot{\theta} = H(t)\varepsilon(t) \tag{C.7}$$

where $H(t)$ is a time-varying gain vector that depends on the measured signals. Equation (C.7) is an 'online' estimation scheme, also known as an *adaptive law*. Indeed, a wide class of adaptive laws can be realized with different choices of $H(t)$ and $\varepsilon(t)$.

Least Squares Algorithm with Forgetting Factor

To derive the adaptive law presented here, consider the cost function

$$J(\theta) = \frac{1}{2}\int_0^t e^{-\beta(t-\tau)} \frac{\left[z(\tau) - \theta^T(t)\phi(\tau)\right]^2}{m_s^2(\tau)} d\tau + \frac{1}{2} e^{-\beta t} \left(\theta - \theta_0\right)^T Q_0 \left(\theta - \theta_0\right) \tag{C.8}$$

where $\theta, \phi \in \mathbb{R}^n$, $z \in \mathbb{R}$; $Q_0 = Q_0^T > 0$, $\beta \geq 0$ are design constants, and $\theta_0 = \theta(0)$ is the initial parameter estimate. The terms in (C.8) for which e is raised to an exponent are sometimes referred to as a 'forgetting factor', as they put more weight on recent data relative to earlier data. If $\frac{z}{m_s}$ and $\frac{\phi}{m_s}$ are bounded, $J(\theta)$ is a convex function of θ over $\mathbb{R}^n$ for every time t. Hence, $J(\theta)$ has a global minimum that satisfies

$$\nabla J(\theta(t)) = 0 \qquad \forall t \geq 0 \tag{C.9}$$

The least squares algorithm for generating $\theta(t)$, the estimate of θ^* in (C.3), is therefore achieved by solving

$$\nabla J(\theta) = e^{-\beta t} Q_0(\theta(t) - \theta_0) - \int_0^t e^{-\beta(t-\tau)} \frac{z(\tau) - \theta(t)^T\phi(\tau)}{m_s^2(\tau)} \phi(\tau) d\tau = 0 \tag{C.10}$$

for $\theta(t)$ yielding the *nonrecursive* least squares algorithm

$$\theta(t) = P(t)\left[e^{-\beta t}Q_0\theta_0 + \int_0^t e^{-\beta(t-\tau)}\frac{z(\tau)\phi(\tau)}{m_s^2(\tau)}d\tau\right] \tag{C.11}$$

where

$$P(t) = \left[e^{-\beta t}Q_0 + \int_0^t e^{-\beta(t-\tau)}\frac{\phi(\tau)\phi^T(\tau)}{m_s^2(\tau)}d\tau\right]^{-1} \tag{C.12}$$

is known as the *covariance matrix*. Since $Q_0 = Q_0^T > 0$ and $\phi\phi^T$ is positive definite, $P(t)$ exists at each time t. By using the identity

$$\frac{d}{dt}PP^{-1} = \dot{P}P^{-1} + P\frac{d}{dt}P^{-1} = 0 \tag{C.13}$$

and $\varepsilon m_s^2 = z - \theta^T\phi$ from (C.6), and differentiating $\theta(t)$ with respect to time, the *recursive* least squares algorithm with forgetting factor is obtained:

$$\begin{aligned} \dot{\theta} &= P\varepsilon\phi & \theta(0) &= \theta_0 \\ \dot{P} &= \beta P - P\frac{\theta\theta^T}{m_s^2}P & P(0) &= P_0 = Q_0^{-1} \end{aligned} \tag{C.14}$$

The stability properties of the algorithm are discussed in [51]. A key aspect of the algorithm is that if $\frac{\phi}{m_s}$ is *persistently exciting*, i.e.

$$\int_0^{t+T_0}\frac{\phi(\tau)\phi(\tau)^T}{m_s^2}d\tau > \alpha_0 T_0 I \qquad \forall t \geq 0, T_0, \alpha_0 > 0 \tag{C.15}$$

then $\theta(t) \to \theta^*$ as $t \to \infty$, the convergence being exponentially fast when $\beta > 0$.

Appendix D

Publications

T. N. Kigezi and J. F. Dunne. A model-based control design approach for linear free-piston engines. *ASME Journal of Dynamic Systems, Measurement, and Control*, 139 (11): 111010, 2017.

T. N. Kigezi and J. F. Dunne. Development of an in-cylinder pressure observer for free-piston engines. *IEEE Conference on Control Technology and Applications*, Copenhagen, Denmark, 2018.

T. N. Kigezi and J. F. Dunne. General free-piston engine motoring strategies for misfire mitigation and compression ratio control. *Mechanical Systems and Signal Processing*, 2019 (In Process).

T. N. Kigezi, J. A. Gonzalez Anaya, and J. F. Dunne. Stochastic stability assessment of a semi-free piston engine concept. *Journal of Physics: Conference Series*, 744 (1), 2016.

T. Kigezi and J. Dunne. Optimal and resonant start of free-piston engines. *International Conference on Dynamical Systems—Theory and Applications*, Łodz, Poland, 2017.